ILLINOIS CENTER FOR TRANSPORTATION

Report No. FHWA-ICT-25-013

Investigation of Dolomite Aggregate Long-Term Cementation and Its Potential Advantage for Building Roads

Taeyun Kong
Chirayu Kothari
Issam I.A. Qamhia
Erol Tutumluer
Nishant Garg

ICT Project R27-248

December 2025

ISSN: 0197-9191
ICT Series Report No. 25-013
https://doi.org/10.36501/0197-9191/25-013

TECHNICAL REPORT DOCUMENTATION PAGE

1. Report No.	2. Government Accession No.	3. Recipient's Catalog No.
FHWA-ICT-25-013	N/A	N/A

4. Title and Subtitle	5. Report Date
Investigation of Dolomite Aggregate Long-Term Cementation and Its Potential Advantage for Building Roads	December 2025
	6. Performing Organization Code N/A

7. Authors	8. Performing Organization Report No.
Taeyun Kong (https://orcid.org/0009-0004-7495-9799), Chirayu Kothari (https://orcid.org/0000-0003-4468-1138), Issam I.A. Qamhia (https://orcid.org/0000-0002-2020-8437), Erol Tutumluer (https://orcid.org/0000-0003-3945-167X), and Nishant Garg (https://orcid.org/0000-0001-9292-8364)	ICT-25-013 UILU-2025-2013

9. Performing Organization Name and Address	10. Work Unit No.
Illinois Center for Transportation Department of Civil and Environmental Engineering University of Illinois Urbana-Champaign 205 North Mathews Avenue, MC-250 Urbana, IL 61801	N/A
	11. Contract or Grant No. R27-248

12. Sponsoring Agency Name and Address	13. Type of Report and Period Covered
Illinois Department of Transportation (SPR) Bureau of Research 126 East Ash Street Springfield, IL 62704	Final Report 7/1/22–12/31/25
	14. Sponsoring Agency Code

15. Supplementary Notes

Conducted in cooperation with the U.S. Department of Transportation, Federal Highway Administration.

https://doi.org/10.36501/0197-9191/25-013

16. Abstract

This study investigated the mechanical strength and freeze-thaw durability of carbonate-based aggregate quarry by-products (QBs) stabilized with cement alone and in combination with calcined clay (metakaolin, MK) for potential use in pavement foundation layers. The primary objective was to evaluate the chemical and physical characteristics of dolomitic and limestone QBs and determine how these factors influence strength development and durability under different stabilization conditions. Four QBs with varying carbonate compositions, ranging from highly dolomitic aggregates to nearly pure limestone, were examined. QBs were stabilized with 3% cement and tested under short- and long-term curing conditions. Short-term testing indicated the curing period was insufficient for the mineralogical properties of carbonate aggregates to fully manifest; instead, performance was governed primarily by physical characteristics, particularly particle packing. In contrast, long-term testing showed the effects of carbonate mineralogy became more pronounced, as the mineral components began contributing more noticeably to overall performance. Dolomitic QBs demonstrated superior strength and stiffness development along with higher retention of these properties after 10 freeze-thaw cycles due to the formation of hydrotalcite, a magnesium-aluminum layered double hydroxide phase. When cement was partially replaced with MK at the optimum MK-to-cement ratio of 1:4, both early-age and long-term performance improved relative to cement-only specimens. Chemical analyses showed that MK participated in pozzolanic and carboaluminate reactions, producing additional calcium-alumino-silicate-hydrate (C-A-S-H) gels and carboaluminate phases. Since MK rapidly consumed available calcium hydroxide to form C-A-S-H gel and carboaluminate phases, hydrotalcite formation was suppressed. This mechanism resulted in comparable long-term performance for all QBs, irrespective of carbonate types. The findings demonstrate that carbonate-based QBs can be transformed into high-performing, durable, and sustainable pavement foundation materials when their physical and mineralogical properties are considered properly and supplementary cementitious materials such as MK are incorporated effectively.

17. Key Words	18. Distribution Statement
Quarry By-Product, Underutilized Quarry Material, Carbonate Aggregate, Dolomite, Hydrotalcite, Freeze-Thaw Durability, Chemical Stabilization	No restrictions. This document is available through the National Technical Information Service, Springfield, VA 22161.

19. Security Classif. (of this report)	20. Security Classif. (of this page)	21. No. of Pages	22. Price
Unclassified	Unclassified	62 + appendices	N/A

ACKNOWLEDGMENT, DISCLAIMER, MANUFACTURERS' NAMES

This publication is based on the results of **ICT-R27-248: Investigation of Dolomite Aggregate Long-Term Cementation and Its Potential Advantage for Building Roads**. ICT-R27-248 was conducted in cooperation with the Illinois Center for Transportation; the Illinois Department of Transportation; and the U.S. Department of Transportation, Federal Highway Administration.

Members of the Technical Review Panel (TRP) were the following:

- Tim Peters, TRP Chair, Illinois Department of Transportation
- Andrew Stolba, TRP Co-Chair, Illinois Department of Transportation
- David Adedokun, Federal Highway Administration
- Matthew Austin, Illinois Department of Transportation
- Dennis Bachman, Federal Highway Administration
- Dan Barnstable, Vulcan Materials Company
- Steve Chery, Illinois Department of Transportation
- Dan Eichholz, Illinois Association of Aggregate Producers
- Dominique Ganier, Illinois Department of Transportation
- Amy Harms, Illinois Department of Transportation
- Paul Rasch, Shakespeare Oil Co., Inc
- Heather Shoup, Illinois Department of Transportation
- James Wooten, Plote Construction Inc.

The authors wish to express their sincere gratitude to the TRP Chairs and members for their valuable time, guidance, and significant contributions throughout the course of this research project. Special thanks are extended to the participating quarries, Northern Illinois Service Co., Heidelberg Materials, Vulcan Materials, Holcim, and Twin Rivers Stone, for generously providing the aggregate quarry by-product materials used in this study.

The authors also gratefully acknowledge the assistance of Illinois Center for Transportation research engineers Greg Renshaw, Mohsen Motlagh, and Uthman Mohamed Ali for their technical support, as well as McCall Macomber for her editorial assistance. Appreciation is further extended to Kristi Anderson, Brian Lorbiecki, and Audrey Donoho for their contributions to ICT project management.

Finally, the authors sincerely thank the University of Illinois graduate students and members of Professor Erol Tutumluer's research group for their dedicated efforts in conducting experimental work and for offering valuable insights and ideas during project discussions.

EXECUTIVE SUMMARY

This report presents the findings from a laboratory study that investigated the mechanical, durability, and microstructural behavior of carbonate-based quarry by-products (QBs) stabilized with cement and calcined clay (metakaolin, MK). The primary objective of this study was to evaluate the characteristics of carbonate aggregate QBs (i.e., dolomite or limestone), including their chemical, mineralogical, and physical properties, and to assess how these factors influence strength development and freeze-thaw durability when stabilized with cement alone and when combined with MK. The research built upon previous Illinois Center for Transportation projects (R27-125, R27-168, and R27-SP38), which demonstrated the potential of chemically stabilized QBs for pavement foundation applications while highlighting unresolved questions regarding the superior freeze-thaw durability observed in dolomitic QBs compared to limestone QBs in project R27-SP38. This study took an additional step toward enhancing the sustainability of QB applications in pavement foundations by incorporating MK as a supplementary cementitious material (SCM) to improve performance and reduce cement consumption.

The experimental program was organized into four major phases. The first phase involved a detailed characterization of the physical and chemical properties of QBs collected from Illinois quarries, aiming to capture a representative range of carbonate compositions, including both dolomitic and limestone materials. Laboratory testing included particle size distribution, compaction characteristics (moisture-density relationship), modified methylene blue test, X-ray fluorescence, atomic absorption spectroscopy, and X-ray diffraction. Based on the characterization results, four of the eight collected QBs were selected for detailed analyses in the subsequent phases: two highly dolomitic QBs, one mixed dolomite-limestone QB, and one nearly pure limestone QB. These materials exhibited a range of magnesium oxide (MgO) contents from 19.8% to 0.8% (determined by atomic absorption spectroscopy), which is the key criterion used by the Illinois Department of Transportation to classify aggregates as dolomitic or limestone. The variation in MgO content among the materials enabled a direct comparison of their performance in the later phases of the study, relating observed mechanical and chemical behavior to their MgO content.

The short-term results indicated that physical properties, particularly particle gradation and packing, governed performance more than the mineralogical or chemical composition of the QB materials. The QB that consistently exhibited the highest unconfined compressive strength (UCS) values and superior freeze-thaw resistance owed its performance to a well-graded particle distribution that minimized interconnected voids, closely following the optimum packing curve defined by Talbot's equation. Optical microscopy provided visual confirmation of this relationship, showing that specimens with denser packing and fewer voids developed fewer microcracks and experienced less particle loss during freeze-thaw conditioning. These findings proved that optimizing particle gradation is a critical factor in improving the short-term strength and durability of cement-stabilized QBs.

The third phase evaluated the long-term performance of cement-stabilized QB specimens, which were cured for 120 days at an elevated temperature of 104°F (40°C) to accelerate hydration reactions and simulate extended field curing. The objective was to assess the influence of carbonate mineralogy, specifically the distinction between dolomitic and limestone aggregates, on chemical

reactivity and its subsequent effects on mechanical performance and freeze-thaw durability. Over the long-term curing period, a clear difference in mechanical and freeze-thaw performance was observed between dolomitic and limestone QBs. Dolomitic QBs exhibited greater UCS development than the limestone control specimen, with the analysis accounting for fines content (passing the No. 200 sieve), which is more reactive during hydration compared to coarser particles. Measurements from bender element sensors placed in the specimens further confirmed this trend, showing higher shear wave velocities (V_s) and small-strain shear moduli (G_{max}) for dolomitic QB specimens. Furthermore, results from the resonant frequency test and UCS testing after freeze-thaw conditioning revealed that dolomitic QBs retained higher strength and stiffness with smaller percent reductions compared to limestone QBs.

The superior performance trends of dolomitic materials when stabilized with cement were attributed to their higher MgO content, which promoted the formation of hydrotalcite, a magnesium-aluminum layered double hydroxide known to refine microstructure and enhance long-term durability. The presence of hydrotalcite was confirmed through X-ray diffraction, thermogravimetric/differential thermogravimetric analysis, and Raman imaging, all of which indicated more extensive hydrotalcite formation in dolomitic systems than in limestone. Raman imaging revealed hydrotalcite formation localized around dolomitic grains, a feature absent in limestone QBs. Moreover, a strong correlation was observed between the strength development of QB specimens and the formation of hydrotalcite, underscoring the role of carbonate mineralogy in long-term stabilization. The results indicated that in cement stabilization, carbonate mineralogy can influence long-term performance, with dolomite imparting superior durability and strength development.

The fourth phase investigated the influence of incorporating metakaolin (MK) as a partial cement replacement to enhance both performance and sustainability. Several MK-to-cement ratios (1:2, 1:4, and 1:6) were tested using representative QB material, with the total stabilizer content fixed at 3% by weight. The 1:4 MK-to-cement ratio was identified as the optimum mix, providing the best balance between strength development and binder efficiency. Short-term (seven-day) curing results showed that even a lower total stabilizer content (2% cement + 0.5% MK) achieved UCS values comparable to or greater than the 3% cement-only control. Long-term testing further demonstrated continued strength and stiffness gains across all carbonate types, with MK incorporation leading to significant improvements in both mechanical performance and freeze-thaw durability. Chemical analyses revealed that MK accelerated pozzolanic and carboaluminate reactions, producing additional calcium-alumino-silicate-hydrate (C-A-S-H) gels and carboaluminate phases that refined pore structure and enhanced overall strength and durability. These reactions consumed available calcium hydroxide during the early stages of hydration, which may have resulted in the undersaturation for the formation of hydrotalcite. As a result, uniform chemical development was observed across both dolomitic and limestone QBs. Consequently, any differences in performance between the two carbonate types diminished, indicating that MK-induced hydration mechanisms dominated over the effects of the mineralogical composition of QB.

Overall, the findings from this study confirm that carbonate-based QBs can be stabilized effectively for use in pavement base and subbase layers when their physical, chemical, and mineralogical properties are considered properly. The results demonstrated that carbonate mineralogy strongly

influences long-term behavior in cementitious systems, with dolomitic QBs exhibiting higher strength development and freeze-thaw durability compared to limestone-based QBs. The inclusion of MK as a SCM further enhanced strength performance at both early- and long-term curing stages while improving resistance to freeze-thaw damage. MK incorporation, achieved through partial replacement of cement at an MK-to-cement ratio of 1:4 (i.e., 2.4% cement and 0.6% MK), demonstrated potential for reducing cement content without compromising performance, providing both environmental and economic benefits. Notably, the addition of a small amount of MK (0.75%) in combination with 3% cement produced the highest strength and durability among all tested specimens, indicating potential reductions in maintenance costs and an extended service life for pavement foundations. These findings provide valuable insight into the stabilization behavior of carbonate QBs, demonstrating that optimal performance can be achieved by leveraging their intrinsic properties and integrating SCMs such as MK. The study highlights a sustainable and technically viable pathway for utilizing QBs in transportation infrastructure, enhancing performance while reducing environmental impact and economic burden.

TABLE OF CONTENTS

LIST OF FIGURES

LIST OF TABLES

CHAPTER 1: INTRODUCTION

BACKGROUND AND MOTIVATION

The production of construction aggregates generates large quantities of fine residuals known as quarry by-products (QBs), also referred to as quarry screenings, quarry fines, and, more recently, underutilized quarry materials. Generated during quarrying operations such as blasting, crushing, washing, and screening, QBs account for up to 25% of total aggregate production, depending on the rock type and production method. The National Cooperative Highway Research Program reported that aggregate QB accumulation in the United States exceeds 4 billion tons (3.6 billion metric tons), originating from more than 3,000 active quarries, with annual QB production estimated to exceed 175 million tons (159 million metric tons) (Stroup-Gardiner & Wattenberg-Komas, 2013). In Illinois, a survey of aggregate producers conducted as part of Illinois Center for Transportation (ICT) project R27-125 indicated that annual production of QBs can be substantial, with quantities estimated to reach as high as 950,000 tons (860,000 metric tons) (Tutumluer et al., 2015). Due to the substantial quantities of QBs generated, their stockpiling and disposal are a major challenge for the aggregate industry. Consequently, evaluating the engineering characteristics of QBs and exploring their potential for sustainable pavement applications is becoming increasingly important.

Unstabilized QBs exhibit low compressive strength, typically less than 10 psi (69 kPa), which makes them unsuitable for direct use in pavement base or subbase layers without treatment. Previous research at ICT, conducted under project R27-125, demonstrated that chemical stabilization with small amounts of cement and Type C fly ash (e.g., 2% cement and 10% fly ash) can significantly improve the strength properties of QBs, making them suitable for pavement foundation applications (Tutumluer et al., 2015). A subsequent ICT project, R27-168, further confirmed the effectiveness of chemically stabilized carbonate aggregate QBs (limestone and dolomite) through the construction of full-scale test sections with various QB applications in foundation layers, followed by accelerated pavement testing (Qamhia et al., 2018). The study found that QBs stabilized with 3% cement provided satisfactory rutting resistance and adequate layer modulus for use in base and subbase applications. A follow-up ICT study, R27-SP38, investigated the wet-dry and freeze-thaw durability of stabilized QB specimens extracted from the full-scale test sections constructed in project R27-168 (Qamhia et al., 2019). The results revealed notable differences between dolomitic and limestone QBs. Dolomitic specimens exhibited less than 10% weight loss, meeting the acceptance threshold, after 12 freeze-thaw cycles with intermediate wire brushing in accordance with AASHTO T 136, even though the specimens had been extracted from the field section after two years. In contrast, limestone QB specimens failed completely, showing 100% weight loss under the same test conditions. These findings suggest that dolomitic and limestone QBs may respond differently to chemical stabilization and/or freeze-thaw exposure, highlighting the potential superiority of dolomitic materials against durability performance.

Limestone and dolomite are both sedimentary carbonate rocks that share a similar origin, containing carbonate minerals, but they differ in their composition. Limestone is primarily composed of calcite (calcium carbonate, $CaCO_3$), whereas dolomite consists mainly of calcium magnesium carbonate, $CaMg(CO_3)_2$, a mineral that incorporates Mg^{2+} ions into its crystal structure. In cementitious matrices,

the dissolution rate of dolomite or calcite governs their ability to supply carbonate ions for carboaluminate phase formation. Studies have shown that dolomite dissolves more slowly than calcite, suggesting the two minerals may participate differently in the hydration process (Morse & Arvidson, 2002; Pokrovsky & Schott, 2001). Several studies have examined the reaction mechanisms of dolomite fines when used as a substitution in concrete; however, no consensus has been reached regarding the fundamental mechanisms or the final hydrated phases produced (García et al., 2003; Xu et al., 2021; Zajac, Bremseth, et al., 2014; Zhang et al., 2020). Therefore, developing a clearer understanding of the role of dolomitic aggregates, specifically QBs, during cement stabilization is critical. Such knowledge can provide both economic and sustainability benefits in pavement construction by leveraging the mineralogical characteristics of dolomite to enhance performance and reduce long-term maintenance costs, while using an underutilized industrial by-product as an alternative aggregate source. This potential is especially significant in Illinois, where carbonate aggregates are abundant, offering significant opportunities to advance more sustainable and resource-efficient pavement foundation construction practices.

Although conventional stabilizers, such as cement and fly ash, have demonstrated satisfactory performance in QB applications, the pursuit of more sustainable and high-performance alternatives has generated growing interest in supplementary cementitious materials (SCMs), such as calcined clays. Calcined clays, such as metakaolin (MK), are highly reactive, amorphous aluminosilicates produced through the thermal treatment of clay. In the case of MK, hydroxyl groups are removed from the crystalline kaolinite structure during the calcination process, resulting in a disordered, amorphous phase. The amorphous MK phase participates in a pozzolanic reaction by reacting with calcium hydroxide from cement. This reaction forms calcium-alumino-silicate-hydrate gel. Numerous studies have confirmed the effectiveness of MK as an SCM in concrete applications, where it improves compressive and splitting tensile strength while reducing shrinkage strain (Güneyisi et al., 2008; Kim et al., 2007; Poon et al., 2006). However, limited research has addressed its role in cement stabilization of soils, particularly in systems involving sand-sized aggregate materials such as QBs (Wang et al., 2018). Furthermore, no study to date has specifically investigated the reaction mechanisms of dolomitic and limestone aggregates in cementitious matrices in the presence of MK, raising essential questions about whether dolomitic QBs will continue to exhibit superior performance over limestone QBs under freeze-thaw exposure.

Therefore, this project aimed to evaluate the characteristics of carbonate aggregate QBs, including their chemical, mineralogical, and physical properties, and to assess how these factors influence the development of mechanical strength and freeze-thaw durability when stabilized with either cement alone or a combination of cement and MK. To accomplish this, a range of material characterization techniques was employed to monitor phase evolution during hydration and to link these microstructural changes to the observed mechanical and durability performance. The outcomes of this study are synthesized in this report to provide recommendations for optimizing the use of QBs by accounting for their physical, chemical, and mineralogical attributes as well as the incorporation of SCMs, with the goal of promoting more sustainable and durable applications in pavement construction.

OBJECTIVE AND SCOPE

The objective of this project is to evaluate the chemical, mineralogical, and physical characteristics of carbonate aggregate QBs and to assess how these properties affect mechanical strength development and freeze-thaw durability when stabilized with cement alone or a combination of cement and MK. The study focuses on understanding the effect of particle gradation, fines content, and carbonate type (dolomite vs. limestone) on strength development, durability, and microstructural evolution under short- and long-term curing conditions. By linking the performance outcomes of QB specimens with their chemical and physical properties, the project aims to identify the governing mechanisms for different carbonate aggregate QBs during stabilization and to optimize their application by leveraging their intrinsic properties.

The scope of this study includes systematic laboratory testing of various QB materials collected from multiple quarries in Illinois, encompassing material characterization, short- and long-term mechanical evaluations with cement or cement-MK stabilization, and durability assessments under freeze-thaw exposure. Representative QBs with varying MgO contents and carbonate compositions were selected for detailed investigation. The experimental program involved unconfined compressive strength (UCS) testing, resonant frequency testing (RFT), bender element (BE) sensor measurements, and microstructural analyses using an optical microscope, X-ray diffraction (XRD), X-ray fluorescence (XRF), thermogravimetric analysis/differential thermogravimetric analysis (TGA/DTG), and Raman imaging. Particular emphasis was placed on comparing the performance of dolomitic and limestone QBs under both cement and cement-MK stabilization, with a focus on reaction mechanisms, strength development, durability, and sustainability, especially the potential of MK to enhance performance while reducing cement usage.

To achieve the overall objective of this project, the following tasks were conducted:

- Task 1—*Identifying Illinois sources and collection of dolomite aggregate materials.* Conduct research on the availability and types of carbonate aggregate QBs in Illinois and acquire a wide range of QB materials with varying carbonate compositions, including one limestone source for comparison.

- Task 2—*Characterization tests for physical, chemical, and mineralogical properties.* Evaluate the fundamental aggregate properties of the collected QB materials, including particle size distribution, compaction characteristics, clay content, oxide composition, and mineralogical phases.

- Task 3—*Laboratory testing for unconfined compressive strength under soaking and freeze-thaw environments.* Evaluate the mechanical strength of QB specimens stabilized with cement after short- and long-term curing, and compare results across different QB types to relate mechanical performance to material characteristics. Conduct freeze-thaw conditioning on the specimens to assess their durability, and compare freeze-thaw resistance among the various QB types.

- Task 4—*Additional characterization tests and interpretation of test results.* Implement material characterization tests over the curing period to monitor phase evolution during hydration reactions among different QB types and compare the results with the mechanical strength and freeze-thaw resistance observed in Task 3 to establish the relationship between mineralogical properties and performance.

- Task 5—*Sample preparation using calcined clay (metakaolin) and laboratory testing for strength and durability*. Prepare QB specimens with the addition of MK and evaluate their mechanical strength after short- and long-term curing to determine the effects of MK and QB type in MK-stabilized systems. Conduct freeze-thaw conditioning on the specimens to assess their durability performance.

- Task 6—*Chemical and microstructure analysis*. Perform a series of material characterization tests on specimens stabilized with MK and cement over the curing period to capture the evolution of distinct mineral phases and relate the results to the performance of QB specimens observed in Task 5.

- Task 7—*Final report and implementation*. Present all research findings and recommendations to IDOT to provide updated guidance on the optimal use of QB materials in pavement foundations by considering their physical, chemical, and mineralogical characteristics and by incorporating MK as a SCM.

REPORT ORGANIZATION

This report consists of six chapters, including this introductory chapter.

Chapter 2 describes the quarries from which eight QB materials were acquired and presents the fundamental properties of the collected carbonate-based aggregates. Laboratory evaluation tests included particle size distribution, compaction characteristics (moisture-density relationships), clay content, as well as chemical and mineralogical composition determined by XRF, XRD, and AAS (atomic absorption spectroscopy). Four representative QBs were selected for more detailed study: two highly dolomitic QBs (QB-1 and QB-2), one mixed dolomite and limestone QB (QB-7), and one limestone QB (QB-L). The stabilizers, cement and MK, were also introduced with their chemical and mineral phase compositions characterized. In addition to materials characterization, this chapter outlines the testing methods employed in this study, including UCS, RFT, BE sensor measurements, XRF, XRD, optical microscopy, TGA, and Raman imaging.

Chapter 3 investigates the short-term mechanical behavior of QB specimens stabilized with 3% cement after seven days of curing at room temperature. UCS, RFT, and freeze-thaw durability tests were conducted, and the results were compared across different QB types. In addition, optical microscopy was used to examine the relationship between particle size distribution and particle packing at a finer scale, both before and after freeze-thaw exposure.

Chapter 4 shifts the focus to the influence of chemical and mineralogical factors of aggregate QB on long-term stabilization performance. Cement-stabilized QBs were cured for up to 120 days at an

elevated temperature of 104°F (40°C) and subsequently tested for strength, stiffness, and freeze-thaw durability. Complementary chemical and microstructural analyses (XRD, TGA, and Raman imaging) were performed to monitor phase evolution during the hydration process and to establish potential links between phase formation and mechanical strength.

Chapter 5 examines the effect of partially replacing cement with MK to enhance performance and sustainability as well as the impact of combining MK and cement on mechanical performance. A range of MK-to-cement ratios was tested, and the optimum proportion was identified. QB specimens stabilized with MK and cement were subjected to both short- and long-term curing and subsequently tested for strength, stiffness, and freeze-thaw durability. Chemical and microstructural analyses were also conducted to investigate how carbonate aggregates behave in cementitious systems in the presence of MK.

Chapter 6 provides a summary of the overall testing program and the major findings. This chapter also presents recommendations for future implementation of QBs in pavement foundations to maximize their benefits.

CHAPTER 2: MATERIALS AND TESTING PROGRAM

AGGREGATE QUARRY BY-PRODUCTS

This research study investigated the effects of intrinsic chemical and mineralogical properties of carbonate-based aggregates (i.e., dolomite and limestone) on chemical stabilization using cement and metakaolin. Various types of carbonate aggregates, particularly quarry by-products (QB), were collected and analyzed. The materials were selected carefully to represent a range of carbonate aggregate properties, from highly dolomitic to pure limestone, based on sources available within the state of Illinois. Laboratory tests were conducted on the collected QB specimens to characterize their physical and chemical properties. These tests included grain size distribution, compaction characteristics (moisture-density relationships), a modified methylene blue test (MMB), X-ray fluorescence (XRF), X-ray diffraction (XRD), and atomic absorption spectroscopy (AAS).

Acquisition of Quarry By-Products

The primary chemical distinction between dolomite and limestone lies in the presence of the Mg^{2+} ion. According to IDOT aggregate specifications, the elemental composition of magnesium oxide (MgO) serves as the criterion for classifying carbonate aggregates as either dolomite or limestone. Aggregates with MgO content greater than 11% are considered dolomitic, while those with less than 11% MgO content are classified as limestone (Illinois Department of Transportation, 2022). The theoretical maximum MgO content in pure dolomite can reach approximately 22%.

The aggregate QB acquisition process began with an IDOT-approved source list, which specifies the average MgO content of quarry ledges across the state of Illinois. To capture a broad spectrum of carbonate aggregates with varying chemical properties, the quarries listed were reviewed carefully and ranked according to the MgO content, from highest to lowest. Based on this analysis, eight quarries were selected to cover a range of MgO content in roughly 1%–2% increments. Seven of the selected quarries were classified as dolomitic, and one was included as a typical limestone source in Illinois for comparison. Efforts were also made to include quarries previously studied in ICT projects related to QB materials (i.e., R27-125 and R27-168), to enable easier referencing of their known properties or past performance (Qamhia et al., 2018; Tutumluer et al., 2015). Table 1 summarizes the selected quarries, including their corresponding MgO content and geographic locations within the state of Illinois. The collected materials are hereafter referred to as QB-1 through QB-7 for the dolomitic samples and as QB-L for the control limestone sample. A close-up view of sand-sized aggregate QBs and a photograph of the collected materials are provided in Appendix A.

Particle Size Distribution

The particle size distributions of all aggregate QB materials were determined using both dry and washed sieving methods, following ASTM C136 and ASTM C117 guidelines, respectively. The inclusion of washed sieve analysis provided more accurate measurements of fine particle content, particularly those passing the No. 200 sieve (smaller than 75 µm). Figure 1 presents the particle size distributions of all collected QB samples. The results indicate that all QB materials exhibit well-graded characteristics. The materials generally show particle sizes smaller than 0.25 in. (6.35 mm). While

most of the QBs followed typical gradation trends, QB-5 showed a coarser profile with a significant portion of material retained on the ¼ in. sieve (6.35 mm). Additionally, all QB materials showed fine contents ranging from approximately 10% to 20%, consistent with observations from previous ICT projects that studied QB materials.

Table 1. MgO Content and Geographical Locations of Quarries Used in the QB Acquisition Process

Quarry No.	Quarry Location	Avg. MgO (%)	Location in Map
1	Roscoe	20.1	
2	Thornton	18.8	
3	McCook	18.1	
4	McCook	16.5	
5	N. Utica	14.5	
6	Romeoville	13.3	
7	Godfrey	11.9	
8	Fairmount	1.8	

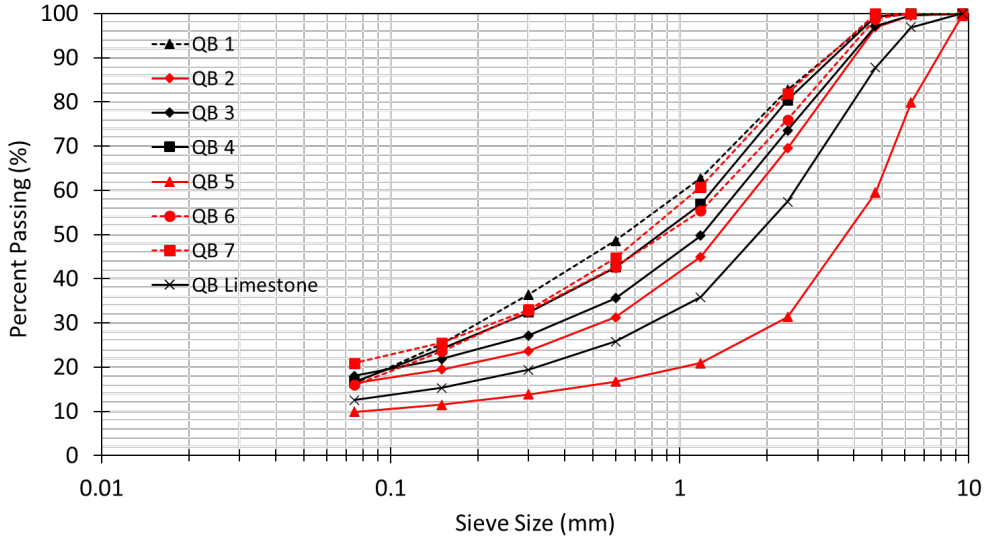

Figure 1. Graph. Particle size distributions for the studied QB materials.

Moisture-Density Relationship

The compaction characteristics of the QB materials were determined using the standard Proctor test, in accordance with ASTM D698, to establish moisture-density relationships. The optimum moisture content (OMC) and maximum dry density (MDD) were determined after the addition of 3% cement to the QB materials. These values were then used to prepare cement-stabilized specimens with 3% cement content. Table 2 summarizes the OMC and corresponding MDD for each QB material studied. The OMC and MDD values fall within similar ranges to those reported in previous ICT projects (Tutumluer et al., 2015), with MDD ranging from 119 to 136 pcf (18.7 to 21.4 kN/m^3) and OMC ranging from 8.5% to 10.7%. Moisture-density relationship curves for all QB materials are provided in Appendix B.

Table 2. Summary of OMC and MDD Properties for QB Materials Sourced from Stone Quarries

Quarry By-Product Type	Maximum Dry Density (pcf)	Optimum Moisture Content (%)
QB-1	129	10
QB-2	137	8.5
QB-3	135.5	8.6
QB-4	134	8.6
QB-5	118.5	8.6
QB-6	132.7	8.3
QB-7	124	10.7
QB-L	130	9.2

Deleterious Clay Content

The presence of excessive clay content in aggregate can induce swelling and expansion, leading to significant volume changes upon water absorption, which in turn may cause pavement distress. Furthermore, clay minerals can negatively impact the long-term strength of soil stabilization by interfering with the bond between the aggregate and the cement paste. To assess the presence of clay in the collected QB materials, the MMB test, a rapid and effective method, was employed. QB particles passing the No. 4 sieve (4.75 mm) were mixed with a methylene blue test solution ($C_{16}H_{18}ClN_3S$), and a colorimeter was used to measure the light transmittance through the diluted suspension. Figure 2 illustrates the apparatus required for the MMB test. Detailed testing procedures can be found in Pitre (2012). Table 3 presents the results obtained from the MMB tests for all tested QB materials. In general, deleterious clay contents were less than 1% across all samples. Based on these findings, the potential for strength reduction or swelling due to clay interference during cement hydration was minimal.

Figure 2. Photo. Modified methylene blue test kit.

Table 3. Measured Clay Contents of the Studied QB Materials Using the MMB Test

QB Type	QB-1	QB-2	QB-3	QB-4	QB-5	QB-6	QB-7	QB-L
Clay content (%)	0.35	0.63	1.00	0.27	0.94	0.21	0.82	0.79

Chemical and Mineralogical Properties

The QB samples were further analyzed for their chemical properties to confirm their mineralogy. The complete elemental compositions of QBs are provided in Appendix C. The carbonate-based QBs exhibited varying levels of MgO content across QB-1 through QB-7, as shown in Table 4. While following the general decline in MgO content from QB-1 to QB-7, XRF measurements of the dolomitic QBs indicated consistently lower values than those reported by IDOT. The only exception was QB-4, whose MgO content (15.4%) was nearly identical to that of QB-1 (15.6%). The discrepancy in MgO content between the IDOT list (11.9%–20.1%) and the XRF results (7.3%–15.6%) arises from the intrinsic differences in the measurement methods. The MgO values reported by IDOT were obtained using AAS, which measures the absolute quantity of magnesium present in the sample (i.e., g/g of sample). In contrast, XRF provides relative elemental compositions, where the MgO content is calculated as a proportion of all detectable elements rather than as an absolute quantity. Additionally, the off-trend MgO content of QB-4 was likely due to the acquisition of QB material from different ledges than those used to report the MgO content. Therefore, all collected QB materials were retested for MgO content using AAS with the assistance of the chemistry laboratory at the IDOT Central Bureau of Materials. The AAS results are presented in the third column of Table 4 and are generally consistent with the values reported by IDOT. However, QB-4 again exhibited a higher MgO content than the reported value, confirming the trend previously observed with XRF. By contrast, QB-L displayed minimal MgO content across all methods (0.3%–1.8%), underscoring its calcitic composition.

Table 4. Comparison of MgO Contents in QB Materials Using Different Measurement Approaches

QB Type	Avg. MgO from the IDOT List (%)	MgO from XRF[#] (%)	MgO from the AAS[*] (%)
QB-1	20.1	15.6	19.8
QB-2	18.8	14.3	19.5
QB-3	18.1	13.7	18.4
QB-4	16.5	15.4	19.7
QB-5	14.5	9.9	8.9
QB-6	13.3	10.9	15
QB-7	11.9	7.3	10.4
QB-L	1.8	0.3	0.8

[#]X-ray Fluorescence [*]AAS = Atomic Absorption Spectroscopy

The MgO content of a sample does not provide sufficient information regarding the mineralogy or carbonate type of the QB, even though IDOT specifications define carbonate type based on MgO content. Therefore, XRD analysis was performed on powdered QB samples to identify and quantify the mineral phases (Figure 3). Results showed that although MgO content decreases from QB-1 to QB-5, these materials primarily consist of dolomite as the dominant phase. In contrast, QB-6 and QB-7 exhibited a mixture of dolomite and limestone as the major phases, while QB-L was composed predominantly of calcite (limestone). Rietveld refinement was also conducted on the XRD patterns to quantify mineral phases, and the compositions are reported in Table 5. Overall, all QB materials were primarily composed of carbonates with minor impurities, including quartz, sanidine, and augite. All QBs contained more than 90% carbonate phases, except for QB-5 (80.2%), which had a higher amount of impurities, including quartz (11.4%) and sanidine (8.4%).

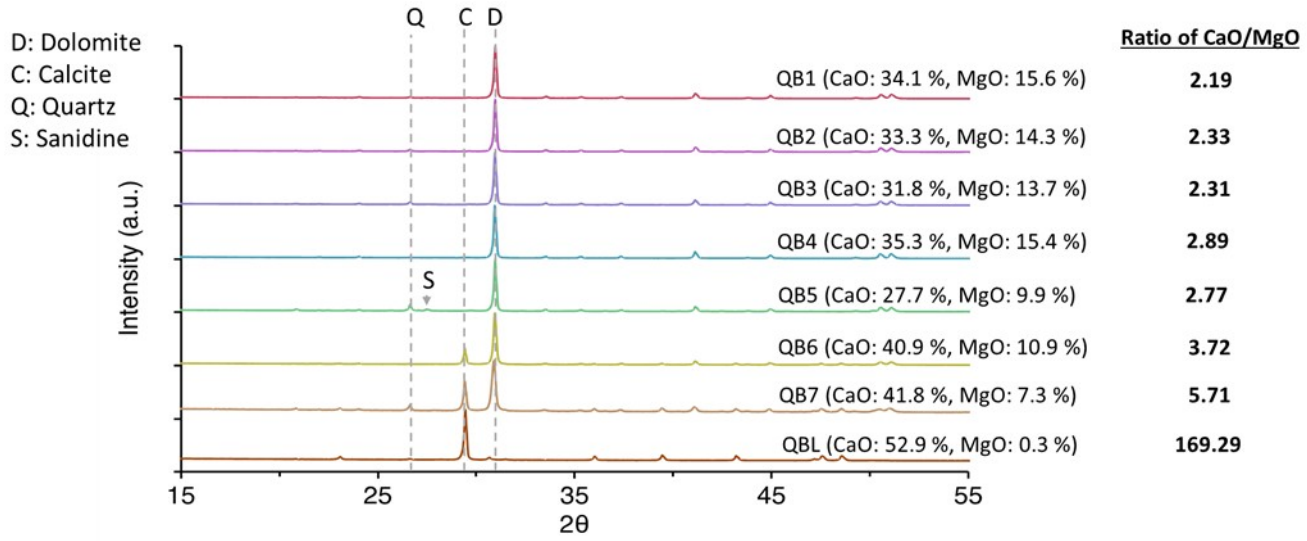

Figure 3. Graph. XRD patterns of the studied QB materials.

Table 5. Quantification of Mineral Phases in Studied QB Materials Using Rietveld Refinement of XRD Patterns

	QB-1	QB-2	QB-3	QB-4	QB-5	QB-6	QB-7	QB-L
Dolomite (%)	96.5	95.6	93.6	98.1	80.2	77.6	58.9	NP
Quartz (%)	2.1	4.5	6	0.8	11.4	0.7	6.8	2.3
Calcite (%)	NP*	NP	0.5	NP	NP	21.7	34.2	96.4
Augite (%)	1.3	NP	NP	1.2	NP	NP	NP	1.3
Sanidine (%)	NP	NP	NP	NP	8.4	NP	NP	NP
R_{wp}**	8.79	9.59	8.76	9.23	9.47	7.82	9.03	7.69

*NP = Not present, **R_{wp} = Weighted residual error

QUARRY BY-PRODUCTS SELECTED FOR FURTHER STUDIES

Among the eight collected aggregate QB materials, four were selected for specimen preparation and further analysis based on their distinct physical and chemical properties. These selected materials were QB-1, QB-2, QB-7, and QB-L, as shown in Figure 4, which presents the particle size distributions for these specific samples. QB-1 and QB-2 were chosen due to their high MgO content (i.e., high dolomite content), but with differing particle size distributions, allowing for comparative analysis of both mineralogical and physical influences. QB-7 was selected for its MgO content, which is near the classification threshold between dolomite and limestone, making it representative of a moderately dolomitic aggregate. Lastly, QB-L was included as a control sample for comparison. Table 6 summarizes the selected materials, along with their corresponding MgO content determined by AAS analysis and their mineralogical composition as determined by XRD analysis.

Fine particles (smaller than approximately 100 μm) tend to be more reactive with cement in soil-cement mixtures due to their larger surface area, which enhances cementitious reactions. These finer materials play a critical role in strength development through chemical interactions with cement. Therefore, evaluating the physical properties of the fine fraction provides valuable insight into their reactivity potential. The particle size distribution of QB fines (QBF), materials passing the No. 200 sieve (smaller than 75 μm), was measured using a laser particle size analyzer, which employs a laser-scattering technique to determine the distribution of particle sizes within a sample, as illustrated in Figure 5. The results show that QBF-L has the finest particle size distribution, while QBF-2 and QBF-7 exhibit similar distribution curves. In contrast, QBF-1 displays a relatively coarser particle size distribution.

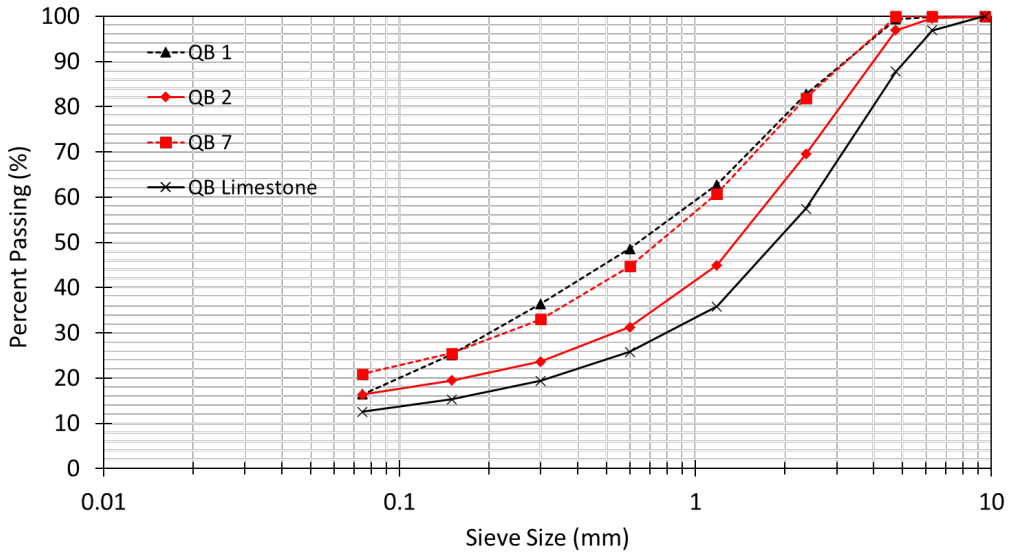

Figure 4. Graph. Particle size distributions of the QB materials selected for further analysis.

Table 6. Mineral Phases and MgO Contents in Selected QB Materials

	Calcite (%)	Dolomite (%)	MgO Content from AAS (%)
QB-1	NP	96.5	19.8
QB-2	NP	95.6	19.5
QB-7	34.2	58.9	10.4
QB-L	96.4	NP	0.8

*NP = Not present

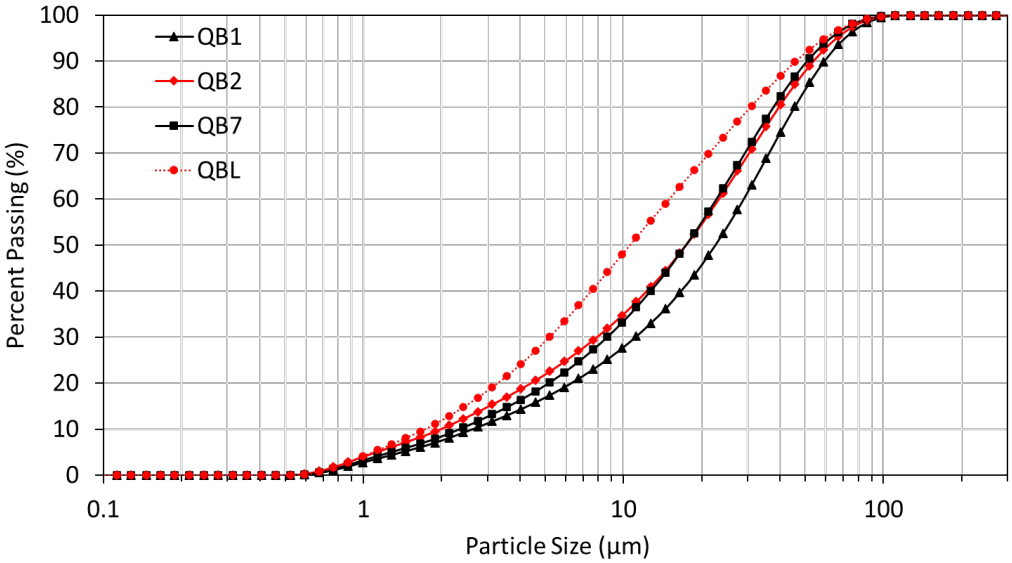

Figure 5. Graph. Particle size distributions of QBF determined by laser particle size analyzer.

CEMENT AND CALCINED CLAY

Type IL cement was used as the primary chemical stabilizer in this study, reflecting current industry trends that favor this cement type for its improved sustainability and reduced carbon footprint. The Rietveld refinement of XRD results, summarized in Table 7, identifies the phase compositions present in the cement used. Additionally, the MK utilized in this study was characterized by using XRF to verify its chemical composition and overall quality. The oxide composition is presented in Table 8. Although there is no universally accepted threshold for defining high-purity MK, materials with a combined silica (SiO_2) and alumina (Al_2O_3) content exceeding 90% by weight are generally associated with high pozzolanic reactivity. In this study, the MK exhibited a combined SiO_2 and Al_2O_3 content of over 96%, confirming its classification as high-purity MK and its suitability for enhancing the performance of cementitious systems.

Table 7. Phase Composition of Cement Used in This Study

Phase (wt.%)	Alite	Belite	Ferrite	Aluminate	Calcite	Gypsum
Type IL Cement	52.5	23.5	8.1	2.4	9.2	4.3

Table 8. Elemental Composition of Calcined Clay (i.e., MK) Used in This Study

Oxide content (%)	Al_2O_3	SiO_2	P_2O_5	SO_3	K_2O	CaO	TiO_2	MnO	Fe_2O_3
MK	42.3	54	0.075	0.0655	0.0895	0.191	1.79	0.0067	1.33

TEST METHODOLOGIES

Unconfined Compressive Strength Test

The mechanical strength of the stabilized QB specimens was determined through UCS tests using the equipment shown in Figure 6. Cylindrical specimens with an aspect ratio of 1:2, measuring 2.8 in. (71 mm) in diameter and 5.6 in. (142 mm) in height, were prepared with the target stabilizer content. After completing their conditioning processes (i.e., curing or freeze-thaw cycles, as detailed in each section), the specimens were stored in a moisture room for 24 hours prior to UCS testing to eliminate any residual matric suction that might otherwise influence the measured compressive strength. A consistent loading rate of 0.056 in. per minute (1.42 mm per minute), equivalent to a strain rate of 1% per minute, was applied. The specimens were loaded until significant failure was observed. Given the inherent variability in UCS measurements, three specimens were tested for each stabilizer type and conditioning stage. The average peak stress, obtained from the stress-strain curves at the point of failure, was used to calculate the UCS for each material.

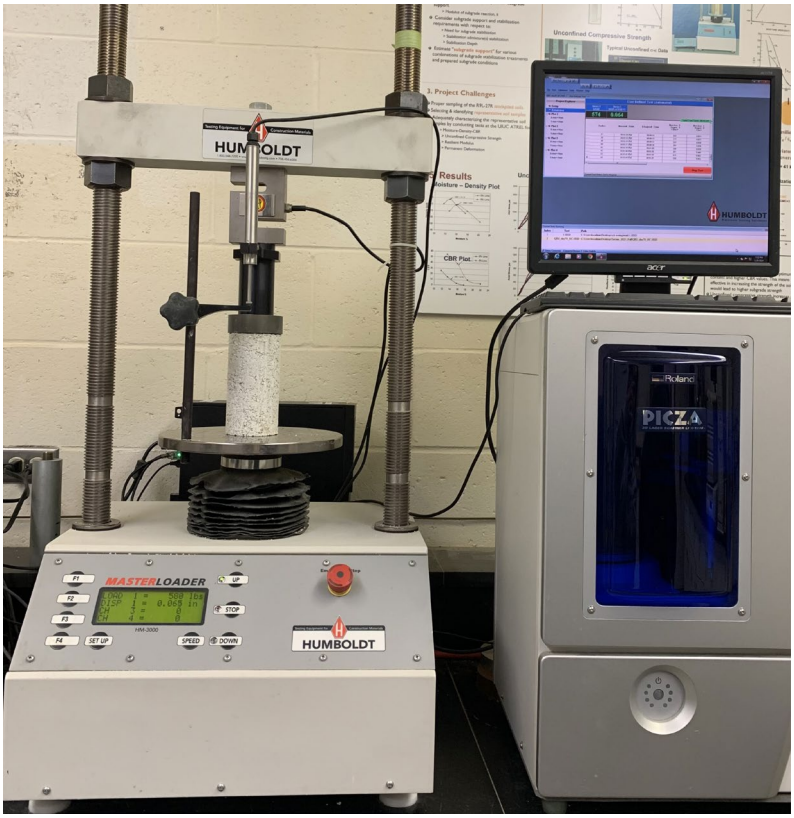

Figure 6. Photo. Loading frame setup during UCS testing of a stabilized QB specimen.

Resonant Frequency Test

Resonant frequency testing, a nondestructive technique for evaluating structural integrity, was employed to assess freeze-thaw damage accumulation in the stabilized QB specimens. This method allows for the evaluation of stiffness and mechanical properties by measuring the natural frequencies at which a material vibrates under dynamic excitation. Generally, higher resonant frequencies are indicative of increased stiffness, offering a better understanding of the internal condition of the material.

In this study, longitudinal RFT was performed using the data acquisition setup illustrated in Figure 7. An accelerometer was attached to one end of each specimen, while an impact was applied to the opposite end. The resulting vibrations were detected by the accelerometer, transmitted through a signal conditioner and data acquisition system, and recorded via a computer interface. The captured signal, initially in the time domain, was transformed into the frequency domain using fast Fourier transform. The peaks observed in the frequency domain indicated the resonant frequencies of the specimens, which reflect the points of maximum vibrational response. The dynamic modulus of elasticity (E_d) was then calculated based on the measured resonant frequency, following ASTM C215 guidelines. The equation presented in Figure 8 was used in this calculation, where ρ is bulk density of the specimen, L is length of the specimen, and f_L is longitudinal resonant frequency. The RFT was conducted at various freeze-thaw intervals to capture stiffness degradation caused by freeze-thaw damage.

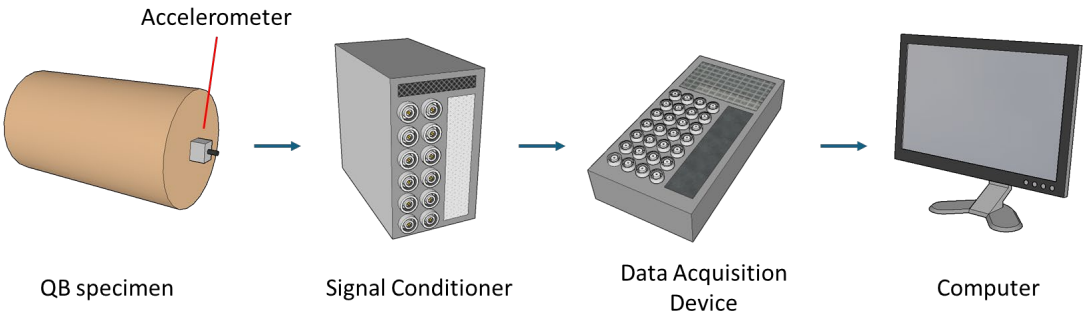

Figure 7. Illustration. Data acquisition setup for RFT.

$$E_d = \rho(2Lf_L)^2$$

Figure 8. Equation. Calculation of the dynamic modulus of elasticity.

Bender Element Sensor Technology

Bender element sensors, consisting of two layers of piezoceramic material bonded to a thin metal shim sandwiched between them, as shown in Figure 9, undergo mechanical deformation when an electric voltage is applied across the sensor. This deformation occurs as one layer contracts while the other expands, thereby generating a shear wave. Shear waves, a type of elastic wave, can propagate through a medium composed of interconnected aggregate particles, providing nondestructive information about a material's internal state. The inherent piezoelectric properties of BE sensors enable the conversion of electrical energy into mechanical deformation, and vice versa. Therefore, BE sensors can function as both transmitters and receivers.

In this study, BE sensors were installed at the top and bottom of the stabilized QB specimens, as illustrated in Figure 10, which shows the overall experimental setup for analyzing stiffness development during the curing period. A signal generator was used to apply a low-voltage excitation to the transmitting BE sensor, and the resulting shear wave propagated through the QB medium. The signal was detected by the receiving BE sensor and transmitted to an oscilloscope for analysis. The output signal was amplified and/or filtered using an electronic filter prior to interpretation. Stiffness development was monitored by evaluating the shear wave velocity (V_s), determined from the first arrival time (i.e., the time it takes for the shear wave to travel through the specimen) as detected by the receiving BE.

According to principles of continuum mechanics, denser microstructures generally exhibit higher stiffnesses and higher elastic moduli, which enable faster transmission of vibrational energy (Santamarina et al., 2001). Therefore, a shorter first arrival time is indicative of stiffer material. The V_s was calculated using the equation shown in Figure 11.

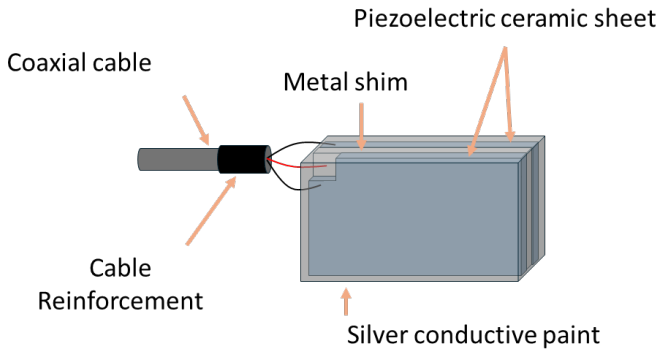

Figure 9. Illustration. Bender element sensor.

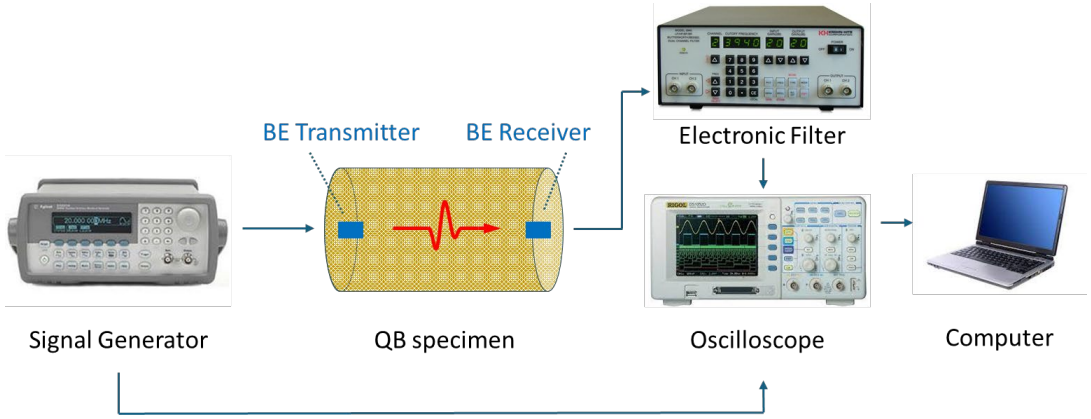

Figure 10. Illustration. Data acquisition setup used in shear wave signal detection using BE sensors.

$$V_s = \frac{L}{t}$$

Figure 11. Equation. Calculation of the shear wave velocity.

where *L* is the known distance between the transmitter and receiver BE sensors, and *t* is the first arrival time representing the travel time through the QB specimen. The V_s was then used to compute the small-strain shear modulus (G_{max}) of the specimens using the equation given in Figure 12.

$$G_{max} = \rho V_s^2$$

Figure 12. Equation. Calculation of the small-strain shear modulus.

where ρ is the bulk density of the QB specimen, and V_s is the calculated shear wave velocity.

X-ray Fluorescence

The bulk oxide content of the samples was measured via an Energy Dispersive X-ray Fluorescence Spectrometer (Shimadzu EDX-7000). The collimator size was 10 mm. The XRF spectrum was acquired

between 0–40 keV in a helium environment. The oxide composition was corrected for loss on ignition.

X-ray Diffraction

XRD analysis was performed using a Bruker D8 advanced diffractometer equipped with a Cu Kα (λ = 1.5418 Å) source and a 2D Eiger2 R 500 K detector. The instrument was operated in a Bragg-Brentano (θ−2θ) setup at 40 kV and 40 mA. It included a Goebel mirror as a monochromator, a 0.2 mm slit for the incidence divergence, and 2.5° Soller slits. Powdered QBF-cement samples hydrated at different ages were placed on polymethylmethacrylate holders and scanned from 5° to 70° (θ), with a step size of 0.01° and a 0.1 second measurement time per step, totaling 14 minutes per sample. Phase identification used the peak search method in DIFFRAC.EVA software. Rietveld refinement was applied to virgin QB samples to determine their mineralogical composition.

Sample Preparation for Microscopy

Small chunks of samples subjected to UCS testing were collected and stored in isopropyl alcohol to stop cement hydration by the water exchange method. Later, the samples were placed in a vacuum desiccator to remove the isopropanol. After the samples were dried in the vacuum desiccator, they were impregnated with low-viscosity epoxy and then placed in the vacuum desiccator for 30 minutes to remove any air bubbles. The samples were then cured at 140°F (60°C) for an additional 24 hours before removing them from the mold. Two parallel cuts were made on the epoxy-impregnated samples using a saw machine and a diamond blade to produce a flat pallet specimen. Finally, the samples were polished using silicon carbide paper (600, 800, and 1200 grit).

Thermogravimetric/Differential Thermogravimetric Analysis

TGA/DTG tests were conducted using a TA Instruments Q50 Thermogravimetric Analyzer, which features a weight sensitivity of 0.1 µg. Samples, weighing around 0.000033 lb (about 15 mg), were placed in an alumina crucible and heated from 86°F (30°C) to 1652°F (900°C) at a rate of 68°F/min (20°C/min), with N_2 gas (2.03 fl. oz/min, roughly 60 ml/min) used as the purging atmosphere.

Raman Imaging

Raman imaging was conducted on cube samples containing QBF-2 (dolomite) and QBF-L (limestone) to analyze phase differences between dolomitic and limestone QBs after long-term curing. The cement-stabilized cubes were cured for 120 days and then stored in a vacuum desiccator, following an isopropanol exchange, to prevent hydration or carbonation until use. The samples were embedded in EpoThin 2 epoxy with the surface facing downward in the mold. After curing, they were demolded and polished in several steps: initially with silicon carbide paper of multiple grits (#400, #600, #800, and #1200) for 10 minutes each, with additional polishing with #1200 grit if needed, followed by optional diamond polishing with 3, 1, and 0.25 µm particles. Between each polishing step, samples were ultrasonicated for three minutes. Optical images and Raman spectra were obtained using a Confocal Raman Microscope (WITec Alpha 300 series SNOM). The scans used a 12 mW excitation at λ = 532 nm, a 600 g/mm grating, and a cooled CCD camera at −76°F (−60°C). A 50x objective scanned an area of 150 µm × 60 µm at 4,500 pixels with a resolution of 0.67 µm per pixel. The depth and lateral resolutions of the CRM, calculated via the equations given in Figures 13 and 14

(Juang et al., 1988; Loh et al., 2021), were diffraction limited. For the 50× objective (working distance 9.1 mm, NA 0.55), the lateral resolution was 0.59 µm and the depth resolution was 1.23 µm in air (n=1). The step size for the scans exceeded the lateral resolution. Each point was scanned for 0.3 seconds, resulting in a total scan time of approximately 34 minutes per sample.

$$\Delta_{depth} = \pm \frac{4.4\,\lambda n}{2\pi(N.A.)^2}$$

Figure 13. Equation. Depth resolution of the objective on the Raman microscope based on the diffraction limit.

$$\Delta_{lat} = \frac{0.61\,\lambda}{N.A.}$$

Figure 14. Equation. Spatial resolution of the objective on the Raman microscope based on the diffraction limit.

Collected data were preprocessed upon completion of the Raman scan. Preprocessing includes cosmic ray correction, background subtraction, and normalization of the prominent peaks of individual spectra to 1.0. After preprocessing, phase identification was performed using basis analysis, also known as true component analysis, in the Witec Project 5 software (Dieing & Ibach, 2010). Basis spectra were obtained from the true component analysis on the Witec Suite. Each basis spectrum was matched with the reference spectrum of a mineral, available in the RRUFF database or in the literature (Lafuente et al., 2015). A detailed procedure for data analysis can be found in a study by Kothari and Garg (2024b). Phase maps were created based on the signal-to-noise ratio of each phase at specific spectral points within individual pixels. The spectra from each pixel were extracted in MATLAB format to produce Raman maps by assigning a phase label to each pixel. A criterion, based on the peak's characteristic position and a signal-to-noise ratio threshold (SNT), was used to assign pixels to specific phases (Kothari & Garg, 2024b). If the ratio of the area under a phase's characteristic peak to the area under noise (SNR) exceeds the detection limit threshold (SNT) of 3.0, then the phase was considered present (Shrivastava & Gupta, 2011). Finally, the binary phase maps were smoothed using a Gaussian blur filter and thresholded with the Isodata algorithm (Lee, 1983; Ridler & Calvard, 1978).

CHAPTER 3: EVALUATION OF SHORT-TERM PERFORMANCE IN CEMENT-STABILIZED CARBONATE-BASED QUARRY BY-PRODUCT SPECIMENS: EFFECT OF PACKING

SAMPLE PREPARATION AND CONDITIONING

A total of 20 specimens were prepared, five for each QB type, without any cement stabilization to evaluate the strength characteristics of the untreated (virgin) QB materials at the optimum moisture content (OMC) and maximum dry density (MDD) values presented in Appendix B. Additionally, 48 cement-stabilized specimens were prepared, as shown in Figure 15, with 12 specimens allocated to each QB type. Cement stabilization was achieved by incorporating 3% cement by weight. The 3% dosage was selected based on prior research involving similar QB materials, where this cement content demonstrated sufficient rutting resistance and wet-dry durability for base and subbase applications. All specimens were prepared in accordance with ASTM D2166, using their respective OMC and MDD values. Compaction was performed in three equal lifts using a standard Proctor hammer. The specimens were molded into cylindrical shapes with an aspect ratio of 1:2, measuring 2.8 in. (71 mm) in diameter and 5.6 in. (142 mm) in height. For the cement-stabilized specimens, a 7-day curing period was implemented in a controlled moisture room maintained at 100% relative humidity and a temperature of 73 ± 5°F (23 ± 2°C).

Upon completing the 7-day curing period, the 3% cement-stabilized QB specimens were subjected to accelerated freeze-thaw conditioning in accordance with ASTM D560, with one modification: the wire brushing procedure was omitted. This step was excluded because the brushing stroke can be subjective, potentially introducing inconsistency in durability evaluation. Instead, unconfined compressive strength (UCS) tests were conducted at selected freeze-thaw stages to assess the mechanical degradation of the specimens. The conditioning process involved exposing the specimens to a 24-hour freezing period at −10°F (−23°C) in a freezing cabinet, followed by a 24-hour thawing period in a moisture room maintained at 73.5°F (23°C) with a relative humidity of 100%. Each freeze-thaw cycle lasted a total of 48 hours. To ensure proper air circulation, the specimens were placed at least 1 in. (2.54 cm) apart inside the freezing cabinet. Additionally, a thick absorptive material was placed between the specimens and the supporting tray, in accordance with ASTM D560 recommendations.

Figure 15. Photo. Cylindrical cement-stabilized QB specimens cured in a moisture room.

MECHANICAL AND DURABILITY PERFORMANCE TRENDS

Compressive Strength Development

Figure 16 shows the UCS test results on both untreated and 3% cement-stabilized QB specimens after a 7-day curing period. As anticipated, the UCS values of the untreated QB materials were very low, with some variation among the QB material types. The average UCS values were 4.2 psi (29 kPa) for QB-1, 2.8 psi (19.3 kPa) for QB-2, 6.2 psi (42.7 kPa) for QB-7, and 2.1 psi (14.5 kPa) for QB-L. In contrast, the inclusion of 3% cement resulted in a substantial increase in strength, with improvements ranging from more than 30 times to over 100 times, depending on the type of QB. The average UCS values for stabilized specimens were 180.3 psi (1,243 kPa) for QB-1, 317 psi (2,186 kPa) for QB-2, 193.7 psi (1,336 kPa) for QB-7, and 265.7 psi (1,832 kPa) for QB-L.

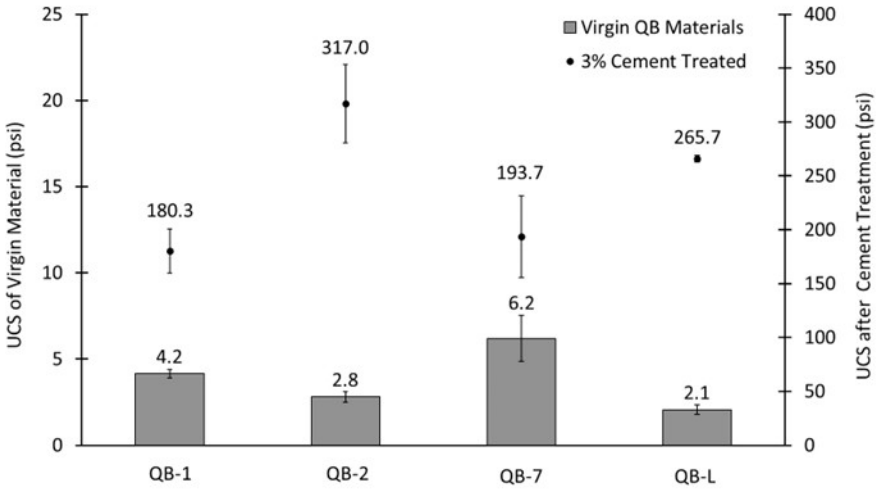

Figure 16. Chart. UCS of untreated and 3% cement-stabilized QB.

Freeze-Thaw Durability Performance

Figure 17 demonstrates the degradation of UCS values for all tested QB types over 10 freeze-thaw cycles. Considering the chemical and mineralogical composition differences among the materials, no clear correlation was found between UCS performance and MgO content or the presence of dolomite. For example, QB-1, which had the highest MgO content, exhibited a strength degradation trend like QB-7, which had higher CaO and lower MgO contents, representing a mixture of limestone and dolomite. Similarly, QB-2, which was also characterized by a high MgO content or a dominant dolomitic phase, showed an equal or even greater reduction in UCS after freeze-thaw cycling compared to QBs with lower MgO content.

These findings are consistent with previous studies (Qamhia et al., 2020; Zhang et al., 2022), which indicated that the enhanced durability typically associated with dolomitic aggregates under freeze-thaw conditions is more evident in long-term field specimens than short-term laboratory samples. For instance, extracted specimens that had been in the field for more than two years showed superior performance of dolomite compared to limestone, whereas 7-day cured laboratory specimens did not exhibit the same trend. Supporting this observation, a study by Xu et al. (2021) found that the UCS of

cement paste incorporating dolomite powder surpassed that of mortar with limestone powder after 90 days of curing (Xu et al., 2021). Therefore, the 7-day curing period used in this study may have been insufficient to fully capture the influence of chemical and mineralogical differences among the carbonate QB materials.

The resonant frequency, which is directly related to a material's stiffness, gradually decreased throughout the freeze-thaw conditioning cycles, as illustrated in Figure 18. Like the UCS trend, no significant effect of MgO content or dolomitic minerals was observed in the degradation of stiffness characteristics. For example, all materials exhibited similar degradation patterns regardless of their chemical and mineralogical composition. This may again suggest that the 7-day curing period was insufficient for the chemical and mineralogical differences to have a significant impact on performance.

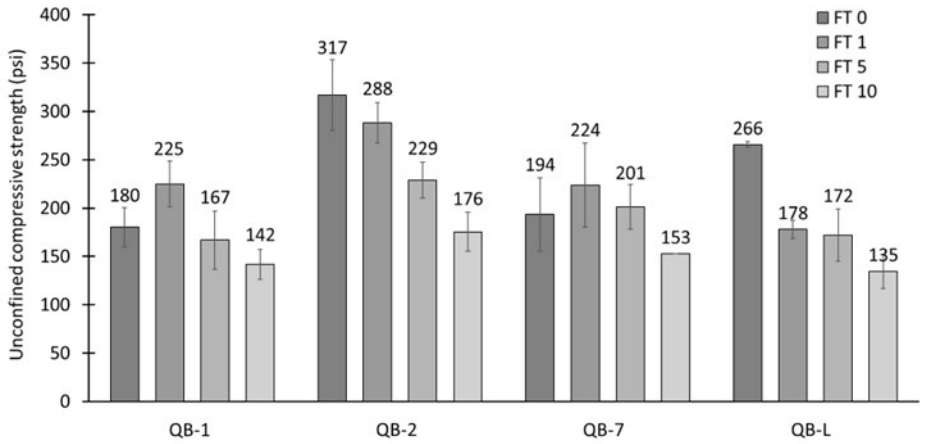

Figure 17. Chart. UCS trends over 10 freeze-thaw cycles for different QB types.

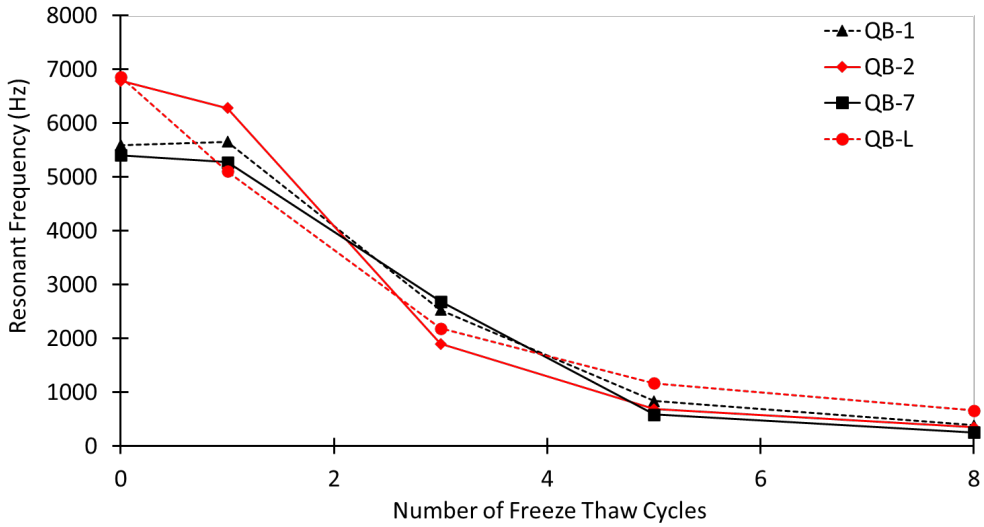

Figure 18. Graph. Resonant frequency trends over 10 freeze-thaw cycles for different QB types.

OPTIMUM PACKING AND MICROSTRUCTURE ANALYSIS

Optimum Packing—Talbot Equation

Physical properties, particularly particle size distribution, had a greater influence on strength development and freeze-thaw damage during the 7-day short-term curing period, compared to chemical and mineralogical effects. As shown in Figure 4, QB-2 and QB-L, which are characterized by relatively coarser particle size distributions, exhibited greater strength reductions compared to QB-1 and QB-7, which had finer particle distributions. Specifically, the total strength reduction observed across all freeze-thaw cycles was 141 psi (972 kPa) for QB-2 and 131 psi (903 kPa) for QB-L, whereas QB-1 and QB-7 experienced smaller reductions of 83 psi (572 kPa) and 71 psi (490 kPa), respectively. This trend may be attributed to the larger surface area of finer particles, which allows for more effective coating by cementitious materials. This enhanced coating likely improves inter-particle bonding, resulting in greater durability of the stabilized QB samples. For this reason, QB-7 exhibited lower strength loss compared to QB-1, despite their similar overall gradations, likely due to QB-7's higher fines content.

QB-2 consistently achieved higher compressive strength than all other QB types throughout the entire freeze-thaw testing period. This superior performance may be linked to optimal particle packing, which is directly influenced by the gradation curve. A previous study examined the effect of gradation and packing on the UCS of chemically stabilized QB materials (Qamhia et al., 2016), using the Fuller curve, commonly referred to as the Talbot equation, as shown in Figure 19.

$$p_i = \left(\frac{D_i}{D_{max}}\right)^n$$

Figure 19. Equation. Calculation of the optimum packing curve.

where p_i is the percentage passing the i^{th} sieve, D_i is the sieve size (in mm or in.), D_{max} is the maximum sieve size, and n is the power exponent (shape factor) of the gradation curve. The study found that an exponent of 0.45 yielded the highest UCS values, suggesting this gradation achieves maximum particle packing and minimal voids (Qamhia et al., 2016). Using this 0.45 exponent, an optimum particle size distribution curve was plotted in Figure 20 along with the particle size distribution curves of the QB materials. The particle gradation of QB-2 closely aligns with the optimum packing curve, resulting in fewer voids in the cement-stabilized aggregate skeleton. These voids, particularly when interconnected, provide pathways for water infiltration. During freeze-thaw cycles, the water trapped within these voids expands upon freezing, exerting internal pressure on the surrounding matrix. Repeated cycles of freezing and thawing can lead to microcracking, loss of fine particles, and gradual breakdown of the cementitious bond, ultimately reducing the material's strength and durability. Therefore, QB-2, which has a particle size distribution aligning with the optimum packing curve, may have achieved the highest UCS both after seven days of curing and throughout all freeze-thaw cycles due to reduced voids and improved particle packing.

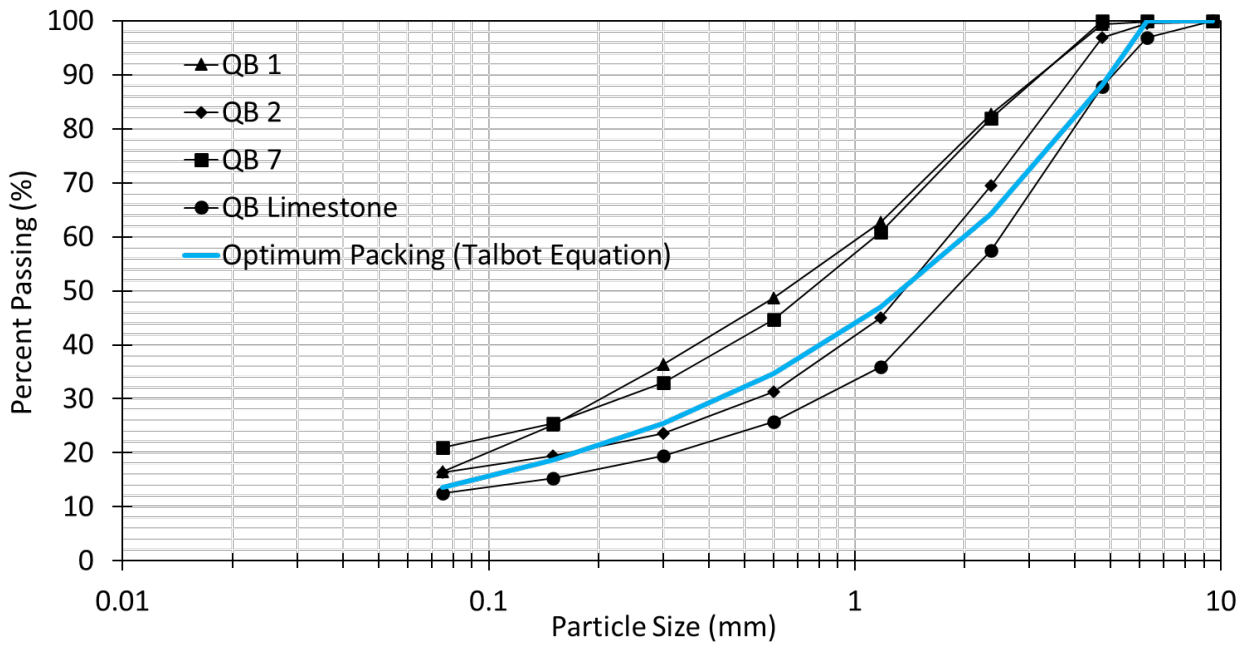

Figure 20. Graph. Particle size distributions of selected QB materials versus optimum packing curve.

Microstructure Analysis—Optimum Packing and Freeze-Thaw Effect

Further verification of the severity of microstructural degradation was carried out through optical microscopy analysis before and after the full freeze-thaw cycle conditioning, as illustrated in Figure 21. The initial micrographs of QB specimens, captured prior to the freeze-thaw conditioning, revealed relatively compact and dense structures with small voids, whereas those taken after conditioning show a noticeable reduction in fine particles surrounding coarse aggregate and an increase in the size of voids between particles. In addition, as the particle size distribution curves deviated further from the optimum packing curve (shown in Figure 20), more voids were visible in the micrographs of the stabilized QB specimens before exposure to freeze-thaw cycles, as highlighted by the red circles in Figure 21. This observation further supports the superior UCS performance of QB-2 compared to the other QBs, as its particle size distribution closely aligns with the optimum packing curve, resulting in fewer initial voids. Although the micrograph in Figure 21 may not represent the entire cement-stabilized aggregate structure, it provides insight into how greater deviation from the optimum packing curve corresponds to increased voids and how the initial presence of abundant voids influences the final void structure after freeze-thaw exposure.

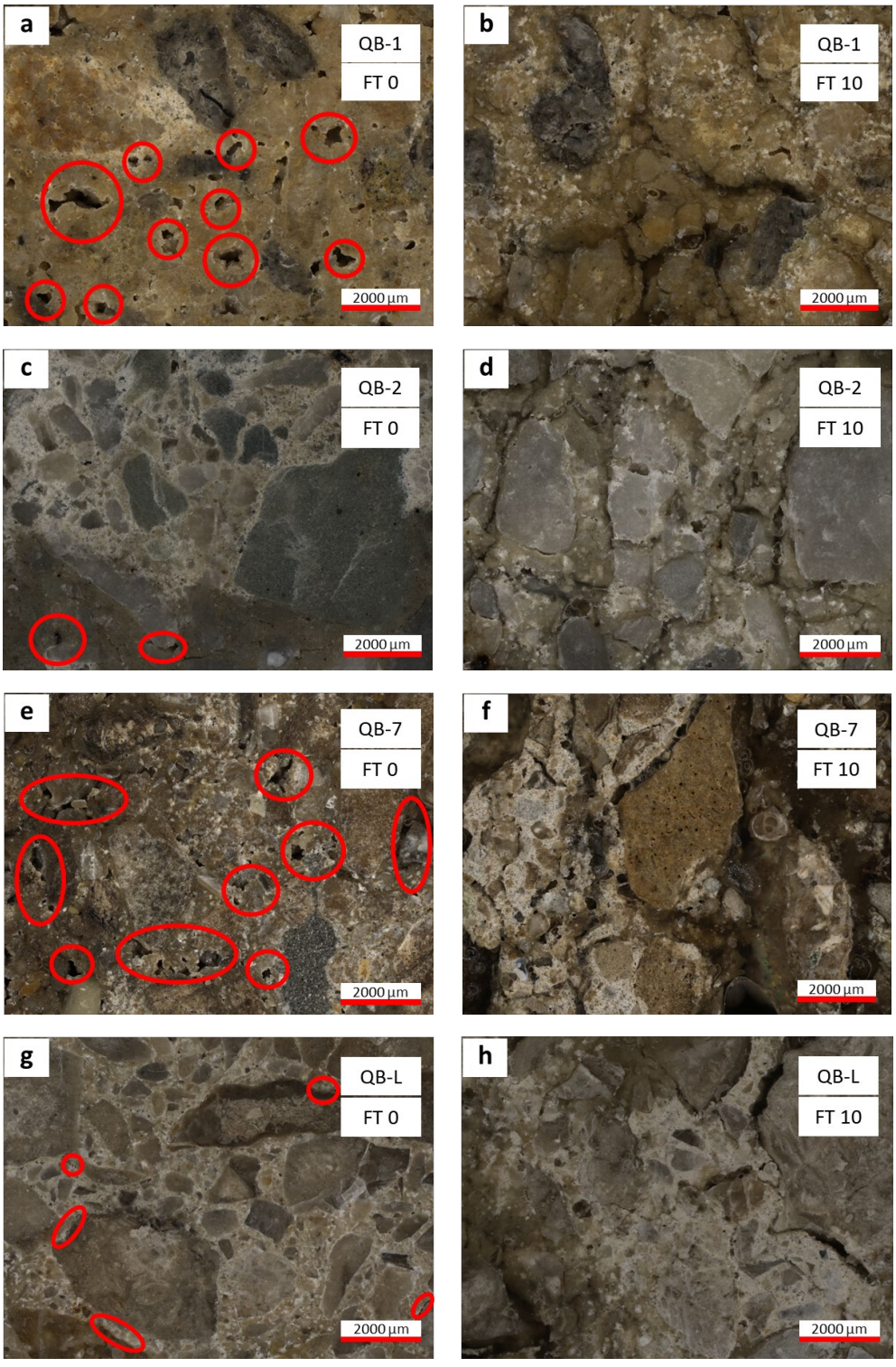

Figure 21**. Photo. Optical micrographs of QB materials: (a) QB-1 before freeze-thaw, (b) QB-1 after freeze-thaw, (c) QB-2 before freeze-thaw, (d) QB-2 after freeze-thaw, (e) QB-7 before freeze-thaw, (f) QB-7 after freeze-thaw, (g) QB-L before freeze-thaw, and (h) QB-L after freeze-thaw.**

CHAPTER 4: EVALUATION OF LONG-TERM PERFORMANCE IN CEMENT-STABILIZED CARBONATE-BASED QUARRY BY-PRODUCT SPECIMENS: EFFECT OF CARBONATE TYPE

SAMPLE PREPARATION AND CONDITIONING

Like the sample preparation method described in Chapter 3 for short-term curing, additional cylindrical specimens with a 1:2 aspect ratio, measuring 2.8 in. (71 mm) in diameter and 5.6 in. (142 mm) in height, were prepared using 3% cement and four different QB types (i.e., QB-1, QB-2, QB-7, and QB-L). These specimens were designed for the long-term curing study to allow sufficient time for carbonate minerals (i.e., dolomite and calcite) to fully precipitate or dissolve within the cementitious matrix, thereby enabling evaluation of their long-term effects. To accelerate the chemical reactions and simulate extended curing, the specimens were cured in an oven at an elevated temperature of 104°F (40°C), as shown in Figure 22. Immediately after compaction and removal from the molds, the cylindrical specimens were wrapped carefully in plastic to prevent moisture loss. The selected curing temperature was chosen specifically to minimize microstructural damage by preventing the decomposition of hydrated AFt phases in the cement system (Kothari & Takahashi, 2022). The specimens were maintained under these conditions for 120 days to simulate long-term cementitious reactions.

In addition to the cylindrical specimens, small cube specimens, measuring 0.4 in. (1 cm) per side, were also prepared for all QB types, as shown in Figure 23-a. These specimens consisted of QB fines (QBF) mixed with 50 wt.% cement and 30.5 wt.% water relative to the total solids. Only QBF was used in the cube specimens, based on the assumption that larger aggregate particles are relatively inert during cement hydration and act primarily as fillers. Furthermore, considering that QB materials typically contain fines in the range of 10% to 20%, the addition of 3% cement may result in a cement content up to 23 wt.% relative to the total solids (fines and cement). However, a higher cement content of 50 wt.%, nearly double that amount, was used in the cube specimens to improve the detectability of phase evolution during cement hydration in material characterization tests. The cube specimens were also subjected to long-term curing for 180 days at the same elevated temperature of 104°F (40°C), as shown in Figure 23-b, by placing them in an open container within a water bath and sealing them with plastic wrap to maintain 100% relative humidity.

Following 120 days of curing, the 3% cement-stabilized cylindrical QB specimens were subjected to freeze-thaw conditioning, consistent with the conditioning procedures detailed in Chapter 3. This involved 24-hour freezing at −10°F (−23°C), followed by 24-hour thawing at 73.5°F (23°C) and 100% relative humidity, with each full cycle spanning 48 hours. Wire brushing was omitted, and unconfined compressive strength (UCS) tests were conducted at selected stages to evaluate strength degradation. Specimens were spaced at least 1 in. (25 mm) apart in the freezing cabinet, with absorptive material placed beneath them in accordance with ASTM D560 recommendations.

Figure 22. Photo. Cement-stabilized cylindrical QB specimens cured in the oven.

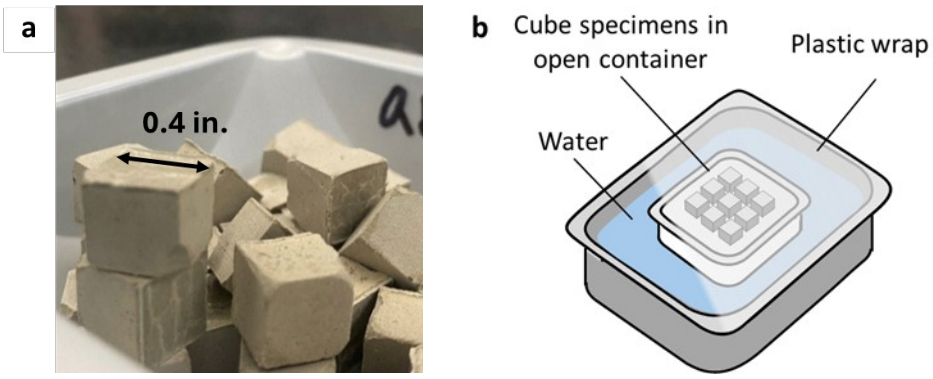

Figure 23. Photo. (a) Cube specimens consisting of QBF materials and cement, and (b) schematics of the curing setup.

MECHANICAL AND DURABILITY PERFORMANCE TRENDS

Compressive Strength Development

After completing 120 days of curing, the 3% cement-stabilized cylindrical QB specimens for all QB types were subjected to UCS testing. The UCS test results were compared to the untreated (virgin) and short-term (7-day) cured specimens discussed in Chapter 3 to evaluate the strength development achieved through long-term curing, as illustrated in Figure 24. The findings revealed significant strength gains across all QB types. Strength improvements from short- to long-term curing ranged from 1.7 to 3.1 times, depending on the specific QB material, with dolomitic QBs exhibiting greater strength development. For example, QB-1 and QB-2, both highly dolomitic materials with high MgO contents, showed increases from 180 psi (12,41 kPa) to 428 psi (2,951 kPa) and from 317 psi (2,186 kPa) to 796 psi (5,488 kPa), reflecting increases of 2.4 and 2.5 times, respectively. QB-7, a mixture of dolomite and calcite, demonstrated the highest relative strength gain, rising from 194 psi (1,337 kPa) to 598 psi (4,123 kPa), an increase of 3.1 times, likely due to its high fines content, which enhances reactivity. Lastly, QB-L, composed primarily of calcite, exhibited the smallest increase, from 266 psi (1,834 kPa) to 451 psi (3,110 kPa), corresponding to a 1.7 times improvement.

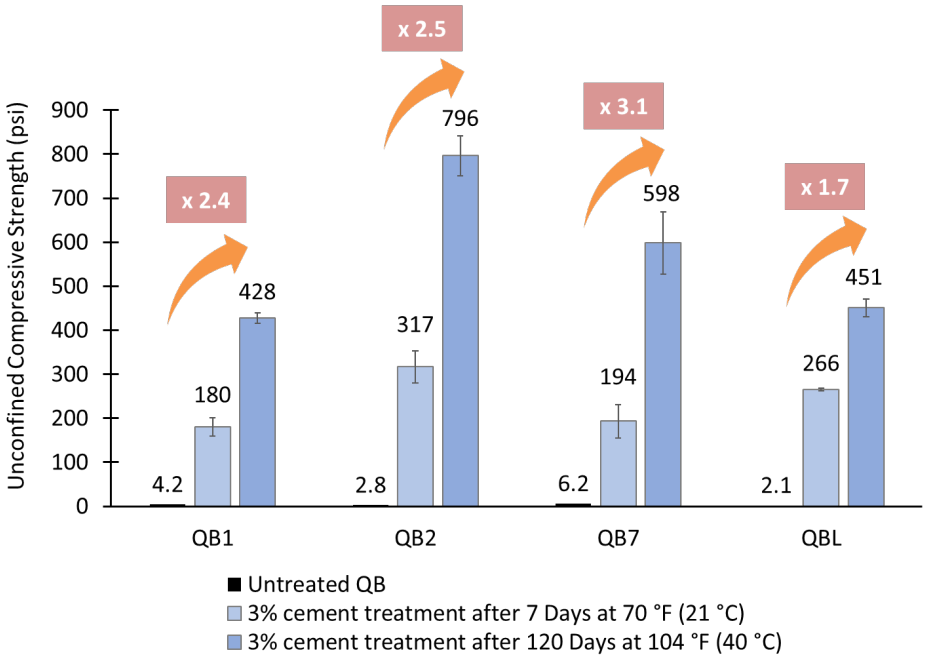

Figure 24. Chart. USC comparison among untreated, short-term cured (7 days), and long-term cured (120 days) specimens.

As demonstrated in Chapter 3, the short-term strength performance of QB materials was primarily influenced by their physical characteristics, especially particle size distribution, as supported by microstructural analysis. However, the strength increase observed between short- and long-term curing can be attributed to the formation of additional phases through chemical reaction between the QBs and cement. In this process, coarse aggregate particles do not actively participate; instead, fine particles play a more significant role due to their higher reactivity and larger surface area. Studies on cement hydration with carbonates have primarily employed fine particles (smaller than 75–100 µm) to investigate their chemical effects, consistently reporting substantial impacts (Xu et al., 2021; Zajac, Bremseth, et al., 2014; Zhang et al., 2022). Therefore, the observed strength increases from short- to long-term curing were attributed to hydration reactions involving QBF materials.

Considering the varying fines content among the aggregate QB materials, the rate of strength development from short- to long-term curing was normalized by the QBF content for each QB type to quantify the proportion of strength gain attributable to the reactive fine fraction. Table 9 presents the QBF contents of the QB materials along with the corresponding strength gains attributed to the fine fraction, evaluated using two approaches: relative strength increase and percent strength increase. The relative strength increase was calculated by normalizing the final strength values with respect to their initial (7-day) strength, providing a ratio that reflects the magnitude of strength development over time. The percent strength increase was determined by dividing the difference between the final and initial strengths by the initial strength, expressing the gain as a percentage of the starting value. Dolomitic QB materials (i.e., QB-1, QB-2, and QB-7) exhibited a greater contribution of fines to long-term strength gain compared to QB-L, as evidenced by the two approaches considered. Both approaches for evaluating strength gain per fine fraction were then

examined in relation to the particle size distribution of QBF in Chapter 2 (Figure 5). The particle size distribution indicates QBF-L has the finest gradation, suggesting the highest potential for strength development due to its larger surface area and reactivity. QB-L, however, demonstrated the lowest strength contribution from fines among the QBs. Furthermore, QB-1 exhibited comparable relative strength gain per fine fraction to QB-7, despite QBF-1 having the coarsest particle size distribution, which can lead to slower chemical reactivity. These findings suggest dolomitic fines may enhance long-term strength development in cement stabilization through chemical reactions during hydration.

Table 9. Strength Increase in Cylindrical QB Specimens Attributed to the Fines Fractions

	Quarry By-Product Fines Content (%)	Relative Strength Gain per Fine Fraction (%)	Percent Strength Gain per Fine Fraction (%)
QB-1	16.5	14.4	8.4
QB-2	16.3	15.4	9.3
QB-7	20.9	14.7	9.9
QB-L	12.5	13.5	5.6

Note: Relative strength gain per fine fraction = $[(UCS_{120\ days} / UCS_{7\ days})/QBF\ content] * 100$
Percent strength gain per fine fraction = $[(UCS_{120\ days} – UCS_{7\ days})/UCS_{7\ days}]/QBF\ content * 100$

Shear Wave Velocity and Small-Strain Shear Modulus Development

The BE sensors installed at the top and bottom of the specimens enabled monitoring of shear wave velocity (V_s) changes over the curing period under both elevated and room temperature conditions. According to continuum mechanics, faster wave velocities correspond to increased stiffness or denser microstructures, as more closely packed particles facilitate faster transmission of vibrational energy. Thus, analysis using BE sensors provided a means to monitor the extent of curing without implementing destructive tests such as UCS. Figure 25 shows V_s changes in dolomitic and limestone QB specimens under two temperature conditions for 120 days of curing. QB-2 specimens exhibited lower V_s values than that of QB-L in the early stages of curing at both elevated and room temperatures because limestone tends to dissolve more rapidly in cement systems. Over time, however, this pattern reversed, as QB-2 specimens began to show higher V_s values, with the transition occurring much faster at the elevated temperature. This reversal may be attributed to microstructural improvement as additional hydrated phases formed and filled more voids, likely influenced by the inherent chemical and mineralogical differences between dolomitic and limestone QBs.

The measured V_s values can be related to stiffness characteristics by calculating G_{max} using the equation presented in Figure 12. Figure 26 shows G_{max} development over the curing period under two temperature conditions. G_{max} trends demonstrated a more pronounced difference between QB-2 and QB-L specimens than V_s results. This difference was further amplified at the elevated temperature due to enhanced chemical reactivity that accelerates hydration. The greater stiffness divergence observed as curing progresses may be attributed to intrinsic chemical and mineralogical differences between the two QB materials, which may play distinct roles in cementitious reactions.

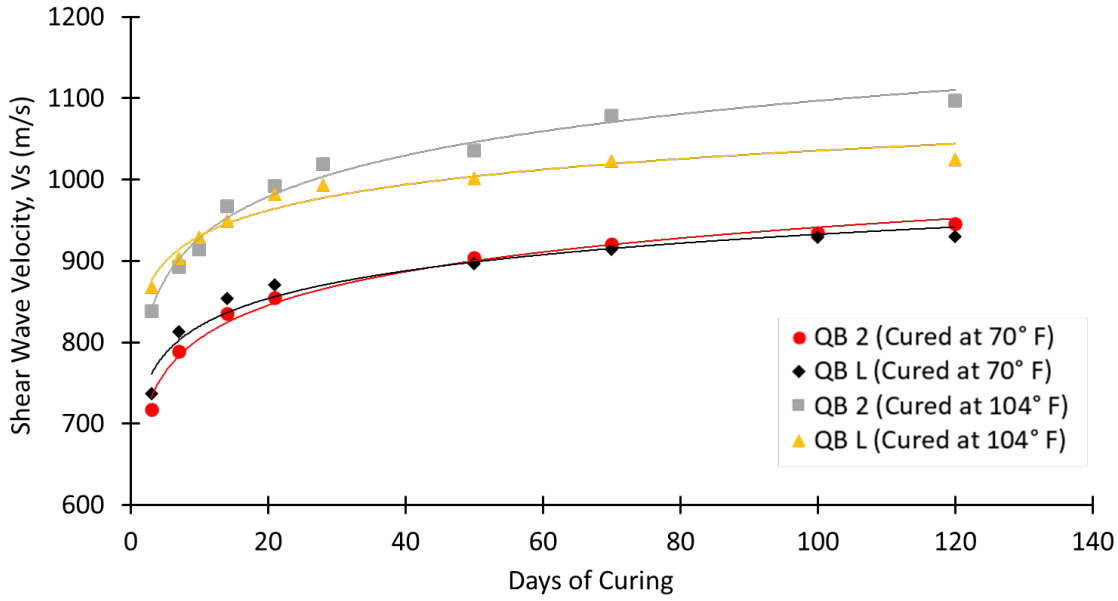

Figure 25. Graph. Shear wave velocity (V_s) trends observed under different curing conditions and periods.

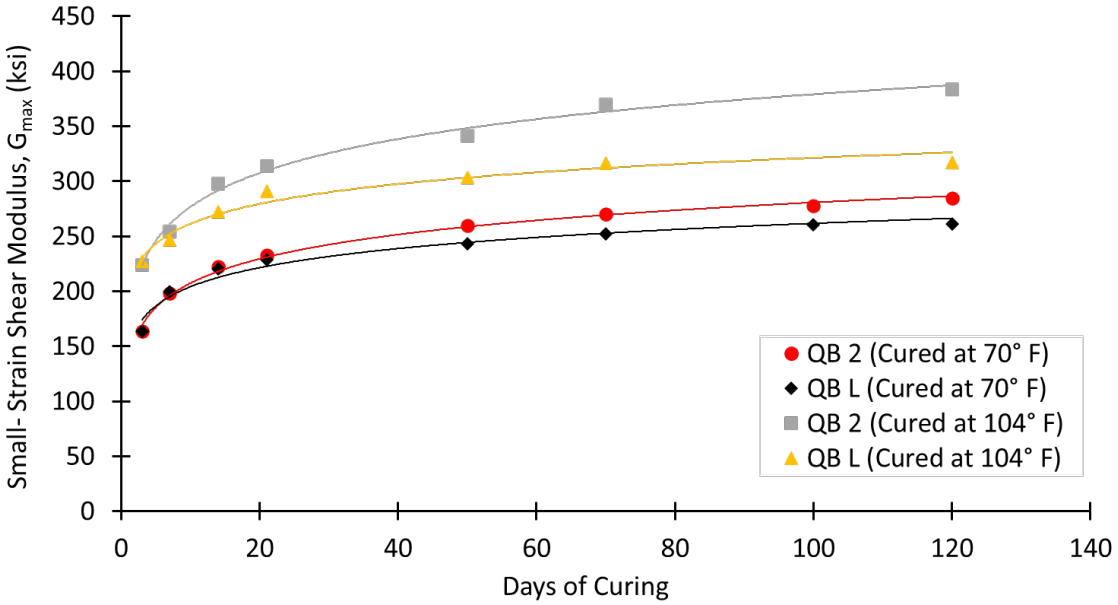

Figure 26. Graph. Small-strain shear modulus (G_{max}) development under different conditions during the curing period.

Freeze-Thaw Durability Performance

The freeze-thaw durability performance trends of the 3% cement-stabilized cylindrical QB specimens were evaluated after 120 days of curing. UCS tests were performed at different freeze-thaw cycle

intervals (i.e., 0, 1, 5, and 10 cycles) to capture strength degradation in each QB type under repeated freeze-thaw conditioning. The overall freeze-thaw durability characteristics of specimens with different QB types are presented in Figure 27, which illustrates progressive strength reduction with increasing number of freeze-thaw cycles. The durability results indicated a general trend of substantial strength loss during the initial freeze-thaw cycles, followed by a more gradual decline in the later stages. After 10 cycles, the strength reductions for QB-1, QB-2, QB-7, and QB-L were 185 psi (1,276 kPa), 345 psi (2,379 kPa), 276 psi (1,903 kPa), and 218 psi (1,503 kPa), respectively. These correspond to relative decreases of 43%, 43%, 46%, and 49% compared to the initial strength, as illustrated in Figure 27. The percent strength reduction relative to the initial strength was inversely proportional to the MgO content or the proportion of dolomite mineral phase in the QB aggregate: QBs with higher MgO content exhibited less strength reduction from freeze-thaw damage than those with lower MgO content. This trend indicates that cement-stabilized dolomitic QBs are less susceptible to freeze-thaw damage compared to limestone QBs, a difference that can be linked to intrinsic mineral effects. The chemical and mineralogical influences of dolomite and limestone on strength and durability are examined later in this chapter using advanced material characterization techniques. Nonetheless, the superior freeze-thaw durability of dolomitic QBs observed here may be attributed to their intrinsic mineral properties, which promote the formation of additional hydrated phases that fill voids and refine the microstructure.

In addition to UCS testing at various freeze-thaw cycle intervals, resonant frequency testing (RFT) was conducted on the 3% cement-stabilized cylindrical QB specimens to assess changes in stiffness characteristics resulting from freeze-thaw effects. RFT, performed using an impact-echo device, is a commonly applied nondestructive method for evaluating the dynamic modulus (E_d) of civil structures or concrete. The technique is also applicable to soil-cement systems for monitoring modulus changes. Figure 28 illustrates the changes in E_d for different QB types over the entire series of freeze-thaw cycles. A similar trend to that observed in the UCS results was identified from RFT, with substantial modulus reduction occurring during the initial stage of freeze-thaw conditioning, followed by a more gradual decrease for all QB types. QB-L exhibited a particularly sharp decline after the first few cycles compared to the dolomitic QBs. The percentage reductions in E_d from the initial to the final cycle after 10 freeze-thaw cycles were 14.9%, 14.8%, 23.6%, and 26.5% for QB-1, QB-2, QB-7, and QB-L, respectively. The modulus reduction trend closely aligned with the UCS reduction shown in Figure 27, indicating that cement-stabilized specimens prepared with QBs containing higher MgO content or dolomitic minerals generally experienced less stiffness loss after repeated freeze-thaw cycling. The superior performance of dolomitic QBs, which exhibited lower susceptibility to freeze-thaw damage in terms of maintaining higher modulus, can be attributed to their intrinsic mineralogical and chemical characteristics during the hydration process. These properties likely promote the formation of additional hydration products over the long term, which fill some voids and refine the microstructure. The detailed chemical and microstructural analyses supporting this interpretation are presented later in this chapter.

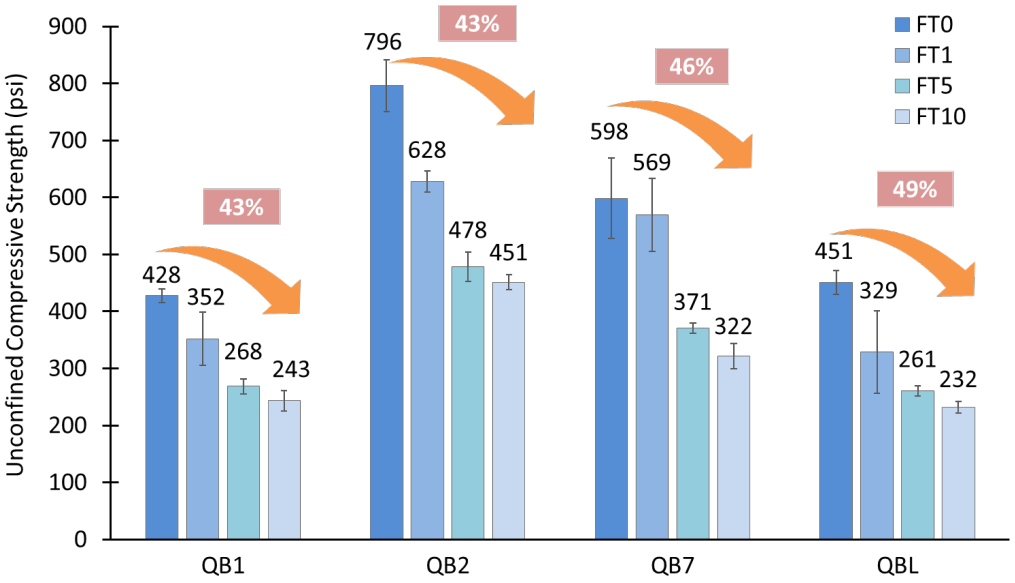

Figure 27. Chart. Freeze-thaw durability performance trends of different quarry by-product types.

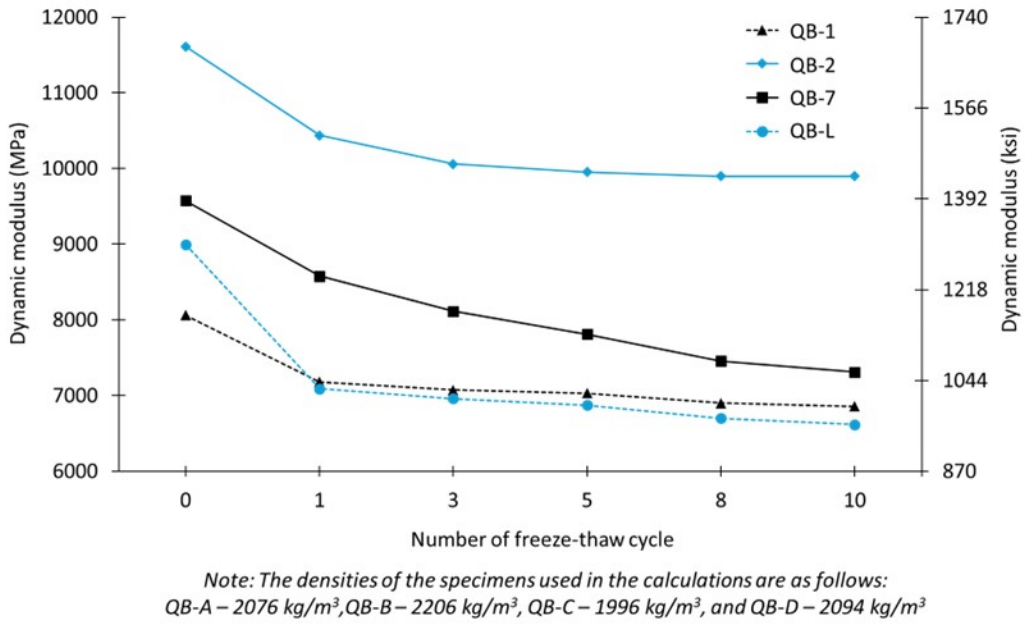

Figure 28. Graph. Dynamic modulus (E_d) trends of QBs versus the number of freeze-thaw cycles.

CHEMICAL AND MICROSTRUCTURAL ANALYSES

When the different types of carbonate-based QB materials were stabilized with cement and tested for UCS after long-term curing, the dolomitic QB materials exhibited greater long-term strength gain per fine fraction compared to the limestone-based QB-L material. Such long-term strength can primarily be attributed to chemical reactions within the system at later ages. These reactions are usually governed by the type of carbonates and their particle size distribution. The influence of limestone on cement hydration and strength development has been explored for application in the

concrete industry, and the reaction mechanism has been well reported in the literature (Matschei et al., 2007; Zajac et al., 2014). Dolomite, however, is hypothesized to undergo two different reactions within the cementitious system and requires further investigation. The first possible reaction, given in Figure 29, involves dolomite, aluminates (from ettringite [$CaAl_2(SO_4)_3(OH)_{12}\cdot 26H_2O$] or monocarbonate [$Ca_4Al_2(CO_3)(OH)_{12}\cdot 5H_2O$]), and calcium hydroxide reacting to form hydrotalcite [$Mg_6Al_2CO_3(OH)_{18}\cdot 3(H_2O)$] and calcium carbonate (Xu et al., 2021; Zajac, Bremseth, et al., 2014). The reacted phase, hydrotalcite, is formed as a solid solution, where different ions, such as CO_3^{2-}, SO_4^{2-}, OH^-, and Cl^-, are present in its crystal structure (Bernard et al., 2022). In the second potential reaction, the dolomite reacts with calcium hydroxide to form magnesium hydroxide and calcium carbonate, as shown in Figure 30 (García et al., 2003; Zhang et al., 2020). This reaction is also known as the dedolomitization reaction and has been observed in geological samples.

$$6CaMg(CO_3)_2 + 2Al(OH)_3 + 6Ca(OH)_2 + 9H_2O \rightarrow Mg_6Al_2CO_3(OH)_{18}\cdot 3H_2O + 12CaCO_3$$

Figure 29. Equation. Formation of hydrotalcite.

$$CaMgCO_3 + Ca(OH)_2 \rightarrow 2CaCO_3 + Mg(OH)_2$$

Figure 30. Equation. Dedolomitization reaction.

Advanced characterization tools, including XRD, TGA/DTG, and Raman imaging, were employed to understand the reaction mechanisms underlying the higher strength gain achieved upon cement stabilization in dolomite-based QB compared to limestone-based QB.

X-ray Diffraction

XRD analysis was performed to probe the reaction between different QB fines and cement. XRD is a widely used tool for identifying and quantifying phases in cementitious systems (Aranda et al., 2012). For QB samples, analyzing the XRD patterns over time could reveal changes in reaction products. The XRD patterns (range: 8−13° 2θ) of the QBF cube specimens at 7, 28, 120, and 180 days of curing are presented in Figure 31. In the case of QB containing dolomite (QBF-1, QBF-2, and QBF-7), a clear shift in intensity from monocarbonate (~11.7° 2θ) to hydrotalcite (~11.4° 2θ) was observed as hydration progressed, especially at later stages. A small intensity for hydrotalcite was also observed in the XRD pattern of the specimen containing QBF-L (limestone). The presence of this small intensity can be potentially attributed to the presence of Mg in cement. These results are consistent with previous studies related to cement blended with carbonates (Xu et al., 2021; Zajac, Bremseth, et al., 2014). The second hypothesis involved the formation of brucite (equation in Figure 30); however, although previous studies (García et al., 2003; Zhang et al., 2020) reported the presence of brucite [$Mg(OH)_2$], the XRD patterns in this study showed no such formation.

Thermogravimetric/Differential Thermogravimetric Analysis

TGA/DTG analysis was used to identify the reaction product of dolomite in the cementitious system. Figure 32 shows the DTG curves of cube specimens mixed with QBF and cement, cured at 104°F (40°C) for various hydration periods at 7, 120, and 180 days. The weight loss during the peak range of

518−770°F (270−410°C) was attributed to hydrotalcite, as it releases H_2O and CO_2 at that temperature. Another observation revealed that the 120-day samples were slightly exposed to natural CO_2, which likely caused some of the calcium hydroxide in these samples to convert to calcium carbonate. Comparing the DTG curves at 7 and 180 days for carbonate phases (932−1472°F [500−800°C]), the intensity of the limestone/dolomite peak increased, and the peak shifted to higher temperatures as curing time extends to 180 days. This temperature shift suggested calcium carbonate formation as part of the reaction producing hydrotalcite from dolomite (equation in Figure 29). The increase and shift were less evident in QBF-L, as the absence of dolomite precludes the formation of hydrotalcite and subsequent calcium carbonate formation. Based on the DTG peaks for dolomite/limestone and the XRD patterns, QBs with dolomite produce more calcium carbonate through reactions involving hydrotalcite formation, compared to limestone-based specimens. A comparative TGA analysis of the hydrotalcite peak and its relationship to strength is presented later in this chapter (Impact of Hydrotalcite Formation).

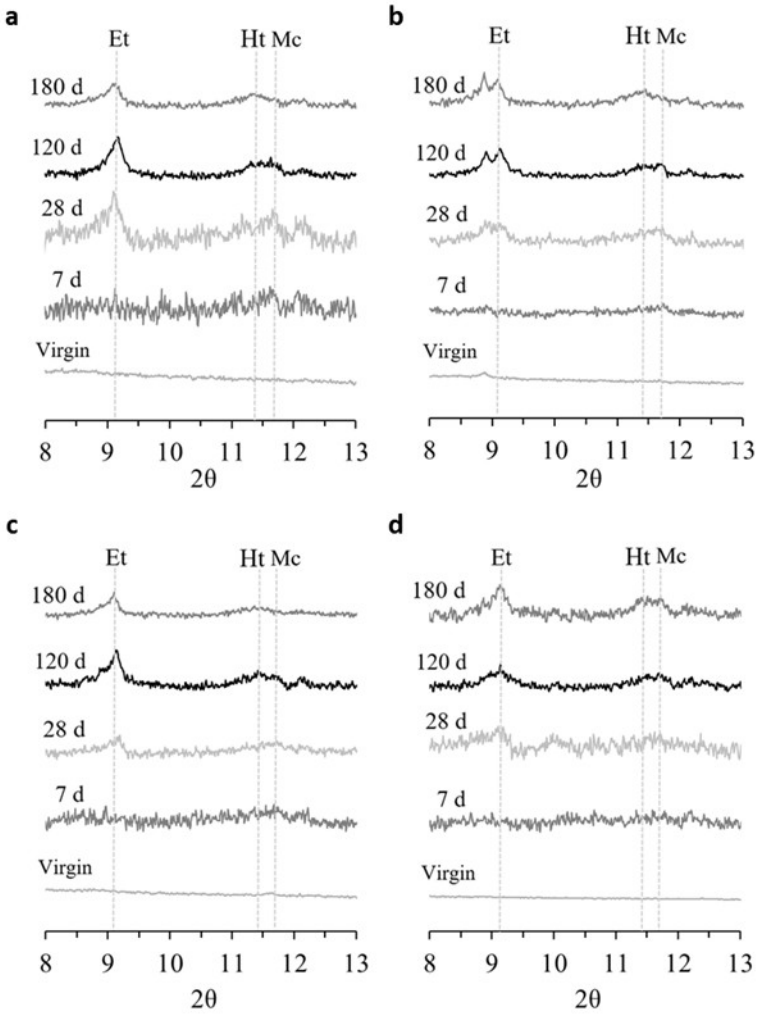

Figure 31. Graph. X-ray diffraction patterns of cube specimens consisting of (a) QBF-1, (b) QBF-2, (c) QBF-7, and (d) QBF-L mixed with cement: primary reflections of ettringite [$CaAl_2(SO_4)_3(OH)_{12}\cdot 26H_2O$] (Et), hydrotalcite [$Mg_6Al_2CO_3(OH)_{18}\cdot 3(H_2O)$] (Ht), and monocarbonate [$Ca_4Al_2(CO_3)(OH)_{12}\cdot 5H_2O$] (Mc).

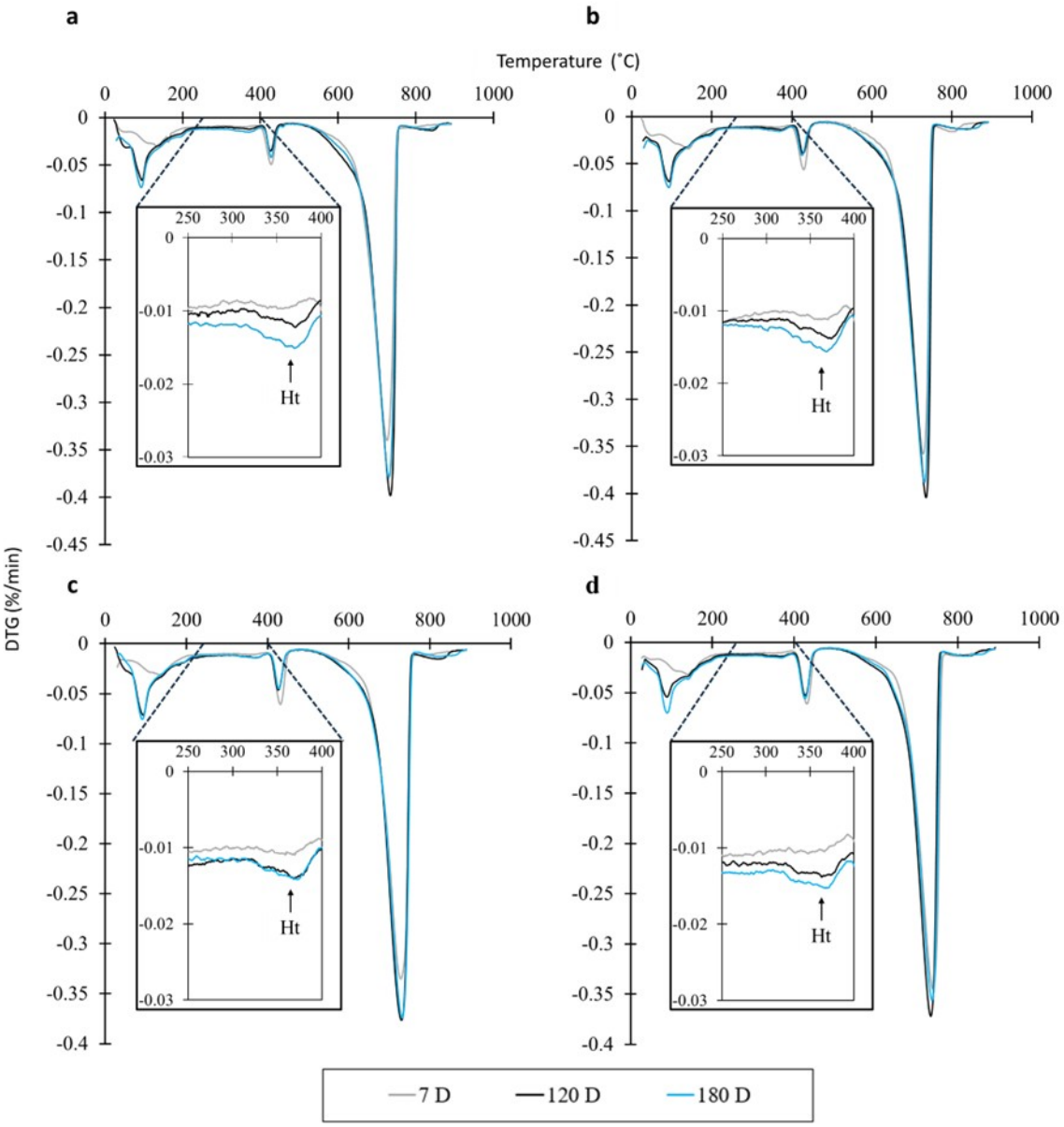

Figure 32. Graph. Differential thermogravimetric analyses of cube specimens containing (a) QBF-1, (b) QBF-2, (c) QBF-7, and (d) QBF-L mixed with cement.

Raman Imaging

Raman imaging was performed on dolomite and limestone-based QBF samples stabilized with cement. It serves as a versatile tool for mapping rocks and cementitious systems (Higl et al., 2016; Kothari & Garg, 2024b; Loh et al., 2021; Polavaram & Garg, 2021), and it can quantify phase composition and phase-specific particle size distributions for various types of anhydrous cement (Kothari & Garg, 2024a, 2024b; Polavaram & Garg, 2023). Additionally, Raman imaging can study cement hydration mechanisms (Higl et al., 2016; Loh et al., 2021). Here, Raman imaging was used to study the microstructure of cement-stabilized QBF samples. Specifically, it was performed on cube specimens containing QBF-2 (dolomite) and QBF-L (limestone) to investigate the differences in phases

present in their microstructures. The Raman phase maps of the cement-stabilized cube specimen containing QBF-2 are presented in Figure 33. Basis analysis showed the presence of phases including calcite (v_1 [CO_3^{2-}] band), belite (v_1 [SiO_4] band), ferrite (v_1[$(Fe,Al)O_4^{5-}$] band), quartz (v_1 [Si – O – Si] band), brucite (SS (OH) band), and hydrotalcite (v_1 [CO_3^{2-}] band and v_1 [SO_4^{2-}] band), as presented in Figure 33-a. The hydrotalcite observed in the microstructure was present as a solid solution, with v_1 [CO_3^{2-}] and v_1 [SO_4^{2-}] bands present in its Raman spectrum. The optical image, individual phase maps, and a combined Raman image of the scan area are reported in Figure 33-b. The combined Raman image reveals where hydrotalcite forms near the dolomite grain. Black pixels indicate areas with no identifiable phase. Calcite appears as a distinct particle within the limestone, embedded in the cement and paste matrix, and may also result from carbonation or hydrotalcite formation during sample preparation. The Raman spectrum labeled for brucite in Figure 33-a could represent either brucite or hydrogarnet, since the 3652 cm^{-1} peak linked to OH^- is common to both. Visually, this particle looked like a separate entity rather than a hydrated form, indicating its presence in the raw QBF-2 material. To confirm the mineralogy, scanning electron microscopy with energy-dispersive X-ray spectroscopy (SEM-EDS) analysis was conducted on the particle using a Hitachi S-4800 SEM with an Oxford Ultim Max EDS detector. Experiments were conducted in a high-vacuum environment at 10 kV for SEM and 20 kV for EDS. The SEM and EDS mappings confirmed that the particle was brucite, not hydrogarnet, as no aluminum was detected, as shown in Figure 33-c and Figure 33-d. The brucite particle observed in the Raman scan area was not found in the XRD analysis, likely due to its very low concentration in the overall sample. Note that the center of the particle is not detected as brucite in the Raman imaging due to a pore/scratch in the particle, as seen in the SEM-EDS map.

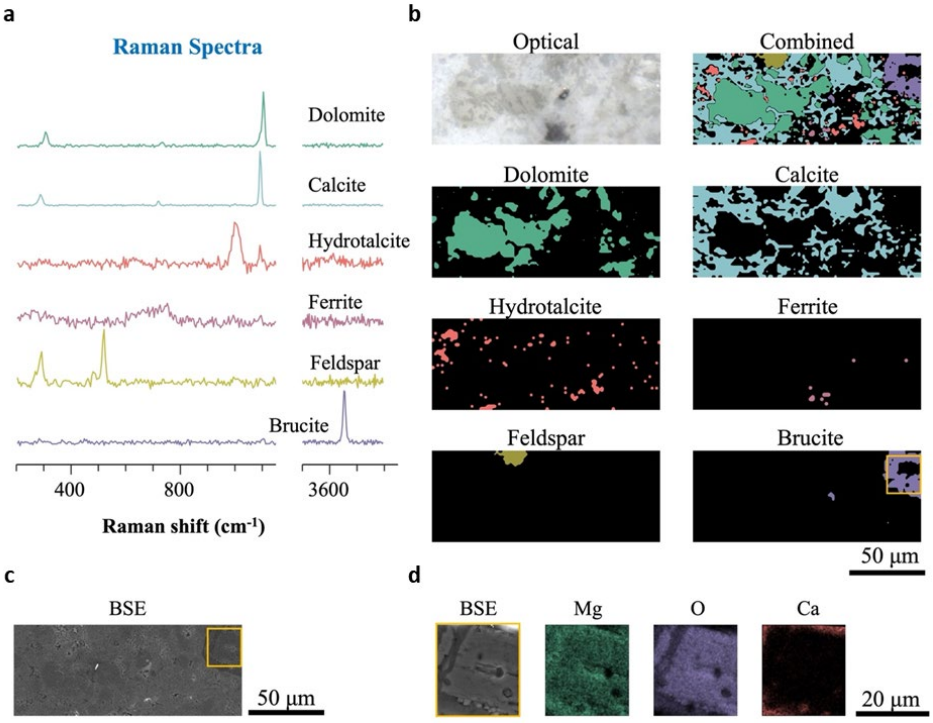

Figure 33. Illustration. (a) Raman spectra of phases from a specimen containing dolomitic QBF (QB-2) cured for 120 days, (b) Raman images of the scan area, (c) back-scattered electron image of the scan area highlighting the particle of interest, and (d) EDS mapping of the particle in the scan area.

Raman imaging was also conducted on the cement-stabilized cube specimen containing QBF-L to analyze microstructural variations. Using basis analysis, calcite (v1 [CO_3^{2-}] band), belite (v1 [SiO_4] band), hydrotalcite (solid solution—v1 [CO_3^{2-}] and v1 [SO_4^{2-}] bands), ferrite (v1[$(Fe,Al)O_4^{5-}$] band), and quartz (v1 [Si – O – Si] band) were identified, as shown in Figure 34-a. The minor presence of hydrotalcite in QBF-L-containing specimens was likely the result of magnesium in the cement, corroborated by XRD and TGA data. Figure 34-b displays optical images, phase maps, and a combined Raman image for the QBF-L specimen's scan area, revealing limited hydrotalcite formation during microstructural development compared to the QBF-2 specimen with dolomite (Figure 33-b). Since the small scan area may not fully represent the entire microstructure, the higher hydrotalcite content in dolomitic QBs compared to limestone QBs was further examined using quantitative TGA in a later section of this chapter (Impact of Hydrotalcite Formation).

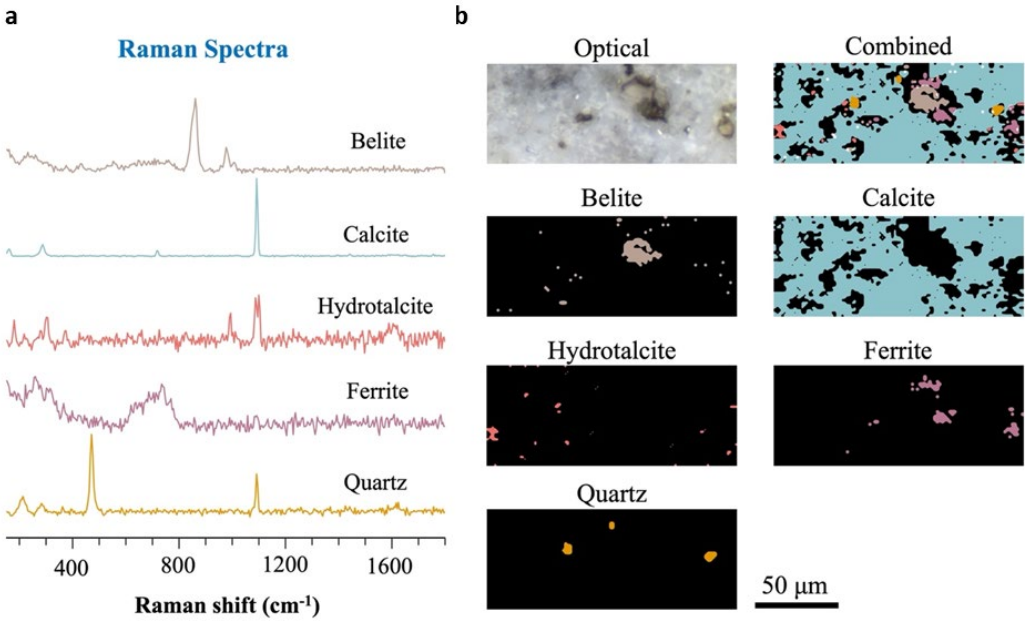

Figure 34. Illustration. Raman spectra of phases from a specimen containing limestone QBF (QB-L) cured for 120 days, and (b) Raman images of the scan area.

THERMODYNAMIC MODELING

Thermodynamic modeling was conducted to examine how hydrated assemblage varies when cement is replaced with limestone and dolomite based on past studies (Machner et al., 2017; Zajac, Bremseth et al., 2014). The study utilized the geochemical modeling program GEMS (Thoenen & Kulik, 2003). It incorporated thermodynamic data from the PSI-GEMS database (Thoenen & Kulik, 2003) and a specific database for cement (Lothenbach et al., 2019). Figure 35-a and Figure 35-b show the phase assemblage of Portland cement mixed with limestone and dolomite, respectively, at a water-to-solid ratio of 0.5. The stabilized phases in the case of limestone and dolomite were similar to those observed in XRD analysis (Figure 31). The modeling predicted the formation of ettringite, carboaluminates, and hydrotalcite at 104°F (40°C) for both the limestone and dolomite systems. This supports the presence of a small amount of hydrotalcite in the QBF-L sample, as detected in the

TGA/DTG results, which is attributed to the magnesium present in the cement. However, a more pronounced formation of hydrotalcite was observed when dolomite was involved. Figure 35-b illustrates the modeled phase assemblage for cement partially replaced with dolomite. The overall phase composition was similar to that of the limestone system, except for the conversion of carboaluminates into hydrotalcite and calcite. This follows the reaction of dolomite with aluminates and portlandite to form hydrotalcite and calcite, as presented in the equation in Figure 29. Since the thermodynamic model does not account for reaction kinetics, it predicted the complete conversion of dolomite into hydrotalcite and calcite. The predicted hydrotalcite content in the dolomite-replacement system was higher than that in the limestone-replacement system, which is consistent with the experimental TGA/DTG results presented in the following section, where hydrotalcite formation was analyzed quantitatively.

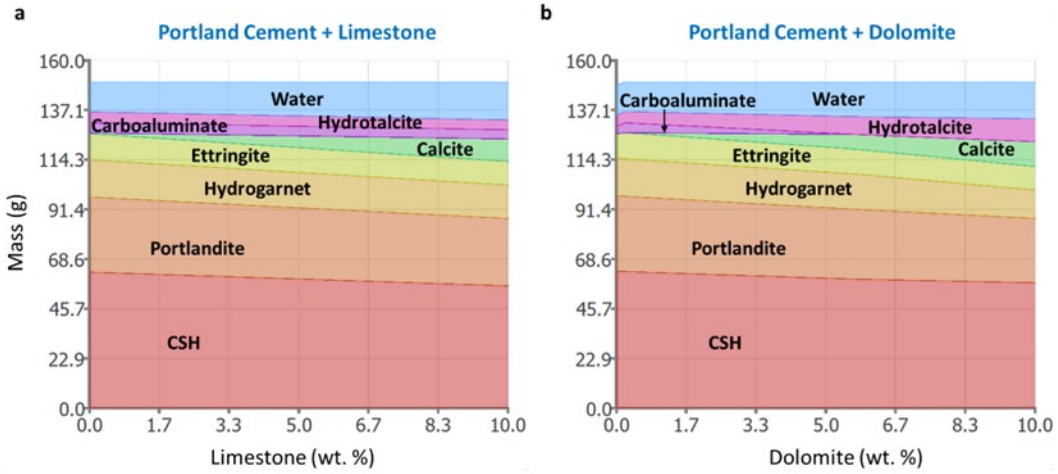

Figure 35. Chart. Thermodynamic modeling results showing phase assemblages of Portland cement replaced with (a) limestone and (b) dolomite at water-to-solid ratio of 0.5.

IMPACT OF HYDROTALCITE FORMATION

DTG curves indicated the formation of hydrotalcite in the dolomite-based QB compared to the limestone-based QB. A quantitative analysis examined how the hydrotalcite peak changed over time across different QBF samples. First, the area under the hydrotalcite peak (518–770°F [270–410°C]) in the DTG curve was measured at 7, 120, and 180 days. The 7-day area was subtracted from the 120- and 180-day areas to track the evolution of hydrotalcite. These results are shown in Figure 36. After 120 days, QBF-1 cubes exhibited less hydrotalcite formation than QBF-2, despite similar chemical compositions (both dolomitic). This difference is likely due to the larger particle size of QBF-1, which slows the chemical reaction (Figure 5). At 180 days, QB-1 showed a loss of 0.137 wt.%, the highest among samples, followed closely by QBF-2 at 0.136 wt.%. QBF-7 and QBF-L demonstrated losses of 0.109 and 0.066 wt.%, respectively, with QBF-L showing the lowest hydrotalcite formation. These findings suggest a higher amount of hydrotalcite formation occurs in samples with higher MgO content after longer curing, as illustrated in Figure 36 alongside the MgO content. Previous studies demonstrated that hydrotalcite formation refines pore structure and may enhance strength (Zajac, Bremseth et al., 2014).

Another comparative analysis was performed on the relationship between hydrotalcite formation and mechanical strength gain to examine the extent of hydrotalcite formation and the relative strength gain per fine fraction in specimens, as shown in Figure 37. It is important to note that the cylindrical QB specimens were cured for 120 days, so the comparisons were based on hydrotalcite formation at 120 days rather than the final measurements at 180 days. The trend in Figure 37 indicates that hydrotalcite formation in dolomitic QBFs likely contributes to greater strength gain per fine fraction of QBs. According to the linear trend, QB-1, which has a similar chemical composition to QB-2, is predicted to show a higher relative strength gain per fine fraction after 180 days of curing, coinciding with the peak of hydrotalcite formation at 180 days, as shown in Figure 36.

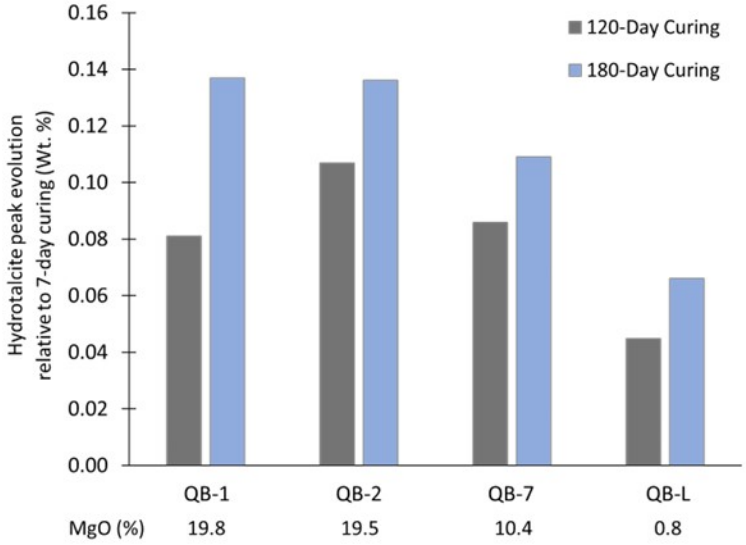

Figure 36. Chart. Hydrotalcite peak evolution in specimens containing QBF over time.

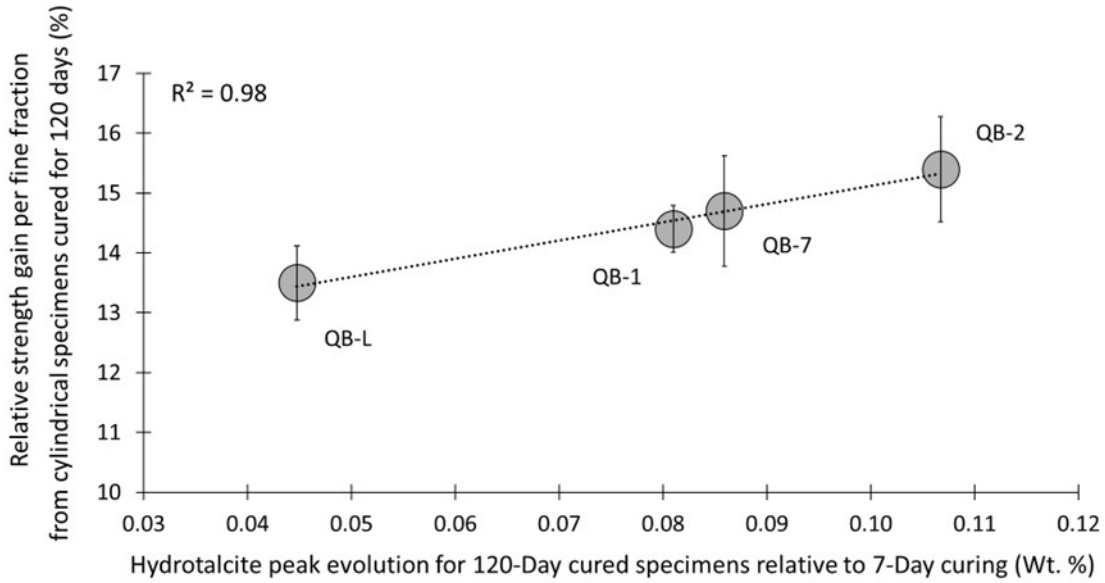

Figure 37. Graph. Comparison of hydrotalcite formation with strength gain per fine fraction.

CHAPTER 5: INFLUENCE OF CALCINED CLAY ADDITION ON PERFORMANCE CHARACTERISTICS OF STABILIZED QUARRY BY-PRODUCTS

SAMPLE PREPARATION AND CONDITIONING

Determination of Optimum Cement and Metakaolin Proportion

The amount of calcined clay (i.e., metakaolin, MK) incorporated with cement in soil stabilization strongly influences the mechanical strength of stabilized specimens. While several studies have investigated the optimum MK-to-cement ratio for various soil types (Wang et al., 2018; Wang et al., 2023; Wu et al., 2016), research on well-graded, sand-sized QB materials remains limited. To identify the optimum MK-to-cement dosage for QB applications, a series of MK-to-cement ratios was tested using QB-2, which represents the mid-range of the particle size distributions among the four QB materials. Specimens without MK were also prepared to evaluate the effect of MK inclusion on mechanical performance. Figure 38 illustrates the MK-to-cement ratios tested in this study, including the control dosage for comparison. The total stabilizer content (i.e., the combined cement and MK content) was fixed at 3% by weight of dry QB material to allow direct comparison with the results presented in Chapters 3 and 4. Within this fixed stabilizer content, MK was used as a partial replacement for cement to investigate how varying the MK dosage influences mechanical performance.

Specimen preparation was conducted in the same manner as described in Chapters 3 and 4 for the 3% cement-stabilized cylindrical specimens. Cylindrical specimens with dimensions of 2.8 in. (71 mm) in diameter and 5.6 in. (142 mm) in height were molded at the optimum moisture content (OMC), determined from the moisture-density relationship established for QB-2 with 3% cement, as described in Chapter 2. Although MK was used as a partial replacement for cement, changes in moisture demand and compaction characteristics were assumed to be minimal at relatively low replacement levels. Therefore, all specimens with different MK-to-cement ratios were compacted at the same moisture content in three equal lifts using a Proctor hammer. Three specimens were prepared for each dosage and target curing period for unconfined compressive strength (UCS) testing. The specimens were then cured for 120 days in a moisture room maintained at 100% relative humidity and a temperature of 73 ± 5°F (23 ± 2°C).

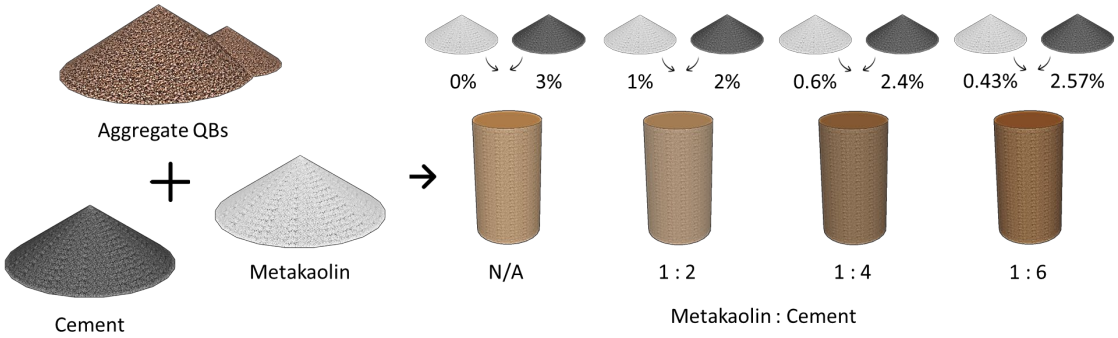

Figure 38. Illustration. Preparation of specimens for determining the optimum MK-to-cement ratio.

Short-Term Performance Monitoring

Based on the results presented later in this chapter, an optimum MK-to-cement ratio of 1:4 was used to prepare same-sized cylindrical QB specimens for evaluating mechanical performance after short-term curing. The same preparation protocol was followed; however, two total stabilizer contents were applied. First, a slightly lower cement content (2% by weight) combined with 0.5% MK at a 1:4 MK-to-cement ratio was tested to compare its performance against the standard 3% cement dosage known to provide satisfactory performance in pavement base and subbase applications. In addition, 0.75% MK was incorporated with 3% cement, also at a 1:4 MK-to-cement ratio, to examine the extent of strength improvement from further MK inclusion. Figure 39 summarizes the two total stabilizer contents used for different QB materials during sample preparation, along with their corresponding OMC and MDD values applied in the process. Three specimens were prepared for each QB type and stabilizer dosage to ensure repeatability in UCS testing, and all specimens were cured for seven days in a moisture room maintained at 100% relative humidity and 73 ± 5°F (23 ± 2°C).

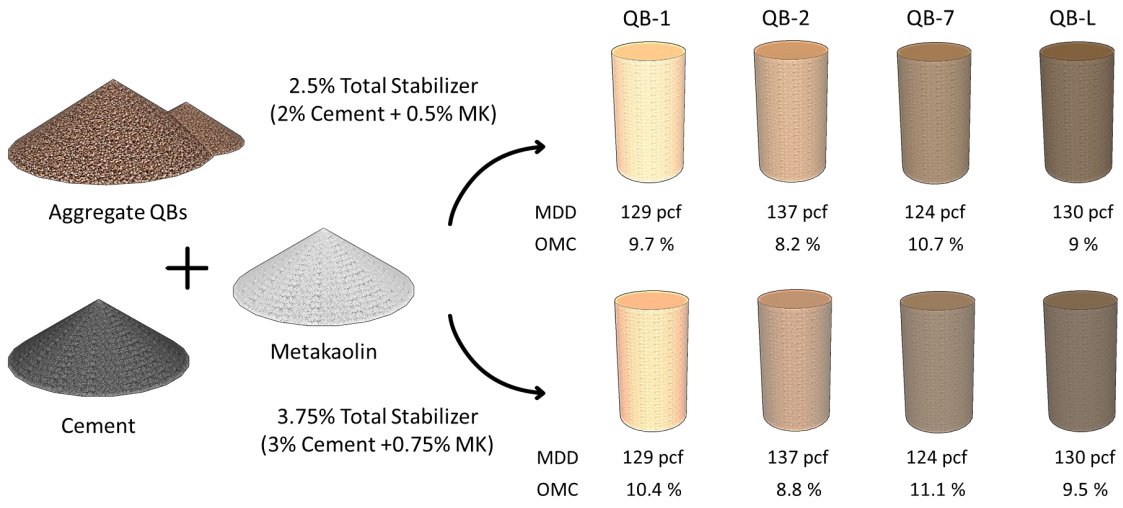

Figure 39. Illustration. Preparation of specimens subjected to short-term curing with two stabilizer contents.

Long-Term Performance Monitoring

The optimum proportion of MK and cement was applied to another set of cylindrical specimens using the same QB types for the long-term study. The same sample preparation procedure described in earlier chapters was followed, using identical cylindrical specimen sizes but with different stabilizer contents. The first set of specimens was prepared with a total stabilizer content of 3% at a 1:4 MK-to-cement ratio, consisting of 0.6% MK and 2.4% cement. This allowed a direct comparison with the long-term performance of the 3% cement-stabilized QB specimens presented in Chapter 4. The second set of specimens was prepared with a total stabilizer content of 3.75% (0.75% MK and 3% cement), also at a 1:4 MK-to-cement ratio, to evaluate the long-term strength improvement from incorporating additional MK beyond the baseline 3% cement dosage. Figure 40 summarizes the two sets of QB specimens prepared with four QB types and two stabilizer contents, along with the OMC and MDD values targeted for specimen preparation.

To evaluate the effect of MK and different carbonate QB aggregates on strength performance, all specimens were subjected to long-term curing, like the specimens described in Chapter 4. The cylindrical QB specimens were placed in sealed containers (Figure 41-a) with an additional water reservoir to maintain 100% relative humidity. The containers were then placed in an oven (Figure 41-b) at a constant temperature of 104°F (40°C) to accelerate curing, following the same protocol used for QB specimens stabilized with cement only. The specimens were kept in sealed containers and cured for up to 210 days.

Following 120 days of curing, certain specimens were removed from the oven and subjected to rapid freeze-thaw cycles to evaluate their durability performance. The conditioning followed the same methods described in Chapters 3 and 4, involving 24-hour freezing at −10°F (−23°C) and 24-hour thawing at 73.5°F (23°C) and 100% relative humidity, with each cycle lasting 48 hours. To avoid subjectivity, the wire-brushing step was omitted, and UCS tests were performed at selected intervals to assess the degradation of strength. Specimens were spaced at least 1 in. (25 mm) apart in the freezing cabinet with an absorptive material placed beneath them, consistent with ASTM D560 recommendations.

In addition to the cylindrical QB specimens used for strength and freeze-thaw testing, small cube specimens measuring 0.4 in. (1 cm) per side were prepared for chemical analysis (Figure 41-c). These cubes were composed of QB fines (QBF) blended with 50% stabilizer at an MK-to-cement ratio of 1:4 and 30.5% water relative to the total solids. As with previous cube preparations containing QBF and cement, only QBF was used, based on the assumption that finer particles are more actively involved in cement hydration, while coarser particles primarily act as inert fillers. A higher stabilizer content of 50% was selected to improve the detectability of hydration products during phase characterization. The cube specimens were cured for 180 days at 104°F (40°C), following the same setup as the cylindrical specimens, in sealed containers with an internal water reservoir to maintain 100% relative humidity. Hydration was stopped at designated curing ages (7 and 180 days) using isopropanol exchange, after which the samples were stored in low-vacuum desiccators until material characterization was performed.

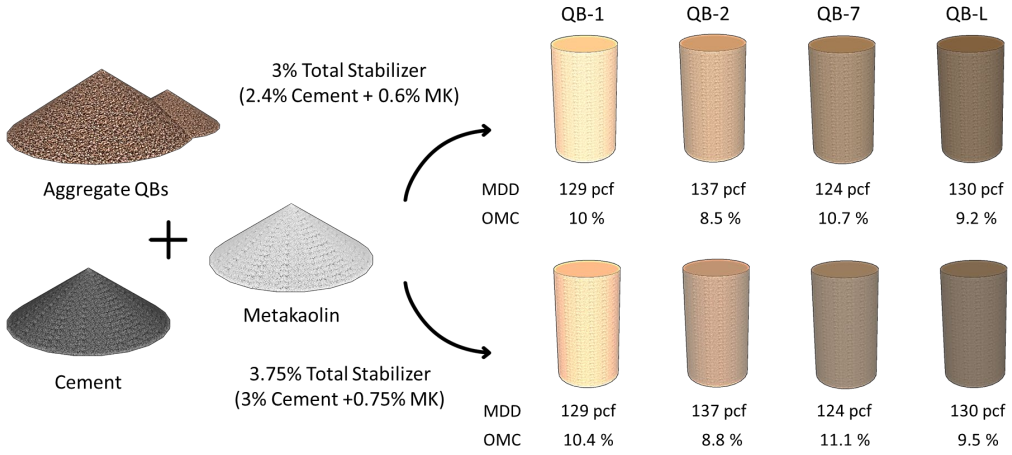

Figure 40. Illustration. Preparation of specimens subjected to long-term curing with two stabilizer contents.

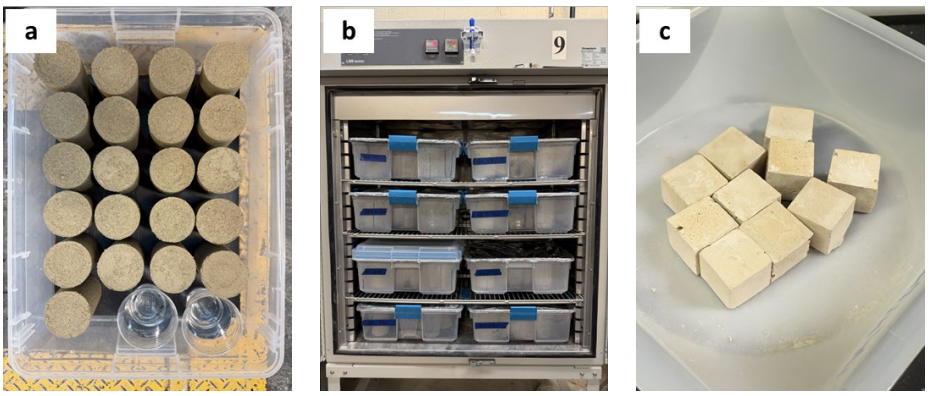

Figure 41. Photo. (a) Cylindrical specimens stabilized with MK and cement, (b) sealed containers with specimens placed in the oven, and (c) cube specimens consisting of QBF, cement, and MK.

OPTIMUM PROPORTION OF CEMENT AND METAKAOLIN

The UCS results of all QB specimens stabilized with different MK-to-cement ratios (i.e., 1:2, 1:4, and 1:6) were monitored over 120 days at curing ages of 7, 28, 60, and 120 days to identify the optimum dosage for sand-sized QB materials. Figure 42 presents the strength development trends of specimens stabilized with MK and cement, along with cement-only controls, highlighting the benefits of MK. Compared to the QB specimens stabilized with only cement, all mixes containing MK demonstrated substantial improvements in early strength, particularly within the first 28 days of curing. These improvements were achieved despite reduced cement content, highlighting the role of MK as an effective supplementary cementitious material (SCM) for lowering cement demand and associated carbon emissions. By 120 days, the differences in UCS among the mixes diminished, likely due to the higher cement content in the control mix and the depletion of available calcium hydroxide in the MK-cement mix that is required for additional pozzolanic reaction. Nevertheless, specimens containing MK achieved UCS values comparable to or greater than the cement-only control.

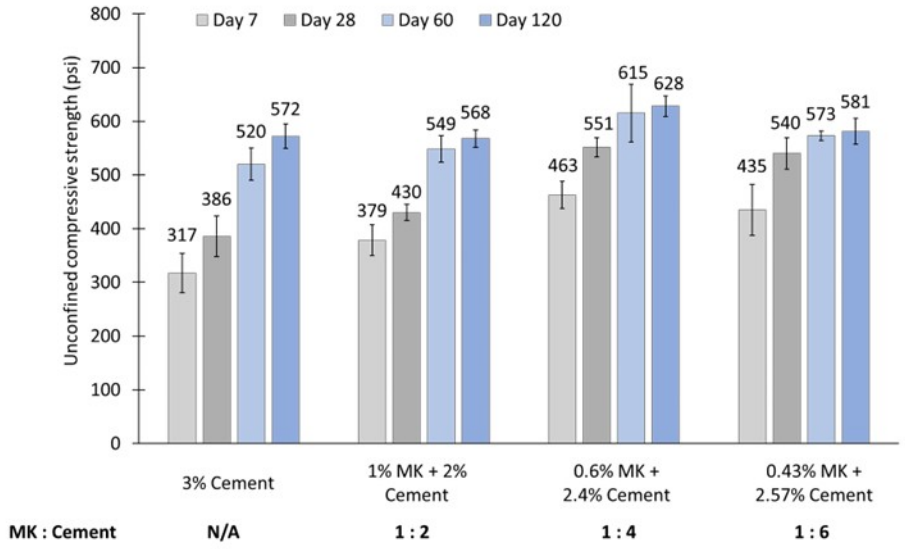

Figure 42. Chart. UCS results for QB specimens prepared at various MK-to-cement ratios.

Among the tested ratios, the blend with 0.6% MK (MK-to-cement ratio of 1:4) consistently produced the highest UCS across all curing periods, indicating an optimal balance between cement hydration and MK reactivity. This optimal ratio was subsequently adopted for all specimen preparation for short- and long-term studies, and it also demonstrates the potential to reduce cement use by 20% while achieving superior compressive strength.

MECHANICAL AND DURABILITY PERFORMANCE TRENDS

Compressive Strength Development after Short-Term Curing

The strength results of the specimens were evaluated through UCS testing after seven days of curing to assess short-term strength development in cement-stabilized mixes incorporating MK with four types of QB materials. The findings were compared with UCS values from QB specimens stabilized with cement only, as reported in Chapter 3. Figure 43 presents the strength values for specimens prepared with 3% cement, 2% cement with 0.5% MK, and 3% cement with 0.75% MK. In general, the results showed that MK incorporation substantially improved the early strength of the stabilized QB materials. Specimens prepared with a total stabilizer content of 2.5% (comprising 2% cement and 0.5% MK) achieved UCS values comparable to or greater than those with 3% cement alone, despite the lower total stabilizer content. The strength difference between the control and the 2.5% stabilizer mix ranged from 0.8 to 1.7 times, depending on QB type, with QB-7 exhibiting the highest improvement. This improvement can be attributed to its higher fines content (particles passing the No. 200 sieve, or smaller than 75 μm), which provides a greater surface area for cementitious reactions and facilitates stronger bonding within the soil matrix. Similarly, the addition of 0.75% MK to 3% cement resulted in significant strength increases over the cement-only control, ranging from 1.7 to 2.6 times, with QB-7 again achieving the highest improvement. Overall, even small MK additions more than doubled the short-term strength values for some QB types, confirming the role of MK in accelerating cement hydration and underscoring its potential to improve the performance of cement-stabilized soils.

Furthermore, the short-term strength performance was not influenced significantly by the chemical or mineralogical characteristics of the QB materials (i.e., dolomite vs. limestone). No clear correlation was found between carbonate type and strength gain after short-term curing. Consistent with earlier findings in Chapter 3, physical properties, particularly particle size distribution, had a greater influence on short-term strength development than chemical and mineralogical properties. In particular, the particle size distribution of QB-2 closely aligned with the curve representing optimum packing derived from Talbot's equation in Chapter 3. Consequently, QB-2 achieved the highest strength under all three stabilizer combinations: 3% cement, 2.5% stabilizer, and 3.75% stabilizer.

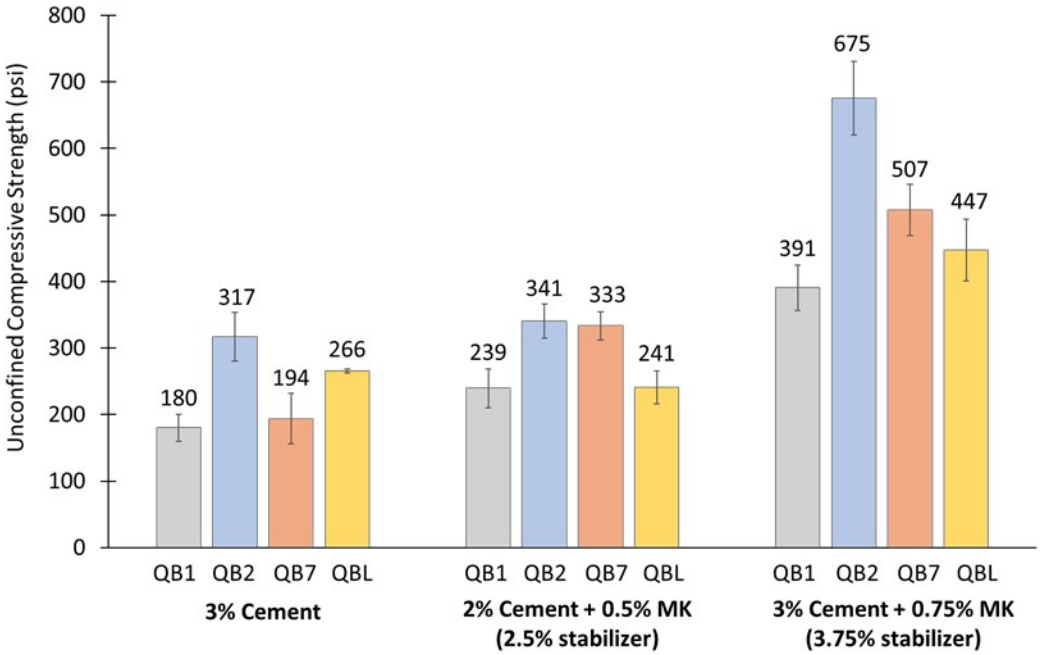

Figure 43. Chart. UCS results for QB specimens incorporating MK after short-term curing.

Compressive Strength Development after Long-Term Curing

QB specimens prepared with two total stabilizer contents (3% and 3.75%) at the optimum MK-to-cement ratio were tested for UCS after long-term curing to evaluate their mechanical performance. The results were compared with those from QB specimens stabilized with 3% cement only, as discussed in Chapter 4, to assess the influence of both MK incorporation and carbonate type of QBs. Figure 44 presents the compressive strengths measured after 120 days of curing for specimens stabilized with 3% cement, 3% total stabilizer (2.4% cement + 0.6% MK), and 3.75% total stabilizer (3% cement + 0.75% MK). Overall, the incorporation of MK provided substantial long-term strength improvements compared with cement-only stabilization. Specimens with 3% total stabilizer achieved strengths of 760 psi (5,240 kPa), 993 psi (6,847 kPa), 905 psi (6,240 kPa), and 710 psi (4,895 kPa) for QB-1 through QB-L, corresponding to improvements of 1.8, 1.3, 1.5, and 1.6 times, respectively, relative to cement-only specimens. Note that these strength gains were achieved with lower cement content, highlighting MK's contribution to more sustainable QB applications in pavement foundations by reducing cement usage while delivering superior performance.

Further improvement was observed with the addition of a small amount of MK to the baseline of 3% cement. Strengths of 1,000 psi (6,895 kPa), 1,262 psi (8,701 kPa), 1,100 psi (7,584 kPa), and 847 psi (5,840 kPa) were achieved by QB-1 through QB-L, corresponding to strength enhancements of 2.3, 1.6, 1.8, and 1.9 times, respectively, relative to specimens stabilized with cement only. On average, the inclusion of MK nearly doubled the strength of lightly cement-stabilized QB specimens compared to those without MK, suggesting the potential to extend pavement foundation lifespan and reduce long-term maintenance costs.

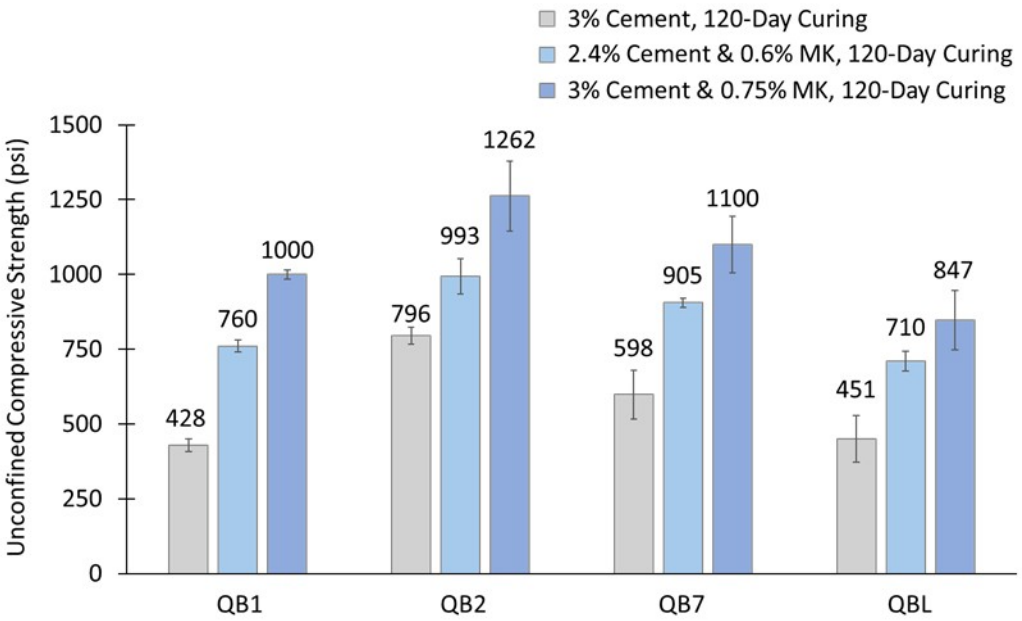

Figure 44. Chart. UCS comparisons among specimens stabilized with 3% cement, 3% total stabilizer, and 3.75% total stabilizer after long-term curing.

Research on the long-term strength performance of carbonate aggregate QB materials presented in Chapter 4 highlighted that the intrinsic mineral properties of dolomite, particularly from QBF, contribute to long-term mechanical strength and freeze-thaw durability by refining the microstructure through the formation of hydrotalcite, an additional phase produced during cement hydration. Building on these findings, UCS trends for each carbonate-based QB were analyzed at multiple curing stages (7, 28, 90, 120, and 210 days) to track long-term strength development and evaluate the potential mineralogical influences of different carbonate types (limestone vs. dolomite) in the presence of MK. Figures 45 and 46 present the UCS development of four carbonate-based QBs stabilized with 3% and 3.75% total stabilizer, respectively, over a period of 210 days.

Overall, the results revealed similar trends to those observed in specimens used to determine the optimum MK-to-cement ratio: significant strength development occurred during the early curing period, while the effect of MK diminished over time as the supply of calcium hydroxide became limited for further pozzolanic reactions. Nevertheless, all QB materials demonstrated substantial long-term strength gains. For example, with 3% total stabilizer, the final strengths were 771 psi (5,316 kPa), 1,050 psi (7,240 kPa), 920 psi (6,343 kPa), and 718 psi (4,950 kPa) for QB-1 through QB-L, corresponding to increases of 1.5, 1.7, 1.6, and 1.4 times their respective 7-day strengths. The addition of 0.75% MK to the baseline 3% cement provided further improvements, yielding up to a 30% increase compared to the final strengths of the 3% total stabilizer specimens at 210 days. The ultimate strengths of the QB materials with 3.75% total stabilizer after 210 days of curing were 1,032 psi (7,115 kPa), 1,321 psi (9,108 kPa), 1,116 psi (7,695 kPa), and 882 psi (6,081 kPa) for QB-1 through QB-L, representing 1.5, 1.7, 1.6, and 1.4 times increases relative to their early 7-day strengths, respectively.

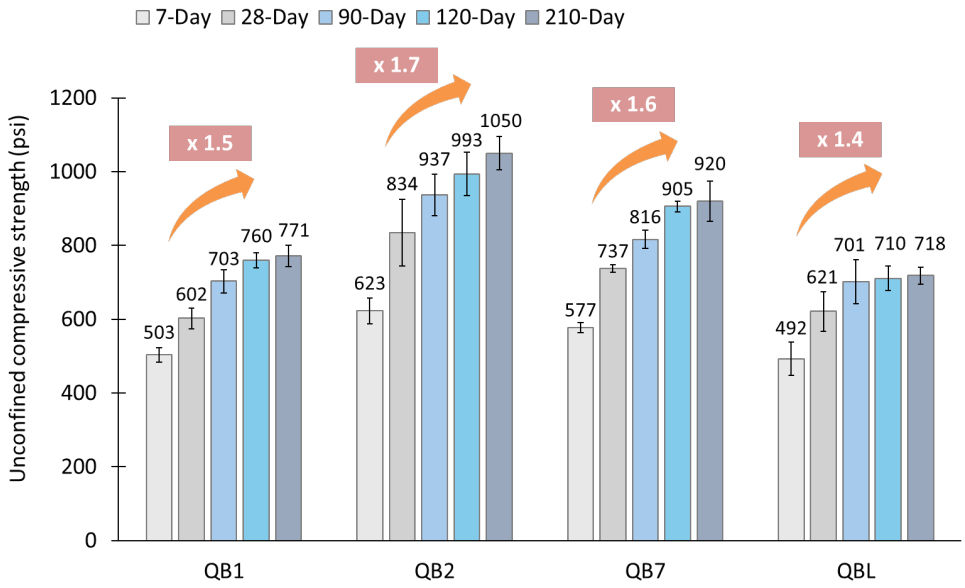

Figure 45. Chart. Long-term strength development trends for various carbonate-based QB materials stabilized with 3% total stabilizer.

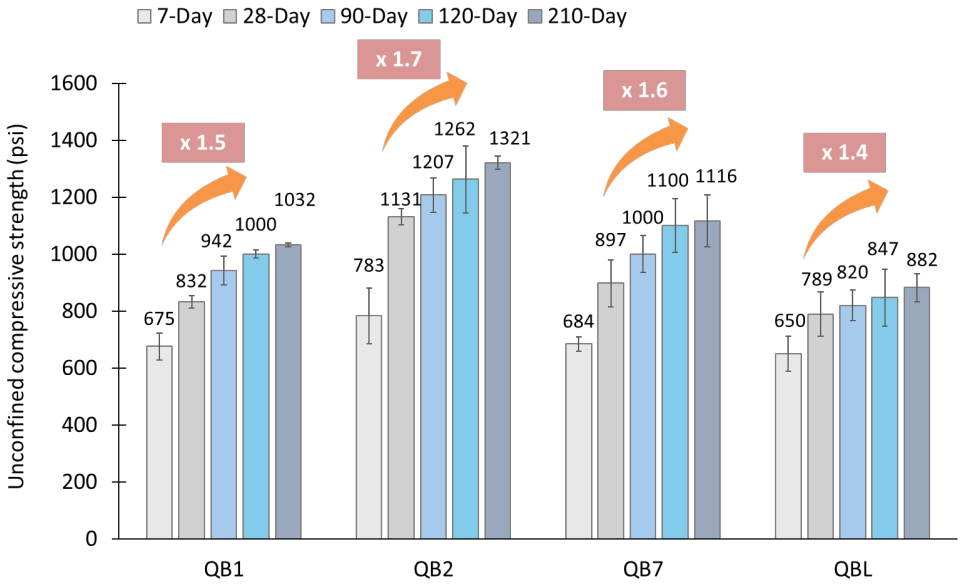

Figure 46. Chart. Long-term strength development trends for various carbonate-based QB materials stabilized with 3.75% total stabilizer.

The UCS development trends shown in Figures 45 and 46 for both 3% and 3.75% total stabilizer indicated slightly higher strength improvements for aggregate QBs with higher dolomitic mineral content or MgO (i.e., QB-1 and QB-2), which reached 1.5 and 1.7 times their initial 7-day strength, compared with QB-L (high in calcite), which reached 1.4 times. However, strength gains attributed to mineralogical properties must also account for the contribution of fines, which are highly reactive due to their larger surface area, whereas coarse aggregate particles are nearly inert. When the fines

content (passing the No. 200 sieve, smaller than 75 µm) of the QB materials is considered (Figure 4), the difference in strength improvement between carbonate types becomes less pronounced than previously reported in the absence of MK, where dolomitic QBs exhibited substantially greater strength development compared to limestone QBs (Chapter 4). Fines largely govern long-term strength development in cementitious systems attributed to chemical interaction, and the slightly lower strength gain of QB-L relative to its initial strength can be attributed to its lower fines content compared with the other QBs. This factor further reduces the difference in strength development between dolomitic and limestone aggregates. Nevertheless, understanding the fundamental chemical interactions of carbonate-based aggregate QBs within cementitious systems in the presence of MK remains essential. A later section in this chapter, Chemical and Microstructure Analysis, provides a detailed analysis of phase evolutions resulting from these chemical reactions.

Dynamic Modulus Development after Long-Term Curing

The development of stiffness characteristics, expressed as the dynamic modulus (E_d), was evaluated from resonant frequency testing (RFT) results using the equation in Figure 8 for all QB types, including both cement-stabilized and MK-cement–stabilized specimens, after 120 days of curing, prior to freeze-thaw conditioning. The calculated E_d values were then compared among specimens to assess the long-term effect of MK on stiffness development. Figure 47 presents the comparison of E_d across three stabilizer contents for different carbonate-based QBs, showing significant stiffness improvement for both partial cement replacement by MK and additional MK incorporation. The results indicated that replacing cement with MK (i.e., 3% total stabilizer, comprising 2.4% cement and 0.6% MK) produced, on average, a 25% increase in stiffness compared to cement-only specimens. This improvement was achieved through a reduction in cement content, underscoring MK's potential for more sustainable QB applications. Moreover, the addition of 0.75% MK to 3% cement nearly doubled the stiffness relative to 3% cement-stabilized specimens, reflecting enhanced structural integrity through additional pozzolanic reactions.

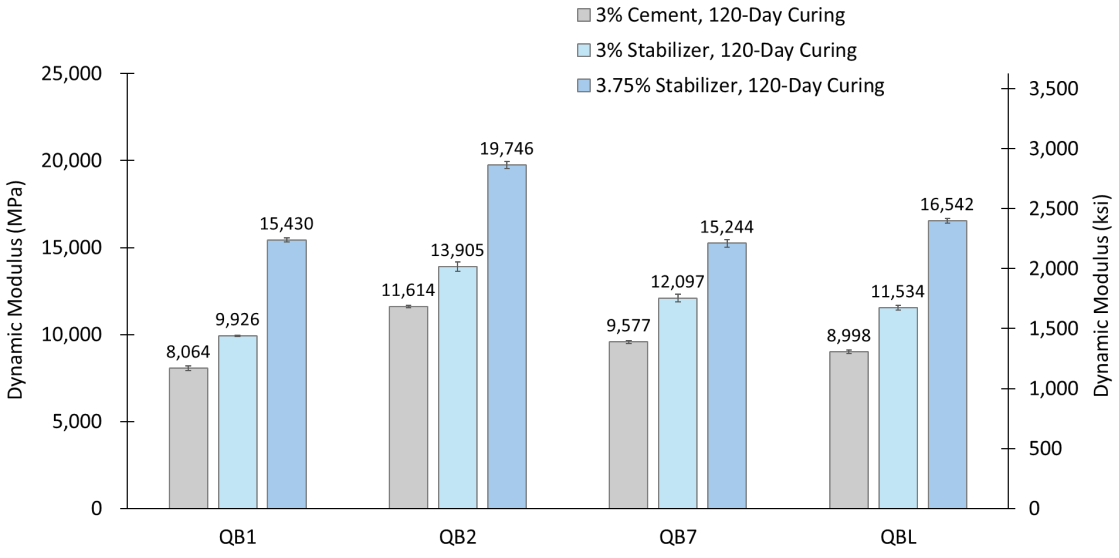

Figure 47. Chart. Dynamic modulus (E_d) comparisons among specimens stabilized with 3% cement, 3% total stabilizer, and 3.75% total stabilizer after long-term curing.

Comparison of Freeze-Thaw Durability Performance

The durability performance of QB specimens stabilized with MK and cement was evaluated through UCS testing before and after 10 freeze-thaw cycles following 120 days of curing. The results were compared with the freeze-thaw performance of cement-only QB specimens presented in Chapter 4. Figure 48 illustrates the UCS changes before and after freeze-thaw cycling for different stabilizer contents.

Overall, the results indicated that MK incorporation significantly enhanced durability. All QB specimens containing 0.6% MK retained higher post-freeze-thaw strength than their cement-only counterparts, despite the reduced cement content. The addition of 0.75% MK provided even greater resistance to freeze-thaw degradation. For specimens treated with a total stabilizer concentration of 3.75%, the UCS values after 10 cycles were comparable to or exceeded those of specimens with a 3% total stabilizer concentration tested before freeze-thaw cycling. This finding suggests that even small additions of MK can substantially extend the service life of pavement foundations under prolonged climatic exposure.

The percent strength reductions for QB specimens with 3% stabilizers were 38%, 32%, 45%, and 42% for QB-1 through QB-L, respectively. For specimens with 3.75% stabilizers, the corresponding reductions for QB-1 through QB-L were notably lower at 21%, 19%, 24%, and 22%, respectively. These results suggest that in the presence of MK, carbonate mineralogy (dolomite vs. limestone) exerted minimal influence on freeze-thaw durability, consistent with the long-term strength development trends observed across QB types during 210 days of curing. Among the QBs, QB-2 consistently demonstrated the best performance at both stabilizer levels, likely due to its particle size distribution closely matching the optimum packing curve for sand-sized aggregates as defined by the Talbot equation (Chapter 3).

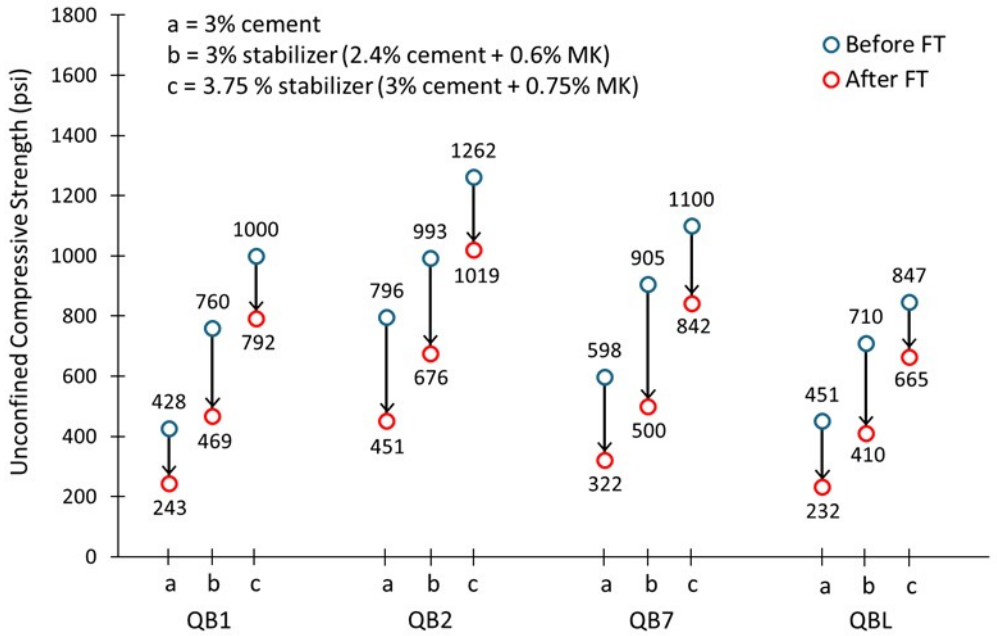

Figure 48. Graph. Changes in the UCS results of stabilized QB specimens after 10 freeze-thaw cycles.

Freeze-thaw durability was also evaluated using longitudinal RFT, where resonant frequency changes were recorded throughout the cycles and subsequently used to calculate E_d according to the equation given in Figure 8. The E_d trends of specimens stabilized with MK and cement were compared with those of cement-only QB specimens discussed in Chapter 4. Figure 49 presents the comparisons as a heatmap, where green indicates higher E_d and red denotes lower E_d.

Consistent with the UCS findings, specimens incorporating MK exhibited substantially higher E_d values during freeze-thaw cycling than their cement-only counterparts. All QB specimens with 3% total stabilizers retained stiffness levels after freeze-thaw cycling that were comparable to those measured before the cycles for cement-only specimens, despite using less cement. Moreover, incorporating 0.75% MK with 3% cement nearly doubled, on average, the E_d of all QB types after completion of the cycles compared with cement-only specimens.

The percent reductions in E_d for QB-1 through QB-L were 16%, 15%, 24%, and 22%, respectively, with 3% stabilizer, whereas for 3.75% stabilizer, the reductions were slightly lower at 14%, 13%, 19%, and 17%. These trends suggest that in the presence of MK, carbonate mineralogy exerts minimal influence on stiffness degradation under freeze-thaw damage, aligning with the UCS results. Among the tested materials, QB-2 consistently demonstrated the least reduction in stiffness, likely due to its particle size distribution aligning closely with the optimum packing curve derived from Talbot's equation (Chapter 3).

Stabilizer Content	Material Type	Freeze-Thaw Cycles						MPa
		FT 0	FT 1	FT 3	FT 5	FT 8	FT 10	
3% cement	QB-1	8,064	7,183	7,074	7,030	6,901	6,858	20,000
	QB-2	11,614	10,438	10,060	9,953	9,900	9,900	
	QB-7	9,577	8,578	8,114	7,812	7,458	7,312	
	QB-L	8,998	7,090	6,960	6,873	6,702	6,617	
3% Stabilizer [2.4% cement + 0.6% MK]	QB-1	9,926	8,800	8,703	8,631	8,440	8,392	
	QB-2	13,905	12,153	12,106	12,039	11,888	11,813	
	QB-7	12,097	10,033	9,619	9,451	9,351	9,152	
	QB-L	11,534	9,653	9,552	9,312	9,168	9,045	
3.75% Stabilizer [3% cement + 0.75% MK]	QB-1	15,430	14,017	13,864	13,712	13,441	13,351	
	QB-2	19,746	17,762	17,624	17,419	17,248	17,101	
	QB-7	15,244	13,387	12,789	12,672	12,440	12,325	
	QB-L	16,542	14,480	14,356	13,966	13,803	13,682	6,000

Figure 49. Chart. Heat map depicting changes in dynamic modulus of stabilized QB specimens under freeze-thaw conditioning.

CHEMICAL AND MICROSTRUCTURAL ANALYSES

X-ray Diffraction and Thermogravimetric Analyses

To investigate the influence of MK on the reaction mechanisms of cement-stabilized carbonate-based QB materials, XRD analysis was performed on cube specimens prepared with QBF mixed with MK and cement. The phase assemblages of these specimens were then compared with those of QBF

specimens stabilized with cement alone at an early hydration stage, as shown in Figure 50. The results revealed that specimens incorporating MK and cement exhibited substantial formation of ettringite [Et, $CaAl_2(SO_4)_3(OH)_{12}\cdot 26H_2O$], hemicarboaluminate [Hc, $Ca_4Al_2(CO_3)_{0.5}(OH)_{13}\cdot 5.5H_2O$], and monocarboaluminate [Mc, $Ca_4Al_2(CO_3)(OH)_{12}\cdot 5H_2O$] at an early hydration age (7 days). Calcium hydroxide [$Ca(OH)_2$] was primarily consumed in specimens containing MK compared with those without MK. This consumption was likely the result of the pozzolanic reaction with MK, as presented in Figure 51, leading to the formation of calcium-alumino-silicate-hydrates (C-A-S-H) (Antoni et al., 2012; Avet & Scrivener, 2018). Furthermore, calcium hydroxide also reacts with carbonates and aluminates from MK and cement to form carboaluminates, as illustrated in Figure 52 (Antoni et al., 2012; Matschei et al., 2007). These reactions contribute to enhanced strength development in the samples treated with MK and cement (Zunino & Scrivener, 2021). Furthermore, all QBF types exhibited similar reactions after seven days, indicating that MK incorporation improves the overall performance of stabilized QBs regardless of carbonate mineralogy.

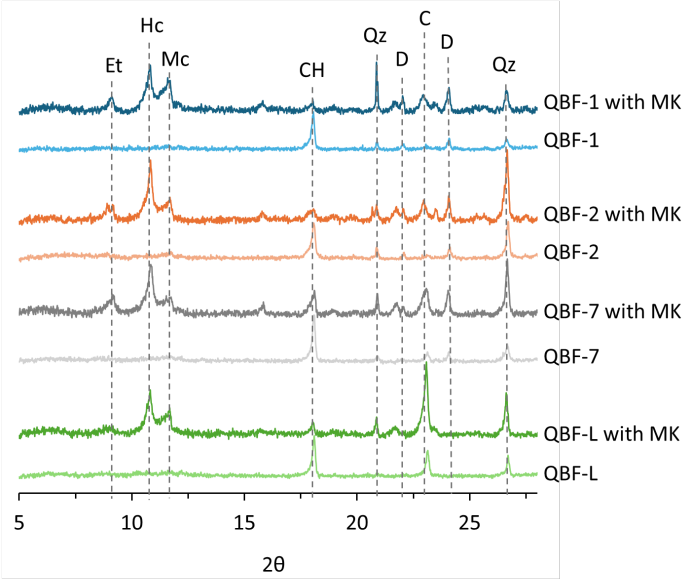

Phase abbreviations: Et = Ettringite; Hc = Hemicarboaluminate; Mc = Monocarboaluminate; CH = Portlandite; Qz = Quartz; D = Dolomite; C = Calcite

Figure 50. Graph. XRD patterns of QBF specimens stabilized with a 1:4 MK-cement blend after seven days of hydration.

$$Al_2Si_2O_7 + 3Ca(OH)_2 + 6H_2O \rightarrow \text{C-A-S-H} + Ca_2Al_2SiO_7.8H_2O$$

Figure 51. Equation. Pozzolanic reaction of metakaolin ($Al_2Si_2O_7$) with calcium hydroxide [$Ca(OH)_2$] from cement hydration.

$$Al_2Si_2O_7 + 0.5CaCO_3 + 3Ca(OH)_2 + 8H_2O \rightarrow Ca_4Al_2(CO_3)_{0.5}(OH)_{13}\cdot 5.5H_2O$$

Figure 52. Equation. Carbonate-based QBs reacting with metakaolin ($Al_2Si_2O_7$) and calcium hydroxide [$Ca(OH)_2$] to form carboaluminate phases.

Previous studies have demonstrated that using dolomitic carbonate, compared to limestone-based carbonate, enhances mechanical performance due to a synergistic reaction that produces hydrotalcite (Zajac, Bremseth, et al., 2014). However, no significant differences in the XRD patterns were observed for QBF samples stabilized with cement and MK, even for long-term curing (Figure 53). Hydrotalcite formation (2θ = 11.4°) was not detected in the dolomitic [$CaMg(CO_3)_2$] QBFs stabilized with cement and MK. This absence is likely due to the limited availability of calcium hydroxide in the system, which is rapidly consumed by the pozzolanic reaction and by the formation of other carboaluminate phases (Machner et al., 2018). These reactions occur much faster than hydrotalcite formation, which typically develops over a longer period. Krishnan and Bishnoi (2018) observed the formation of strätlingite during long-term hydration of limestone, calcined clay cement, and dolomite calcined clay cement systems. However, in this study, no strätlingite was observed in any QB. Moreover, the hemicarbonaluminate peak diminishes at later ages, accompanied by the formation of calcium carbonate polymorphs such as vaterite and calcite, which are likely products of natural carbonation (Bahman-Zadeh et al., 2022). Similar findings were observed in the TGA analyses, as shown in Figure 54. Minimal calcium hydroxide presence (around 450°C) was detected at both early and later ages, while the hydrotalcite peak was not present at later ages (around 400°C). Additionally, the main DTG peak associated with CO_2 release at lower temperatures is due to calcium carbonate polymorphs, specifically aragonite and vaterite (Igami et al., 2025). These DTG findings complement the XRD observations.

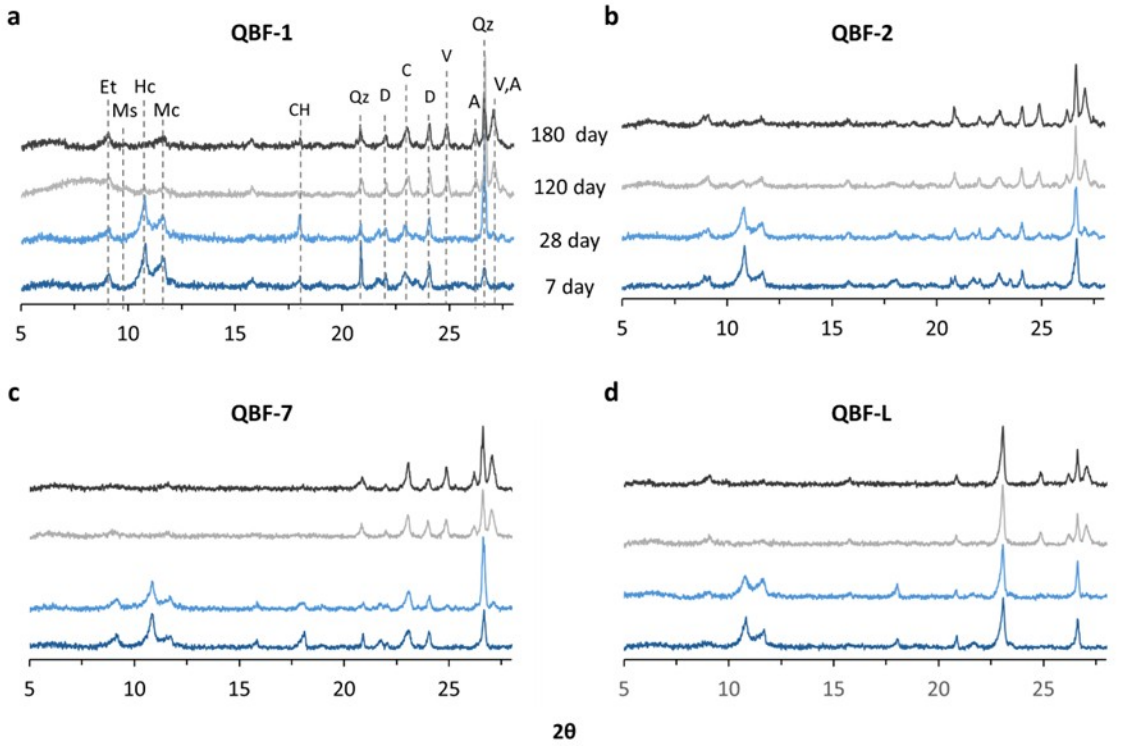

Figure 53. Graph. XRD patterns of hydrated QBF samples stabilized with 1:4 cement-MK blend: (a) QBF-1, (b) QBF-2, (c) QBF-7, and (d) QBF-L samples at 7, 28, 120, and 180 days.

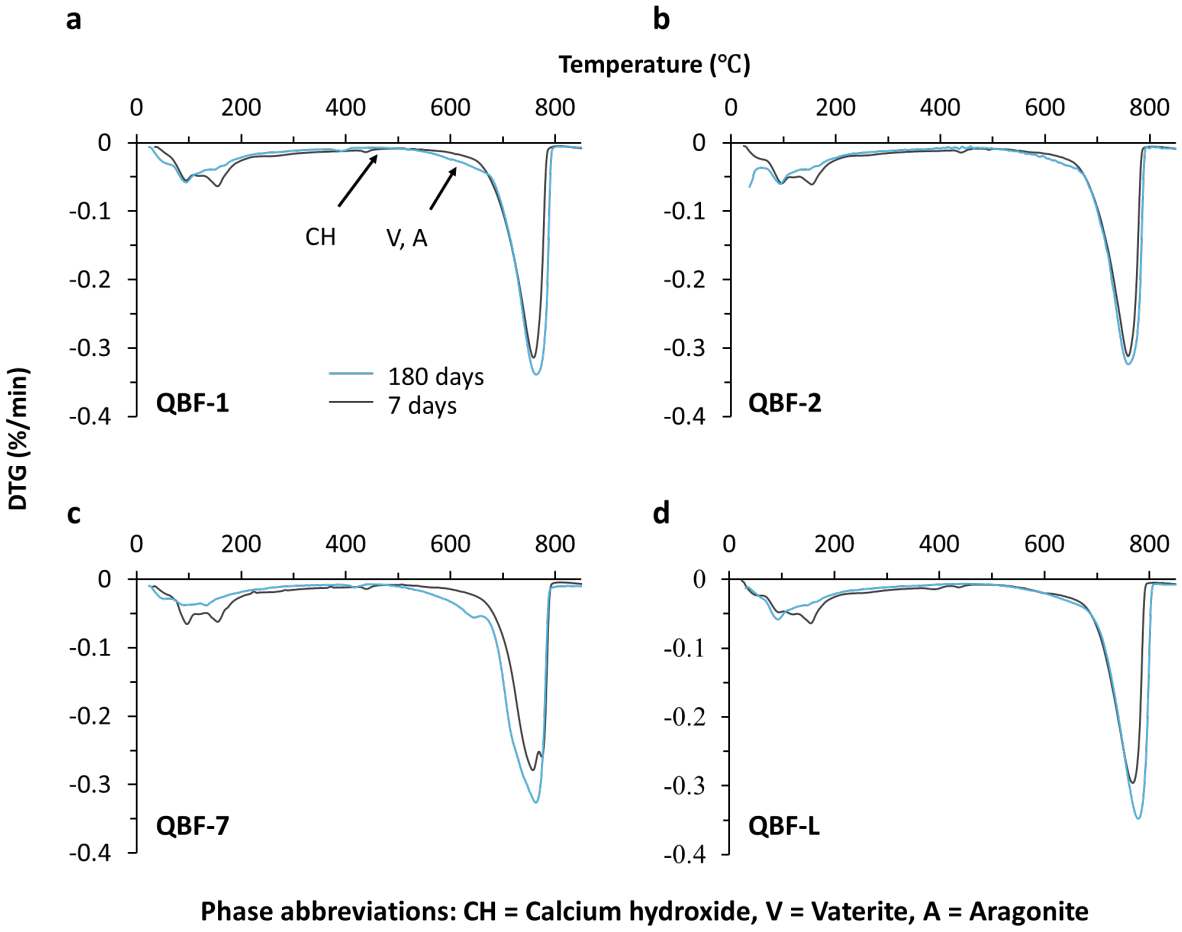

Phase abbreviations: CH = Calcium hydroxide, V = Vaterite, A = Aragonite

Figure 54. Graph. Differential thermogravimetric plots of various hydrated QBF samples stabilized with 1:4 MK-cement blend: (a) QBF-1, (b) QBF-2, (c) QBF-7, and (d) QBF-L at 7 days and 180 days.

ROLE OF CALCINED CLAYS IN STABILIZING CARBONATE-BASED QUARRY BY-PRODUCTS

Calcined clays are essentially aluminosilicates that release aluminum and silicon into the pore solution during the hydration of cement. Silicon reacts with calcium hydroxide formed in the process, leading to the precipitation of C-A-S-H gel. This pozzolanic reaction increases the overall amount of binding gel, thereby enhancing strength. In addition, carbonates from QBs react with aluminum from cement and MK to form carboaluminate phases at early ages, further contributing to strength development. This reaction occurs irrespective of carbonate type, meaning all QB materials exhibit improved performance when stabilized with an MK-cement blend compared to cement alone.

Unlike the case of dolomitic QBs stabilized solely with cement, where hydrotalcite formation enhances long-term strength, the incorporation of MK does not promote the formation of hydrotalcite. This absence is attributed to the rapid consumption of calcium hydroxide by the pozzolanic reaction. Overall, replacing part of the cement with sustainable, low-CO_2 MK results in improved strength across all QB types, regardless of carbonate type.

CHAPTER 6: SUMMARY AND CONCLUSIONS

SUMMARY AND KEY RESEARCH FINDINGS

The report investigated the effect of physical, chemical, and mineralogical properties of carbonate-based aggregate quarry by-products (QBs, of dolomite and limestone) on mechanical performance, such as compressive strength, and freeze-thaw durability performance after stabilizing them with cement or a combination of cement and calcined clay, metakaolin (MK). The scope of the research covered both short- and long-term mechanical and durability behavior of stabilized QB specimens, while also incorporating advanced material characterization techniques to investigate the microstructural and chemical mechanisms that may govern differences in performance trends. Special emphasis was placed on identifying the role of dolomitic versus calcitic QBs, the influence of fines content and particle packing, and the effectiveness of MK in enhancing the strength, durability, and sustainability of stabilized systems. By integrating laboratory testing, advanced characterization, and performance evaluation, the study aimed to provide practical guidelines for sustainable utilization of QBs in pavement foundation layers.

The study began with a characterization of carbonate-based aggregate QBs collected from eight quarries in Illinois, selected to represent a wide range of MgO contents, a key criterion used in IDOT specifications to distinguish dolomite from limestone. The collected materials encompassed highly dolomitic, moderately dolomitic, and limestone QBs, providing a basis for comparative analysis. Laboratory tests were conducted to characterize the QB material properties, including particle size distribution (dry and washed sieve analyses), compaction characteristics determined by Proctor tests, and deleterious clay content assessed using the modified methylene blue test. The chemical and mineralogical properties of the QBs were determined using X-ray fluorescence, atomic absorption spectroscopy, and X-ray diffraction (XRD), with Rietveld refinement applied to quantify the mineral phases. Among the collected QBs, four representative QBs (QB-1, QB-2, QB-7, and QB-L) were selected for further studies: QB-1 and QB-2 are highly dolomitic aggregates with differing particle size distributions, QB-7 is a moderate dolomitic material containing a mixture of dolomite and limestone, and QB-L is a limestone QB characterized by high calcite content. Type IL cement was used to align with current industry trends, and high-purity MK was employed as a supplementary stabilizer.

The short-term behavior of QBs stabilized with 3% cement after seven days of curing was examined alongside untreated QB specimens to evaluate strength development and to assess potential chemical and mineralogical influences on performance. Unconfined compressive strength (UCS) tests confirmed that untreated QB specimens exhibited negligible strength, whereas stabilization with a small amount of cement (i.e., 3% by the dry weight of QB) enhanced compressive strength by more than 30 to 100 times, depending on the QB type. Durability performance was evaluated through rapid freeze-thaw cycling, with UCS and longitudinal resonant frequency tests conducted after selected cycles. Results indicated that short-term strength and durability were governed primarily by physical properties, particularly particle size distribution and fines content, rather than chemical composition. The slow reaction kinetics of carbonates with cement did not influence strength development at an early age. Microstructural analysis using an optical microscope further confirmed that optimal particle packing—particularly in QB-2, which closely followed the optimum packing derived from

Talbot's equation—minimized voids and enhanced strength and durability under freeze-thaw conditioning.

Following the first phase of the project, which focused on the short-term performance of QB materials, the long-term performance trends of cement-stabilized QB specimens were evaluated after 120 days of curing under an elevated temperature to accelerate reactions. UCS tests showed significant strength gains for all QB materials over long-term curing, with dolomitic QB materials exhibiting greater improvements compared to limestone-based QB. Freeze-thaw durability also improved for dolomitic aggregates, as they demonstrated smaller reductions in strength and dynamic modulus of elasticity (E_d) compared to limestone. Bender element sensors installed at the top and bottom of the 3% stabilized specimens tracked stiffness development through shear wave velocity (V_s) measurements and computed small-strain shear modulus (G_{max}) characteristics, revealing that dolomitic QBs outperformed limestone QBs over extended curing. Advanced chemical and microstructural analyses using XRD, thermogravimetric analysis/differential thermogravimetric analysis (TGA/DTG), and Raman imaging confirmed that dolomitic QBs, particularly their fine fraction (passing the No. 200 sieve, smaller than 75 μm), led to the formation of hydrotalcite, an additional phase evolving during cement hydration. This phase formed around dolomite grains, refining the microstructure and contributing to improved strength and durability. A strong correlation was observed between hydrotalcite formation, quantified through TGA analysis, and the strength improvements of QB materials over the long-term curing period.

The final experimental phase investigated the impact of MK as a supplementary cementitious material in stabilizing carbonate-based aggregate QBs, focusing on its effects on the short- and long-term strength development and durability of the QBs as well as on the role of carbonate minerals in the presence of MK. Using different MK-to-cement ratios, the study identified 1:4 as the optimum ratio for the two-stabilizer blend, which consistently improved strength while reducing cement demand by 20%. Short-term performance improvements after seven days of curing were particularly notable, as mixes with reduced cement content partially replaced with MK (i.e., 2% cement and 0.5% MK) achieved compressive strengths comparable to or greater than the cement-only controls. Furthermore, the addition of 0.75% MK to the 3% cement baseline produced significant strength gains, nearly doubling strength on average in comparison to cement-only specimens. These results confirm MK's role in accelerating cement hydration and underscore its potential to enhance the performance of cement-stabilized QBs. In the long-term evaluation, incorporating MK improved the strength and freeze-thaw durability of all carbonate-based QBs, while the performance differences previously observed between dolomitic and limestone aggregate QBs in cement-only systems became less pronounced.

In cement-stabilized specimens without MK, dolomitic fines contributed additional reactivity through hydrotalcite formation, thereby outperforming limestone-based QB. By contrast, specimens stabilized with MK and cement exhibited comparable long-term strength gains and freeze-thaw durability across all carbonate types. Chemical and microstructural analyses indicated that this convergence was driven by the dominant pozzolanic activity involving MK. XRD analyses confirmed that MK accelerated the consumption of calcium hydroxide and promoted the continuous formation of calcium-alumino-silicate-hydrate (C-A-S-H) gels. Additionally, calcium hydroxide reacted with

carbonates and aluminates from MK and cement to form carboaluminate phases, thereby further enhancing the strength development in specimens treated with MK and cement. Therefore, hydrotalcite did not form in dolomitic QB fines, as indicated by TGA, because the available calcium hydroxide had already been consumed during C-A-S-H and carboaluminate reactions. Although the predominant superiority of dolomitic QBs was not evident in the presence of MK, all carbonate aggregate types benefited from MK inclusion in both the short- and long-term evaluations. The QBs stabilized with MK and cement displayed better performance than the cement-stabilized QBs. Hence, the inclusion of MK highlights the potential for more sustainable practices using industrial by-product materials in road construction.

CONCLUSIONS

The study systematically evaluated the stabilization of carbonate-based QB materials using cement and MK, with consideration of their physical and mineralogical characteristics as well as their mechanical and freeze-thaw durability performance under different curing conditions. The results demonstrated that carbonate-based QBs can be stabilized effectively for pavement base and subbase applications using either cement alone or a combination of cement and MK.

The findings highlight that the performance of stabilized QBs is governed by a dual mechanism involving both physical and mineralogical factors. Physical parameters such as particle size distribution, fines content and packing density primarily influence early-age strength and durability, while mineralogical attributes, particularly chemical reactivity and microstructural development, become more dominant over longer curing periods. Dolomitic QBs exhibited superior long-term strength and freeze-thaw durability due to favorable hydration reactions associated with their magnesium-rich mineralogy, which promote the formation of additional hydrated phases such as hydrotalcite. The presence of hydrotalcite contributes to pore refinement, enhanced microstructural integrity, and improved mechanical performance.

The utilization of aggregate QB materials can be optimized to achieve maximum short- and long-term strength and durability by considering several key factors. First, gradation control can be emphasized, as particle packing significantly affects both early- and long-term strength development as well as resistance to freeze-thaw damage. Applying particle packing principles, such as Talbot's equation, is recommended to optimize compaction and minimize interconnected voids, resulting in more consistent and reliable field performance. Second, the distinct mineralogical differences between dolomitic and limestone QBs can be recognized and considered in stabilization design and performance evaluation. Aggregates with higher MgO content generated greater amounts of hydrotalcite when stabilized with cement, which in turn contributed to improved long-term strength and reduced susceptibility to freeze-thaw degradation. As a result, aggregates with high MgO content and particle gradation close to the optimum packing curve, derived from Talbot's equation, are expected to yield the highest overall performance. In this study, QB-2 exhibited these characteristics and consequently demonstrated the most favorable mechanical strength and durability outcomes.

Additionally, the incorporation of MK as a supplementary cementitious material (SCM) demonstrated strong potential to enhance both the performance and sustainability of all types of carbonate-based

QB stabilization. Laboratory results indicated that replacing a portion of cement with MK at an MK-to-cement ratio of 1:4 improved strength, stiffness, and freeze-thaw durability, while reducing CO_2-intensive cement content by approximately 20%. Moreover, the addition of a small amount of MK (0.75%) to the 3% light cement stabilization mixture led to a notable improvement in strength and resistance to freeze-thaw damage. The use of MK is expected to contribute to the extended service life of pavement foundations, reduced maintenance requirements, lower-carbon construction practices, and decreased dependence on cement. This approach may represent a cost-effective and environmentally responsible advancement in material technology that can enhance the long-term durability and resilience of transportation infrastructure.

RECOMMENDATIONS FOR FUTURE WORK

This project successfully demonstrated the potential of carbonate-based QBs by leveraging their chemical and mineralogical properties to enhance mechanical and durability characteristics. The incorporation of MK further improved performance, supporting its use in pavement foundation applications aimed at achieving more sustainable, stronger, and longer-lasting pavement construction practices. However, additional research is needed to further optimize the effective utilization of QBs in pavement foundations and to expand the current understanding of their behavior under varying field conditions. The following discussion points outline the primary recommendations for future research:

- The current findings are limited to laboratory-scale conditions. There is a need for field-scale studies to validate the findings of the current study and further investigate additional factors influencing long-term performance. Future research should include pilot field demonstrations using both dolomitic and limestone QBs stabilized with cement or with a cement-MK blend to monitor in situ performance indicators such as distress accumulation, changes in layer modulus, and rutting potential. Moreover, the elevated-temperature curing employed in this study to accelerate chemical reactions requires further investigation to establish correlations with field conditions and to predict the time frame for hydrotalcite formation in dolomitic aggregate QBs, as field environments are subject to natural fluctuations in temperature and moisture.

- The search for alternative stabilizers that can reduce dependence on energy-intensive materials such as cement, beyond the use of MK, is necessary. Although MK demonstrated strong potential for improving mechanical performance while lowering cement content, its availability remains limited, as no local producers have been identified to date in the state of Illinois. Therefore, to promote broader utilization of QBs in pavement foundation applications, future research should explore other types of self-cementitious materials or SCMs, such as slags or other industrial by-products, that may offer similar performance and sustainability benefits.

- Life cycle assessment (LCA) and life cycle cost analysis (LCCA) studies are recommended to evaluate the use of QBs comprehensively, particularly when comparing dolomitic and limestone sources, in terms of their long-term performance and sustainability. Such analyses

can help quantify environmental impacts (e.g., energy consumption and material reuse potential), economic feasibility (e.g., construction and maintenance costs over the service life), and social benefits (e.g., practical utilization of QBs and reduction of QB stockpiles). Integrating LCA and LCCA into future studies would provide a holistic understanding of the overall sustainability of QB stabilization practices, supporting data-driven decision-making for pavement foundation applications.

REFERENCES

AASHTO T136. (2013). *Method of Test for Freezing and Thawing Test of Compacted Soil-Cement Mixtures*. American Association of State Highway and Transportation Officials.

ASTM C117. (2017). *Standard Test Method for Materials Finer than 75-µm (No. 200) Sieve in Mineral Aggregates by Washing*. ASTM International.

ASTM C136. (2015). *Standard Test Method for Sieve Analysis of Fine and Coarse Aggregates*. ASTM International.

ASTM C215. (2019). *Standard Test Method for Fundamental Transverse, Longitudinal, and Torsional Resonant Frequencies of Concrete Specimens*. ASTM International.

ASTM D2166. (2006). *Standard Test Method for Unconfined Compressive Strength of Cohesive Soil*. ASTM International.

ASTM D560. (2003). *Standard Test Methods for Freezing and Thawing Compacted Soil-Cement Mixtures*. ASTM International.

ASTM D698. (2021). *Standard Test Methods for Laboratory Compaction Characteristics of Soil Using Standard Effort* (12,400 ft-lbf/ft3 (600 kN-m/m3)). ASTM International.

Antoni, M., Rossen, J., Martirena, F., & Scrivener, K. (2012). Cement substitution by a combination of metakaolin and limestone. *Cement and Concrete Research*, *42*(12), 1579–1589. https://doi.org/10.1016/j.cemconres.2012.09.006

Aranda, M. A. G., De La Torre, Á. G., & León-Reina, L. (2012). Rietveld quantitative phase analysis of OPC clinkers, cements and hydration products. *Reviews in Mineralogy and Geochemistry*, 74, 169–209. https://doi.org/10.2138/rmg.2012.74.5

Avet, F., & Scrivener, K. (2018). Investigation of the calcined kaolinite content on the hydration of limestone calcined clay cement (LC3). *Cement and Concrete Research*, *107*, 124–135. https://doi.org/10.1016/j.cemconres.2018.02.016

Bahman-Zadeh, F., Ramezanianpour, A. A., & Zolfagharnasab, A. (2022). Effect of carbonation on chloride binding capacity of limestone calcined clay cement (LC3) and binary pastes. *Journal of Building Engineering*, *52*, 104447. https://doi.org/10.1016/j.jobe.2022.104447

Bernard, E., Zucha, W. J., Lothenbach, B., & Mäder, U. (2022). Stability of hydrotalcite (Mg-Al layered double hydroxide) in presence of different anions. *Cement and Concrete Research*, *152*, 106674. https://doi.org/10.1016/j.cemconres.2021.106674

Dieing, T., & Ibach, W. (2010). Software requirements and data analysis in confocal Raman microscopy. In *Confocal raman microscopy* (pp. 61–89). Springer.

García, E., Alfonso, P., Labrador, M., & Galí, S. (2003). Dedolomitization in different alkaline media: Application to Portland cement paste. *Cement and Concrete Research*, *33*(9), 1443–1448. https://doi.org/10.1016/S0008-8846(03)00095-4

Güneyisi, E., Gesoğlu, M., & Mermerdaş, K. (2008). Improving strength, drying shrinkage, and pore structure of concrete using metakaolin. *Materials and Structures*, *41*, 937–949. https://doi.org/10.1617/s11527-007-9296-z

Higl, J., Köhler, M., & Linden, M. (2016). Confocal Raman microscopy as a non-destructive tool to study microstructure of hydrating cementitious materials. *Cement and Concrete Research*, *88*, 136–143. https://doi.org/10.1016/j.cemconres.2016.07.005

Igami, R., Igarashi, G., Aili, A., Minato, D., Kurihara, R., & Maruyama, I. (2025). Clinker mineral formation and thermal decomposition of calcium carbonates in carbonated tobermorites: Mechanism of CO2 release in low-temperature ranges. *Cement and Concrete Research*, *197*, 107969. https://doi.org/10.1016/j.cemconres.2025.107969

Illinois Department of Transportation. (2022). *Standard Specifications for Road and Bridge Construction*. https://public.powerdms.com/IDOT/documents/1945348

Juang, C., Finzi, L., & Bustamante, C. J. (1988). Design and application of a computer-controlled confocal scanning differential polarization microscope. *Review of Scientific Instruments*, *59*(11), 2399–2408. https://doi.org/10.1063/1.1139918

Kim, H.-S., Lee, S.-H., & Moon, H.-Y. (2007). Strength properties and durability aspects of high strength concrete using Korean metakaolin. *Construction and Building Materials*, *21*(6), 1229–1237. https://doi.org/10.1016/j.conbuildmat.2006.05.007

Kothari, C., & Garg, N. (2024a). Phase quantification of anhydrous CSA cements: A combined X-ray diffraction and Raman imaging approach. *Advances in Cement Research*, 1–27. https://doi.org/10.1680/jadcr.23.00238

Kothari, C., & Garg, N. (2024b). Quantitative phase analysis of anhydrous Portland cement via combined X-ray diffraction and Raman imaging: Synergy and impact of analysis parameters. *Cement and Concrete Research*, *186*, 107662. https://doi.org/10.1016/j.cemconres.2024.107662

Kothari, C., & Takahashi, Y. (2022). The effect of heat treatment on the kinetics of the delayed ettringite formation – An improved chemo-thermal-hygral model. *Construction and Building Materials*, *331*. https://doi.org/10.1016/j.conbuildmat.2022.127358

Krishnan, S., & Bishnoi, S. (2018). Understanding the hydration of dolomite in cementitious systems with reactive aluminosilicates such as calcined clay. *Cement and Concrete Research*, *108*, 116–128. https://doi.org/10.1016/j.cemconres.2018.03.010

Lafuente, B., Downs, R. T., Yang, H., Stone, N., Armbruster, T., & Danisi, R. M. (2015). The power of databases: The RRUFF project. *Highlights in Mineralogical Crystallography*, *1*, 25.

Lee, J.-S. (1983). Digital image smoothing and the sigma filter. *Computer Vision, Graphics, and Image Processing*, *24*(2), 255–269. https://doi.org/10.1016/0734-189X(83)90047-6

Loh, H.-C., Kim, H.-J., Ulm, F.-J., & Masic, A. (2021). Time-space-resolved chemical deconvolution of cementitious colloidal systems using Raman spectroscopy. *Langmuir*, *37*(23), 7019–7031. https://doi.org/10.1021/acs.langmuir.1c00609

Lothenbach, B., Kulik, D. A., Matschei, T., Balonis, M., Baquerizo, L., Dilnesa, B., Miron, G. D., & Myers, R. J. (2019). Cemdata18: A chemical thermodynamic database for hydrated Portland cements and alkali-activated materials. *Cement and Concrete Research*, *115*, 472–506. https://doi.org/10.1016/j.cemconres.2018.04.018

Machner, A., Zajac, M., Ben Haha, M., Kjellsen, K. O., Geiker, M. R., & De Weerdt, K. (2017). Portland metakaolin cement containing dolomite or limestone—similarities and differences in phase assemblage and compressive strength. *Construction and Building Materials*, *157*, 214–225. https://doi.org/10.1016/j.conbuildmat.2017.09.056

Machner, A., Zajac, M., Ben Haha, M., Kjellsen, K. O., Geiker, M. R., & De Weerdt, K. (2018). Limitations of the hydrotalcite formation in Portland composite cement pastes containing dolomite and metakaolin. *Cement and Concrete Research*, *105*, 1–17. https://doi.org/10.1016/j.cemconres.2017.11.007

Matschei, T., Lothenbach, B., & Glasser, F. P. (2007). The role of calcium carbonate in cement hydration. *Cement and Concrete Research*, *37*(4), 551–558. https://doi.org/10.1016/j.cemconres.2006.10.013

Morse, J. W., & Arvidson, R. S. (2002). The dissolution kinetics of major sedimentary carbonate minerals. *Earth-Science Reviews*, *58*(1–2), 51–84. https://doi.org/10.1016/S0012-8252(01)00083-6

Pitre, B. T. (2012). *Application of the modified methylene blue test to detect clay minerals in coarse aggregate fines*. Texas A&M University.

Pokrovsky, O. S., & Schott, J. (2001). Kinetics and mechanism of dolomite dissolution in neutral to alkaline solutions revisited. *American Journal of Science*, *301*(7), 597–626. https://doi.org/10.2475/ajs.301.7.597

Polavaram, K. C., & Garg, N. (2021). High-fidelity and high-resolution phase mapping of granites via confocal Raman imaging. *Scientific Reports*, *11*(1), 8022. https://doi.org/10.1038/s41598-021-87488-1

Polavaram, K. C., & Garg, N. (2023). Elucidating the size and shape of individual clinker phases via Raman imaging: Impact on cement hydration. *The Journal of Physical Chemistry C*, *127*(34), 17157–17170. https://doi.org/10.1021/acs.jpcc.3c03453

Poon, C. S., Kou, S. C., & Lam, L. (2006). Compressive strength, chloride diffusivity and pore structure of high performance metakaolin and silica fume concrete. *Construction and Building Materials*, *20*(10), 858–865. https://doi.org/10.1016/j.conbuildmat.2005.07.001

Qamhia, I. I. A., Cheung, J., Hou, W., Mwumvaneza, V., Ozer, H., & Tutumluer, E. (2016). Gradation effects on the strength properties of cement and fly ash stabilized quarry by-products. In *Geo-Chicago 2016* (pp. 610–620). https://doi.org/10.1061/9780784480137.058

Qamhia, I. I. A., Tutumluer, E., Ozer, H., Boler, H., Shoup, H., & Stolba, A. J. (2020). Durability aspects of chemically stabilized quarry by-product applications in pavement base and subbase. *Transportation Research Record*, *2674*(6), 339–350.

Qamhia, I. I. A., Tutumluer, E., & Ozer, H. (2018). *Field performance evaluation of sustainable aggregate by-product applications* (Report No. FHWA-ICT-18-016). Illinois Center for Transportation. https://doi.org/10.36501/0197-9191/18-019

Qamhia, I. I. A., Tutumluer, E., Ozer, H., & Boler, H. (2019). *Durability aspects of stabilized quarry by-product pavement base and subbase applications* (Report No. FHWA-ICT-19-012*)*. Illinois Center for Transportation. https://doi.org/10.36501/0197-9191/19-015

Ridler, T. W., & Calvard, S. (1978). Picture thresholding using an iterative selection method. *IEEE Trans. Syst. Man Cybern*, *8*(8), 630–632. https://doi.org/10.1109/TSMC.1978.4310039

Santamarina, J. C., Klein, A., & Fam, M. A. (2001). Soils and waves: Particulate materials behavior, characterization and process monitoring. *Journal of Soils and Sediments*, *1*(2), 130. https://doi.org/10.1007/BF02987719

Shrivastava, A., & Gupta, V. B. (2011). Methods for the determination of limit of detection and limit of quantitation of the analytical methods. *Chron. Young Sci*, *2*(1), 21–25. https://doi.org/10.4103/2229-5186.79345

Stroup-Gardiner, M., & Wattenberg-Komas, T. (2013). *Recycled materials and byproducts in highway applications, Volume 4: Mineral and quarry byproducts*. NCHRP Synthesis of Highway Practice, 4 (Project 20-05, Topic 40-01).

Thoenen, T., & Kulik, D. (2003). Nagra/PSI chemical thermodynamic data base 01/01 for the GEM-Selektor (V. 2-PSI) Geochemical Modeling Code: Release 28-02-03. *Paul Scherrer Institute: Villigen, Switzerland*.

Tutumluer, E., Ozer, H., Hou, W., & Mwumvaneza, V. (2015). *Sustainable aggregates production: green applications for aggregate by-products* (Report No. FHWA-ICT-15-012). Illinois Center for Transportation.

Wang, L., Li, X., Cheng, Y., & Bai, X. (2018). Effects of coal-metakaolin on the properties of cemented sandy soil and its mechanisms. *Construction and Building Materials*, *166*, 592–600. https://doi.org/10.1016/j.conbuildmat.2018.01.192

Wang, S., Zhang, X., Zhang, P., & Chen, Z. (2023). Strength performance and stabilization mechanism of fine sandy soils stabilized with cement and metakaolin. *Sustainability*, *15*(4), 3431. https://doi.org/10.3390/su15043431

Wu, Z., Deng, Y., Liu, S., Liu, Q., Chen, Y., & Zha, F. (2016). Strength and micro-structure evolution of compacted soils modified by admixtures of cement and metakaolin. *Applied Clay Science*, *127*, 44–51. https://doi.org/10.1016/j.clay.2016.03.040

Xu, J., Lu, D., Zhang, S., Xu, Z., & Hooton, R. D. (2021). Reaction mechanism of dolomite powder in Portland-dolomite cement. *Construction and Building Materials*, *270*. https://doi.org/10.1016/j.conbuildmat.2020.121375

Zajac, M., Bremseth, S. K., Whitehead, M., & Ben Haha, M. (2014). Effect of CaMg(CO3)2 on hydrate assemblages and mechanical properties of hydrated cement pastes at 40°C and 60°C. *Cement and Concrete Research*, *65*, 21–29. https://doi.org/10.1016/j.cemconres.2014.07.002

Zajac, M., Rossberg, A., Le Saout, G., & Lothenbach, B. (2014). Influence of limestone and anhydrite on the hydration of Portland cements. *Cement and Concrete Composites*, *46*, 99–108. https://doi.org/10.1016/j.cemconcomp.2013.11.007

Zhang, X., Luo, Y., & Yao, W. (2022). An innovative material with strong frost resistance—concrete containing dolomite powder. *Materials*, *15*(5), 1721. https://doi.org/10.3390/ma15051721

Zhang, X., Wei, Y., Zuo, J., Luo, Y., Wang, B., & Yao, W. (2020). Evolution of hydration process of cement-based material containing high volume of dolomite powder. *Fullerenes Nanotubes and Carbon Nanostructures*, *29*(5), 343–351. https://doi.org/10.1080/1536383X.2020.1842739

Zunino, F., & Scrivener, K. (2021). The reaction between metakaolin and limestone and its effect in porosity refinement and mechanical properties. *Cement and Concrete Research*, *140*, 106307. https://doi.org/10.1016/j.cemconres.2020.106307

APPENDIX A: MATERIAL ACQUISITION

Figure 55. Photo. Close-up view of aggregate QB depicting sand-sized gradation.

Figure 56. Photo. Aggregate QB collected from quarry 1 through quarry 7.

APPENDIX B: MOISTURE-DENSITY RELATIONSHIPS

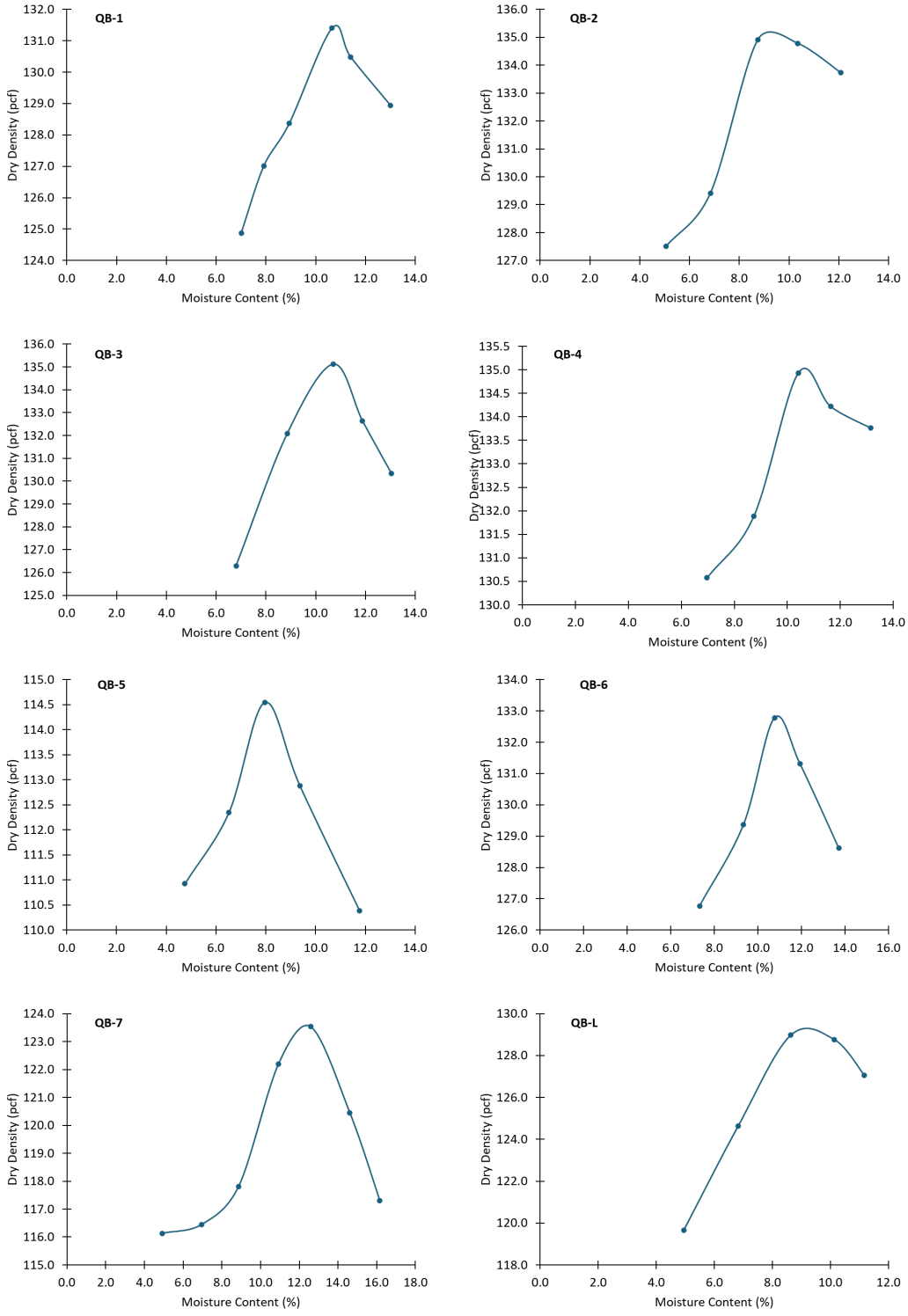

Figure 57. Graph. Moisture-density relationships of virgin QB materials without cement treatment (ASTM D698).

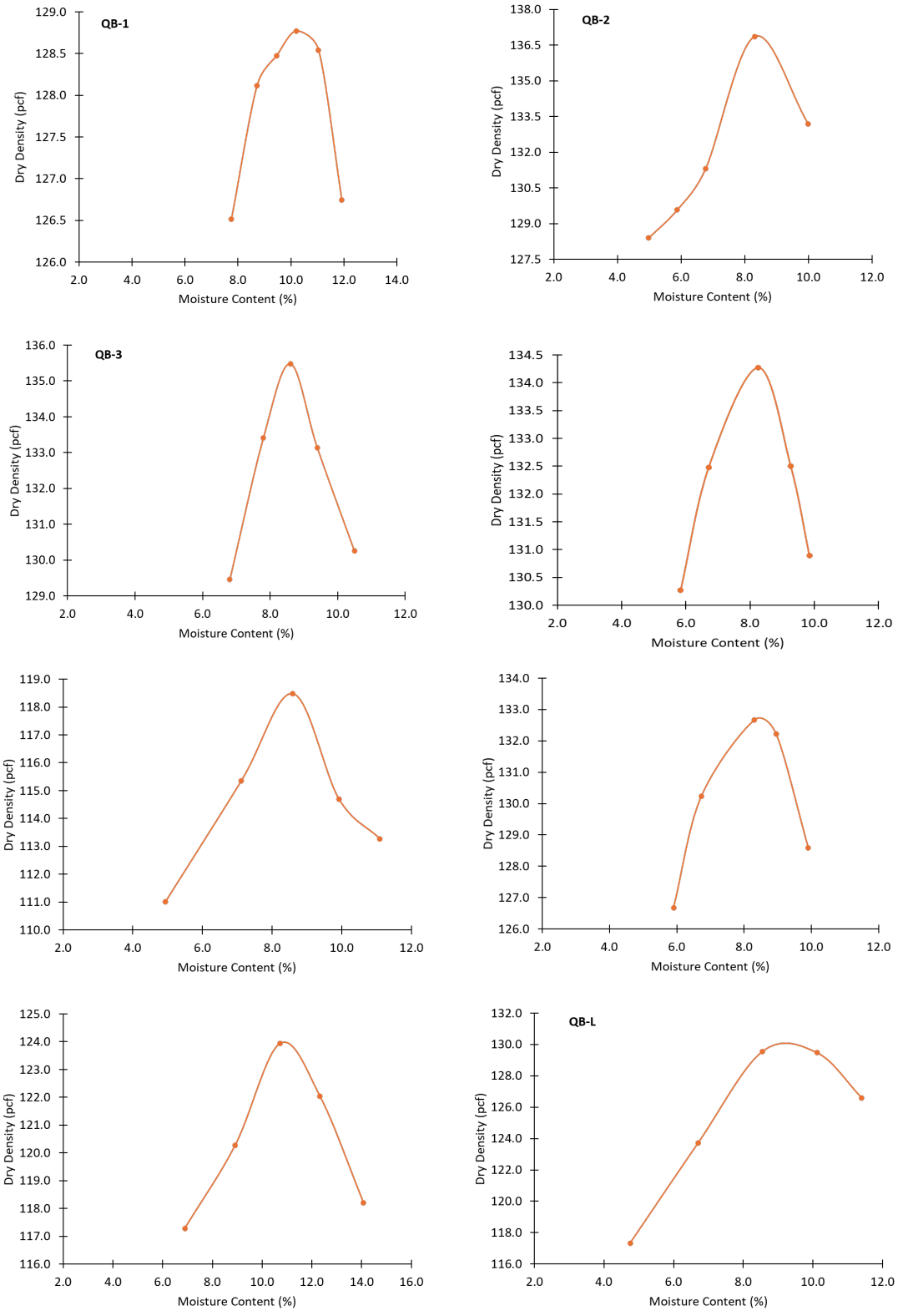

Figure 58. Graph. Moisture-density relationships of QB materials mixed with 3% cement (ASTM D698).

APPENDIX C: ELEMENTAL COMPOSITIONS OF AGGREGATE QUARRY BY-PRODUCTS

Table 10. Full Oxide Components of QB Materials Obtained from XRF Analysis

Oxide/Sample	QB1	QB2	QB3	QB4	QB5	QB6	QB7	QBL
CaO	34.19	33.31	31.85	35.33	27.75	40.93	41.88	52.89
MgO	15.63	14.25	13.74	15.44	10.00	10.99	7.33	0.31
Fe_2O_3	0.874	0.794	0.778	0.694	0.901	0.716	1.918	1.725
SiO_2	3.530	6.210	9.178	2.376	19.281	1.506	6.183	2.569
MnO	0.057	0.035	0.041	0.053	0.034	0.045	0.059	0.223
SO_3	0.139	0.239	0.113	0.297	0.116	0.335	0.435	0.159
K2O	0.329	0.518	0.787	0.260	2.014	0.164	0.190	0.127
TiO_2	0.057	0.097	0.146	0.061	0.170	0.041	0.067	0.049
SrO	0.011	0.013	0.015	0.015	0.015	0.013	0.031	0.065
Al_2O_3	0.000	0.692	1.228	0.016	2.821	0.000	0.215	0.029
Cl	0.711	0.688	0.000	0.673	0.000	0.601	0.000	0.274
Br	0.003	0.003	0.003	0.001	0.000	0.000	0.000	0.001
Rb_2O	0.000	0.003	0.004	0.000	0.003	0.000	0.000	0.001
V_2O_5	0.000	0.000	0.017	0.000	0.000	0.000	0.000	0.006
CuO	0.000	0.000	0.000	0.000	0.020	0.000	0.000	0.242
LOI	44.47	43.14	42.10	44.79	36.88	44.66	41.70	41.32
Total	100	100	100	100	100	100	100	100


Illinois Department
of Transportation


ILLINOIS